

Dynamics in the quantum Hall effect and the phase diagram of graphene

E.V. Gorbar,^{1,*} V.P. Gusynin,^{1,†} V.A. Miransky,^{2,‡} and I.A. Shovkovy^{3,§}

¹*Bogolyubov Institute for Theoretical Physics, 03680, Kiev, Ukraine*

²*Department of Applied Mathematics, University of Western Ontario, London, Ontario N6A 5B7, Canada*

³*Physics Department, Western Illinois University, Macomb, Illinois 61455, USA*

(Dated: November 5, 2018)

The dynamics responsible for lifting the degeneracy of the Landau levels in the quantum Hall (QH) effect in graphene is studied by utilizing a low-energy effective model with a contact interaction. A detailed analysis of the solutions of the gap equation for Dirac quasiparticles is performed at both zero and nonzero temperatures. The characteristic feature of the solutions is that the order parameters connected with the QH ferromagnetism and magnetic catalysis scenarios necessarily coexist. The solutions reproduce correctly the experimentally observed novel QH plateaus in graphene in strong magnetic fields. The phase diagram of this system in the plane of temperature and electron chemical potential is analyzed. The phase transitions corresponding to the transitions between different QH plateaus in graphene are described.

PACS numbers: 73.43.Cd, 71.70.Di, 81.05.Uw

I. INTRODUCTION

In this paper, we analyze the dynamics in quantum Hall (QH) effect in graphene, a single atomic layer of graphite.¹ As was experimentally discovered in Refs. 2,3 and theoretically predicted in Refs. 4,5,6, an anomalous quantization takes place in this case: the filling factors are $\nu = \pm 4(n + 1/2)$, where $n = 0, 1, 2, \dots$ is the Landau level index. For each QH state, a four-fold (spin and sublattice-valley) degeneracy takes place. These properties of the QH effect are intimately connected with relativistic-like features in the graphene dynamics.^{7,8,9,10,11,12}

In recent experiments,^{13,14} it has been observed that in a strong enough magnetic field, $B \gtrsim 20$ T, the new QH plateaus with $\nu = 0, \pm 1$ and ± 4 occur. This is attributed to the magnetic field induced splitting of the $n = 0$ and $n = 1$ Landau levels (LLs). It is noticeable that while the degeneracy of the lowest LL (LLL), $n = 0$, is completely lifted, only the spin degeneracy of the $n = 1$ LL is removed.

On theoretical side, there are now two leading scenarios for the description of these plateaus. One of them is the QH ferromagnetism (QHF).^{15,16,17,18,19} (The dynamics of a Zeeman spin splitting enhancement considered in Ref. 20 is intimately connected with the QHF.) The second one is the magnetic catalysis (MC) scenario in which Dirac masses are spontaneously produced as a result of the excitonic condensation.^{21,22,23,24} For a brief review of these two scenarios, see Ref. 25.

The QHF scenario is connected with the theory of exchange-driven spin splitting of Landau levels²⁶ and utilizes the dynamical framework developed for bilayer QH systems.²⁷ The underlying physics relies on the fact that the spin and/or valley degeneracy of the one-particle states is lifted by the repulsive Coulomb interaction in a many-body system at half filling. The argument is the same as that behind the Hund's rule in atomic physics. The Coulomb energy of the system is lowered by antisymmetrizing the coordinate part of the many-body wave function. Because of the Fermi statistics of the charge carriers, the corresponding lowest energy state must be symmetric in the spin-valley degrees of freedom, i.e., it is spin and/or valley polarized.

On the other hand, the MC scenario is based on the phenomenon of an enhancement of the density of states in infrared by a strong magnetic field, which catalyzes electron-hole pairing (leading to excitonic condensates) in relativistic-like systems. The essence of the MC phenomenon is the dimensional reduction $D \rightarrow D - 2$ in the pairing dynamics on the LLL with energy $E = 0$ (containing both electron and hole states). In two dimensions, this reduction implies a non-zero, proportional to $|eB|/2\pi\hbar c$, density of states in infrared. The latter is responsible for a Cooper-like electron-hole pairing even at the weakest attractive interaction between electrons and holes. This universal phenomenon was revealed in Ref. 28 and was first considered in graphite in Refs. 9,10.

The difference between the QHF and MC scenarios is in utilizing different order parameters in breaking an approximate $U(4)$ symmetry of the Hamiltonian of graphene. This symmetry operates in the sublattice-valley and spin spaces. While the QHF order parameters are described by densities of the conserved charges connected with diagonal generators of the non-Abelian subgroup $SU(4) \subset U(4)$, the order parameters in the MC scenario are Dirac mass terms.

One may think that the QHF and MC order parameters should compete with each other. However, as was recently pointed out by three of the authors,²⁹ the situation is quite different: these two sets of the order parameters *necessarily* coexist, which implies that they have the same dynamical origin. The physics underlying their coexistence is specific

for relativistic-like dynamics that makes the QH dynamics of the $U(4)$ breakdown in graphene to be quite different from that in the bilayer QH systems²⁷ whose dynamics has no relativistic-like features.

The main goal of this paper is a detailed study of the dynamics responsible for lifting the degeneracy of the Landau levels in the quantum Hall effect in graphene using the model of Ref. 29. To get the benchmark results that are unobscured by the various types of possible disorder,^{30,31,32,33} the analysis in this study is done for graphene in the clean limit. By taking into account a considerable improvement in samples quality seen in graphene suspended above a Si/SiO₂ gate electrode³⁴ or above a graphite substrate,³⁵ it is expected that the clean limit already provides a reasonable qualitative description for some real devices (the role of disorder in this dynamics will be briefly considered in Sec. VI.)

The main tool in our analysis is a gap equation for the propagator of Dirac quasiparticles. The highlights of the analysis are as follows:

1. The coexistence of the QHF and MC order parameters is a robust phenomenon, which is mostly based on the kinematic and symmetric properties of the QH dynamics in graphene.
2. The process of filling the LLs is described by varying the electron chemical potential μ_0 . A set of the solutions of the gap equation at a fixed μ_0 is quite rich. The stable solution is selected as the solution with the lowest free energy density. The obtained results for the QH effect qualitatively agree with the experimental data in Refs. 13,14.
3. The existence of two types of the Dirac masses in the QH dynamics in graphene is established. Both of them play an important role in the dynamics.
4. The phase diagram in the plane of temperature T and electron chemical potential μ_0 is analyzed. The phase transitions corresponding to the transitions between different QH plateaus are described.

The paper is organized as follows. In Sec. II we start by describing the general features of the model itself as well as the many-body approximation used in its analysis. After that, in Sec. III, we derive the gap equation for Dirac quasiparticles in graphene at zero and nonzero temperatures. The necessity of the coexistence of the QHF and MC order parameters in the solutions of the gap equation is shown. The analysis of the quasiparticle dynamics at the LLL, which is relevant to the $\nu = 0, \pm 1$ QH plateaus, is presented in Sec. IV. There we first give a detailed derivation of the analytic results of Ref. 29 at zero temperature. Then, we consider the nonzero temperature case by utilizing numerical calculations. In a similar fashion, in Sec. V, the quasiparticle dynamics at the $n = 1$ Landau level is analyzed. In Sec. VI, we summarize our findings in the form of the phase diagram of graphene in the $T - \mu_0$ plane. The obtained phase diagram is rich and it allows to describe all the recently discovered novel plateaus (as well as the plateaus $\nu = \pm 3$ and $\nu = \pm 5$ which have not been observed yet) in graphene in strong magnetic fields.^{13,14} We also discuss the correspondence between our results and the experimental data and point out that the coexistence of the QHF and MC order parameters could have important consequences for edge states, whose relevance for the dynamics in graphene has been recently discussed in Refs. 20,36,37. Detailed derivations of some key results used in our analysis are presented in four Appendices at the end of the paper.

II. MODEL: GENERAL DESCRIPTION

A. Model: Hamiltonian and gap equation

Our approach is based on the gap equation for the propagator of Dirac quasiparticles. For the description of the dynamics in graphene, we will use the model introduced recently in Ref. 29, which in turn is a modification of the model in Refs. 9,10,21. Let us start from the description of the latter. In this model, while quasiparticles are confined to a 2-dimensional plane, the electromagnetic (Coulomb) interaction between them is three-dimensional in nature. The low-energy quasiparticles excitations in graphene are conveniently described in terms of a four-component Dirac spinor $\Psi_s^T = (\psi_{KAs}, \psi_{KBs}, \psi_{K'Bs}, \psi_{K'As})$ which combines the Bloch states with spin indices $s = \pm$ on the two different sublattices (A, B) of the hexagonal graphene lattice and with momenta near the two inequivalent valley points (K, K') of the two-dimensional Brillouin zone. The free quasiparticle Hamiltonian can be recast in a relativistic-like form with the Fermi velocity $v_F \approx 10^6$ m/s playing the role of the speed of light:

$$H_0 = v_F \int d^2r \bar{\Psi} (\gamma^1 \pi_x + \gamma^2 \pi_y) \Psi, \quad (1)$$

where $\mathbf{r} = (x, y)$ is the position vector in the plane of graphene and $\bar{\Psi} = \Psi^\dagger \gamma^0$ is the Dirac conjugated spinor. In Eq. (1), γ^ν with $\nu = 0, 1, 2$ are 4×4 gamma matrices belonging to a reducible representation of the Dirac algebra, namely,

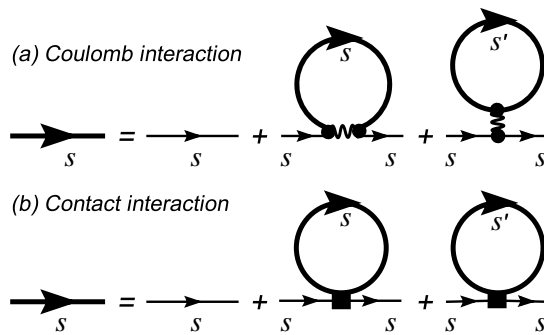


FIG. 1: The diagrammatic form of the gap equation in the Hartree-Fock (mean field) approximation. The upper (lower) diagram corresponds to the form of the gap equation with the long-range Coulomb (contact) interaction. The indices denote quasiparticle spins.

$\gamma^\nu = \tilde{\tau}^3 \otimes (\tau^3, i\tau^2, -i\tau^1)$, where the Pauli matrices $\tilde{\tau}^i$ and τ^i , with $i = 1, 2, 3$, act in the subspaces of the valleys (K, K') and sublattices (A, B), respectively.³⁸ The matrices satisfy the usual anticommutation relations $\{\gamma^\mu, \gamma^\nu\} = 2g^{\mu\nu}$, where $g^{\mu\nu} = \text{diag}(1, -1, -1)$ and $\mu, \nu = 0, 1, 2$. The canonical momentum $\boldsymbol{\pi} \equiv (\pi_x, \pi_y) = -i\hbar\nabla + e\mathbf{A}/c$ includes the vector potential \mathbf{A} corresponding to a magnetic field B_\perp , which is the component of the external magnetic field \mathbf{B} orthogonal to the xy -plane of graphene.

The Coulomb interaction term has the form

$$H_C = \frac{1}{2} \int d^2r d^2r' \Psi^\dagger(\mathbf{r}) \Psi(\mathbf{r}) U_C(\mathbf{r} - \mathbf{r}') \Psi^\dagger(\mathbf{r}') \Psi(\mathbf{r}'), \quad (2)$$

where $U_C(\mathbf{r})$ is the Coulomb potential in a magnetic field, calculated in the random phase approximation (RPA) in Ref. 10, see Eq. (46) there. The Hamiltonian $H = H_0 + H_C$ possesses a global $U(4)$ symmetry discussed in the next subsection. The electron chemical potential μ_0 is introduced by adding the term $-\mu_0 \Psi^\dagger \Psi$ to the Hamiltonian density. This term also preserves the $U(4)$ symmetry. The Zeeman interaction is included by adding the term $\mu_B B \Psi^\dagger \sigma^3 \Psi$, where $B \equiv |\mathbf{B}|$ and $\mu_B = e\hbar/(2mc)$ is the Bohr magneton. Here we took into account that the Lande factor for graphene is $g_L \simeq 2$ (our convention is $e > 0$). The spin matrix σ^3 has eigenvalue $+1$ (-1) for the states with the spin directed along (against) the magnetic field \mathbf{B} .³⁹ Such states will be called spin up (down) states. Because of the Zeeman term, the $U(4)$ symmetry is broken down to a symmetry $U(2)_+ \times U(2)_-$, where the subscript \pm labels the spin of the states on which this subgroup operates (see the next subsection).

The dynamics will be treated in the Hartree-Fock (mean field) approximation, which is conventional and appropriate in this case.^{9,10,15,16,21} Then, at zero temperature and in the clean limit (no impurities), the gap equation takes the form:

$$G^{-1}(u, u') = S^{-1}(u, u') + i\hbar\gamma^0 G(u, u') \gamma^0 \delta(t - t') U_C(\mathbf{r} - \mathbf{r}') - i\hbar\gamma^0 \text{tr} [\gamma^0 G(u, u)] \delta^3(u - u') U_C^{(F)}(0), \quad (3)$$

where $u \equiv (t, \mathbf{r})$, t is the time coordinate, $U_C^{(F)}(0)$ is the Fourier transform of $U_C(\mathbf{r})$ at $\mathbf{k} = 0$, $G(u, u') = \hbar^{-1} \langle 0 | T \Psi(u) \bar{\Psi}(u') | 0 \rangle$ is the *full* quasiparticle propagator, and

$$iS^{-1}(u, u') = [(i\hbar\partial_t + \mu_0 - \mu_B B \sigma^3) \gamma^0 - v_F(\boldsymbol{\pi} \cdot \boldsymbol{\gamma})] \delta^3(u - u') \quad (4)$$

is the inverse *bare* quasiparticle propagator. Note that while the second term on the right hand side of Eq. (3) describes the exchange interaction, the third one is the Hartree term describing the direct interaction. The diagrammatic form of the gap equation is shown in Fig. 1(a).

As will be shown in Sec. III below, in order to determine all the order parameters, the analysis of the gap equation (3) has to be done beyond the LLL approximation, which is a formidable problem. Because of this, we follow the approach of Ref. 29 and replace the Coulomb potential $U_C(\mathbf{r})$ in the gap equation by the contact interaction $G_{\text{int}} \delta^2(\mathbf{r})$. Thus, we arrive at

$$G^{-1}(u, u') = S^{-1}(u, u') + i\hbar G_{\text{int}} \gamma^0 G(u, u) \gamma^0 \delta^3(u - u') - i\hbar G_{\text{int}} \gamma^0 \text{tr} [\gamma^0 G(u, u)] \delta^3(u - u'), \quad (5)$$

where G_{int} is a dimensionful coupling constant. As we will see later, in the analysis it would be more convenient to use a dimensionless coupling constant $\lambda = G_{\text{int}} \Lambda / (4\pi^{3/2} \hbar^2 v_F^2)$ instead of G_{int} (note that Λ is the energy cutoff parameter

which is required when a contact interaction is used). The corresponding diagrammatic form of the equation is given in Fig. 1(b). A similar approximation is commonly used in Quantum Chromodynamics (QCD), where the long range gluon interaction is replaced by the contact Nambu–Jona-Lasinio one. This leads to a good description of many features of the nonperturbative dynamics in low energy region of QCD (for a review see, for example, Ref. 40). By taking into account the universality of the MC phenomenon and the fact that the symmetry and kinematic structures of equations (3) and (5) are the same, we expect that approximate gap equation (5) should be at least qualitatively reliable for the description of the LLL and the first few LLs, say, with $n = \pm 1$.

As to the value of the cutoff Λ , note that, in a strong magnetic field, the Landau scale

$$\epsilon_B \equiv \sqrt{2\hbar|eB_\perp|v_F^2/c} \simeq 424\sqrt{|B_\perp[\text{T}]|} \text{ K} \quad (6)$$

is the only relevant energy scale in the dynamics with the Coulomb interaction. This suggests that the ultraviolet cutoff Λ should be taken of order ϵ_B in the approximation with the contact interaction. The dimensionful coupling constant G_{int} then becomes $G_{\text{int}} \sim 4\pi^{3/2}\hbar^2v_F^2\lambda/\epsilon_B$.

Before concluding this section, the following remark concerning the present approximation is in order. While there is Debye screening at nonzero chemical potential, the situation is more complicated near the Dirac point with $\mu_0 = 0$. In that case, while for subcritical values of the Coulomb coupling constant⁴¹ the polarization effects lead only to its screening without changing the *form* of the Coulomb interactions at large distances,⁴² they lead to a drastic change of the form of the interactions for a supercritical coupling.⁴³ In the present work, the dynamics with a subcritical coupling is utilized, when no dynamical gaps are generated without a magnetic field (this is in agreement with the experiments^{2,3}). In our approximation, utilizing smeared contact interactions with an ultraviolet cutoff $\Lambda \sim \epsilon_B$, the contribution of large energies $\omega > \epsilon_B$ is suppressed much stronger than for the subcritical Coulomb like interactions. However, because the dominant contribution in the gap equation comes from energies $\omega \ll \epsilon_B$, we expect that the present approximation is qualitatively reliable even near the Dirac point.

B. Model: Symmetry and order parameters

The Hamiltonian $H = H_0 + H_C$, with H_0 and H_C given in Eqs. (1) and (2), respectively, possesses the $U(4)$ symmetry with the following 16 generators (see for example Refs. 10,21):

$$\frac{\sigma^\alpha}{2} \otimes I_4, \quad \frac{\sigma^\alpha}{2i} \otimes \gamma^3, \quad \frac{\sigma^\alpha}{2} \otimes \gamma^5, \quad \text{and} \quad \frac{\sigma^\alpha}{2} \otimes \gamma^3\gamma^5, \quad (7)$$

where I_4 is the 4×4 Dirac unit matrix and σ^α , with $\alpha = 0, 1, 2, 3$, are four Pauli matrices connected with the spin degrees of freedom (σ^0 is the 2×2 unit matrix). In the representation used in the present paper (for the definition of the γ^ν matrices, see the previous subsection), the Dirac matrices γ^3 and $\gamma^5 \equiv i\gamma^0\gamma^1\gamma^2\gamma^3$ are

$$\gamma^3 = i \begin{pmatrix} 0 & I \\ I & 0 \end{pmatrix}, \quad \gamma^5 = i \begin{pmatrix} 0 & I \\ -I & 0 \end{pmatrix}, \quad (8)$$

where I is the 2×2 unit matrix. Note that while the Dirac matrices γ^0 and $\boldsymbol{\gamma} = (\gamma^1, \gamma^2)$ anticommute with γ^3 and γ^5 , they commute with the diagonal matrix $\gamma^3\gamma^5 = -\gamma^5\gamma^3$,

$$\gamma^3\gamma^5 = \begin{pmatrix} I & 0 \\ 0 & -I \end{pmatrix}. \quad (9)$$

The matrix $\gamma^3\gamma^5$ is called a pseudospin operator.

The total Hamiltonian

$$H_{\text{tot}} \equiv H + \int d^2r [\mu_B B \Psi^\dagger \sigma^3 \Psi - \mu_0 \Psi^\dagger \Psi] \quad (10)$$

possesses a lower symmetry. Because of the Zeeman term $\mu_B B \Psi^\dagger \sigma^3 \Psi$, the $U(4)$ symmetry is broken down to the ‘‘flavor’’ symmetry $U(2)_+ \times U(2)_-$, where the subscript \pm corresponds to spin up and spin down states, respectively. The generators of the $U(2)_s$, with $s = \pm$, are $I_4 \otimes P_s$, $-i\gamma^3 \otimes P_s$, $\gamma^5 \otimes P_s$, and $\gamma^3\gamma^5 \otimes P_s$, where $P_\pm = (1 \pm \sigma^3)/2$ are the projectors on spin up and down states.

Our goal is to find all solutions of Eq. (5) both with intact and spontaneously broken $SU(2)_s$ symmetry, where $SU(2)_s$ is the largest non-Abelian subgroup of the $U(2)_s$. The Dirac mass term $\tilde{\Delta}_s \bar{\Psi} P_s \Psi \equiv \tilde{\Delta}_s \Psi^\dagger \gamma^0 P_s \Psi$, where

$\tilde{\Delta}_s$ is a Dirac gap (mass),⁴⁴ is assigned to the triplet representation of the $SU(2)_s$, and the generation of such a mass would lead to a spontaneous breakdown of the flavor $SU(2)_s$ symmetry down to the $\tilde{U}(1)_s$ with the generator $\gamma^3\gamma^5 \otimes P_s$.^{9,10,21} There is also a Dirac mass term of the form $\Delta_s \bar{\Psi} \gamma^3 \gamma^5 P_s \Psi$ that is a singlet with respect to $SU(2)_s$, and therefore its generation would not break this symmetry. On the other hand, while the triplet mass term is even under time reversal \mathcal{T} , the singlet mass term is \mathcal{T} -odd (for a recent review of the transformation properties of different mass terms in graphene, see Ref. 45). Note that the possibility of a singlet Dirac mass like Δ was first discussed in relation to graphite about 20 years ago.⁸

The masses Δ_s and $\tilde{\Delta}_s$ are related to the MC order parameters $\langle \bar{\Psi} \gamma^3 \gamma^5 P_s \Psi \rangle$ and $\langle \bar{\Psi} P_s \Psi \rangle$. In terms of the Bloch components of the spinors, the corresponding operators take the following forms:

$$\Delta_s : \quad \bar{\Psi} \gamma^3 \gamma^5 P_s \Psi = \psi_{KA_s}^\dagger \psi_{KA_s} - \psi_{K'A_s}^\dagger \psi_{K'A_s} - \psi_{KB_s}^\dagger \psi_{KB_s} + \psi_{K'B_s}^\dagger \psi_{K'B_s}, \quad (11)$$

$$\tilde{\Delta}_s : \quad \bar{\Psi} P_s \Psi = \psi_{KA_s}^\dagger \psi_{KA_s} + \psi_{K'A_s}^\dagger \psi_{K'A_s} - \psi_{KB_s}^\dagger \psi_{KB_s} - \psi_{K'B_s}^\dagger \psi_{K'B_s}. \quad (12)$$

The expressions on the right hand side further clarify the physical meaning of the Dirac mass parameters as the Lagrange multipliers that control various density imbalances of electrons at the two valleys and the two sublattices. In particular, the order parameter (12), connected with the triplet Dirac mass, describes the charge density imbalance between the two sublattices, i.e., a charge density wave.^{9,21}

As revealed in Ref. 29, and will be discussed in detail in the next section, these MC order parameters necessarily coexist with QHF ones in the solutions of the gap equation (5). More precisely, for a fixed spin, the full inverse quasiparticle propagator takes the following general form [compare with Eq. (4)]:

$$iG_s^{-1}(u, u') = \left[(i\hbar\partial_t + \mu_s + \tilde{\mu}_s \gamma^3 \gamma^5) \gamma^0 - v_F (\boldsymbol{\pi} \cdot \boldsymbol{\gamma}) - \tilde{\Delta}_s + \Delta_s \gamma^3 \gamma^5 \right] \delta^3(u - u'), \quad (13)$$

where the parameters μ_s , $\tilde{\mu}_s$, Δ_s , and $\tilde{\Delta}_s$ are determined from gap equation (5). Note that the full electron chemical potentials μ_\pm include the Zeeman energy $\mp Z$ with

$$Z \simeq \mu_B B = 0.67 B [\text{T}] \text{ K}. \quad (14)$$

The chemical potential $\tilde{\mu}_s$ is related to the density of the conserved pseudospin charge $\Psi^\dagger \gamma^3 \gamma^5 P_s \Psi$, which is assigned to the triplet representation of the $SU(2)_s$. Therefore, unlike the masses Δ_s and $\tilde{\Delta}_s$, the chemical potentials $\mu_3 \equiv (\mu_+ - \mu_-)/2$ and $\tilde{\mu}_s$ are related to the conventional QHF order parameters: the spin density $\langle \Psi^\dagger \sigma^3 \Psi \rangle$ and the pseudospin density $\langle \Psi^\dagger \gamma^3 \gamma^5 P_s \Psi \rangle$, respectively. In terms of the Bloch components, the corresponding operators take the following forms:

$$\mu_3 : \quad \Psi^\dagger \sigma^3 \Psi = \frac{1}{2} \sum_{\kappa=K, K'} \sum_{a=A, B} \left(\psi_{\kappa a+}^\dagger \psi_{\kappa a+} - \psi_{\kappa a-}^\dagger \psi_{\kappa a-} \right), \quad (15)$$

$$\tilde{\mu}_s : \quad \Psi^\dagger \gamma^3 \gamma^5 P_s \Psi = \psi_{KA_s}^\dagger \psi_{KA_s} - \psi_{K'A_s}^\dagger \psi_{K'A_s} + \psi_{KB_s}^\dagger \psi_{KB_s} - \psi_{K'B_s}^\dagger \psi_{K'B_s}. \quad (16)$$

By comparing the last expression with Eq. (12), we see that while the triplet MC order parameter related to $\tilde{\Delta}_s$ describes the charge density imbalance between the two graphene sublattices, the pseudospin density (related to $\tilde{\mu}_s$) describes the charge density imbalance between the two valley points in the Brillouin zone. On the other hand, as seen from Eq. (15), μ_3 is related to the conventional ferromagnetic order parameter $\langle \Psi^\dagger \sigma^3 \Psi \rangle$.

The following remark is in order. Because of the relation $\gamma^5 = i\gamma^0 \gamma^1 \gamma^2 \gamma^3$, the operator in Eq. (16) can be rewritten as $i\bar{\Psi} \gamma^1 \gamma^2 P_s \Psi$. The latter has the same form as the anomalous magnetic moment operator in Quantum Electrodynamics (QED). However, unlike QED, in graphene, it describes not the polarization of the spin degrees of freedom but that of the pseudospin ones, related to the valleys and sublattices. Because of that, this operator can be called the anomalous magnetic pseudomoment operator.

Let us describe the breakdown of the $U(4)$ symmetry down to the $U(2)_+ \times U(2)_-$ flavor symmetry, responsible for a spin gap, in more detail. Because of the Zeeman term, this breakdown is not spontaneous but explicit. The point however is that, as was shown in Ref. 20, a magnetic field leads to a strong enhancement of the spin gap in graphene. Such an enhancement is reflected in a large chemical potential $\mu_3 = (\mu_+ - \mu_-)/2 \gg Z$ and the corresponding QHF order parameter $\langle \Psi^\dagger \sigma^3 \Psi \rangle$. But as was pointed out in Ref. 29 and will be shown below in Sec. IV, it is not all. There is also a large contribution to the spin gap connected with the flavor singlet Dirac mass $\Delta_3 \equiv (\Delta_+ - \Delta_-)/2$ and the corresponding MC order parameter $\langle \bar{\Psi} \gamma^3 \gamma^5 \sigma^3 \Psi \rangle$. This feature leads to important consequences for the dynamics of edge states in graphene (see Secs. IV and VI).

As will be shown in Subsec. IV C, the spin gap may remain large even in the limit when the Zeeman energy $Z = \mu_B B$ goes to zero. In this limit, a genuine spontaneous breakdown of the $U(4)$ takes place. In the realistic case with a nonzero but small Z , one can say that a quasi-spontaneous breakdown of the $U(4)$ is realized.

The $U(2)_+ \times U(2)_-$ is an exact symmetry of the total Hamiltonian H_{tot} (10) of the continuum effective theory. However, as was pointed out in Ref. 17 (see also Refs. 19, 22, and 46), it is not exact for the Hamiltonian on the graphene lattice. In fact there are small on-site repulsion interaction terms which break the $U(2)_+ \times U(2)_-$ symmetry down to a $U(1)_+ \times Z_{2+} \times U(1)_- \times Z_{2-}$ subgroup, where the elements of the discrete group Z_{2s} are $\gamma^5 \otimes P_s + I_4 \otimes P_{-s}$ and the unit matrix. Unlike a spontaneous breakdown of continuous symmetries, a spontaneous breakdown of the discrete symmetry $Z_{2\pm}$, with the order parameters $\langle \bar{\Psi} P_{\pm} \Psi \rangle$ and $\langle \Psi^\dagger \gamma^3 \gamma^5 P_{\pm} \Psi \rangle$, is not forbidden by the Mermin-Wagner theorem at finite temperatures in a planar system.⁴⁷ This observation is of relevance for the description of the ground state responsible for the $\nu = \pm 1$ plateaus (see Subsec. IV D).

Thus, there are six order parameters describing the breakdown of the $U(4)$ symmetry: the two singlet order parameters connected with μ_3 and Δ_3 and the four triplet ones connected with $\tilde{\mu}_{\pm}$ and $\tilde{\Delta}_{\pm}$.

By extracting the location of the poles in full propagator $G(u, u')$, which is given in terms of the sum over separate LL contributions in Eq. (A27) in Appendix A, it is straightforward to derive the dispersion relations for the quasiparticles in graphene. The dispersion relations for LLs with $n \geq 1$ are

$$\omega_{n_s}^{(\sigma)} = -\mu_s + \sigma \tilde{\mu}_s \pm \sqrt{n\epsilon_B^2 + (\tilde{\Delta}_s + \sigma \Delta_s)^2}, \quad (17)$$

where $\sigma = \pm 1$ and the two signs in front of the square root correspond to the energy levels above and below the Dirac point. In the case of the LLL, which is special, the corresponding dispersion relations read

$$\omega_s^{(\sigma)} = -\mu_s + \sigma \left(\tilde{\mu}_s \text{sign}(eB_{\perp}) + \tilde{\Delta}_s \right) + \Delta_s \text{sign}(eB_{\perp}). \quad (18)$$

As shown in Subsec. A 2 in Appendix A, the parameter σ in Eqs. (17) and (18) is connected with the eigenvalues of the diagonal pseudospin matrix $\gamma_3 \gamma_5$ in Eq. (9). For the LLs with $n \geq 1$, the value $\sigma = \pm 1$ in (17) corresponds to the eigenvalues ∓ 1 of $\gamma^3 \gamma^5$. On the other hand, for LLL, the value $\sigma = \pm 1$ in (18) corresponds to $\text{sign}(eB_{\perp}) \times (\mp 1)$, with ∓ 1 being the eigenvalues of $\gamma^3 \gamma^5$.

One can see from Eqs. (17) and (18) that at a fixed spin, the terms with σ are responsible for splitting of LLs. We will return to this issue in Sec. IV.

III. GAP EQUATION: EXPLICIT FORM AT $T = 0$ AND $T \neq 0$ AND COEXISTENCE OF QHF AND MC ORDER PARAMETERS

In this section, we will present the explicit equations for the Dirac masses and the chemical potentials at zero and finite temperature. In particular, it will be shown that the QHF and MC order parameters necessarily coexist.

The equations for the Dirac masses Δ_s and $\tilde{\Delta}_s$ and the chemical potentials μ_s and $\tilde{\mu}_s$ follow from the matrix form of the gap equation in Eq. (5) and expression (13). Their derivation, while straightforward, is rather tedious. It is considered in Appendix A in detail. At zero temperature, the equations are

$$\begin{aligned} \tilde{\Delta}_s = \frac{A}{2} & \left\{ - [\text{sign}(\mu_s - \tilde{\mu}_s) \theta(|\mu_s - \tilde{\mu}_s| - E_{0s}^+) - \text{sign}(\mu_s + \tilde{\mu}_s) \theta(|\mu_s + \tilde{\mu}_s| - E_{0s}^-)] \text{sign}(eB_{\perp}) \right. \\ & \left. + \sum_{n=0}^{\infty} \left[\frac{(\tilde{\Delta}_s + \Delta_s) \theta(E_{ns}^+ - |\mu_s - \tilde{\mu}_s|)}{E_{ns}^+} + \frac{(\tilde{\Delta}_s - \Delta_s) \theta(E_{ns}^- - |\mu_s + \tilde{\mu}_s|)}{E_{ns}^-} \right] [1 + \theta(n-1)] \right\}, \quad (19) \end{aligned}$$

$$\begin{aligned} \Delta_s = \frac{A}{2} & \left\{ - [\text{sign}(\mu_s - \tilde{\mu}_s) \theta(|\mu_s - \tilde{\mu}_s| - E_{0s}^+) + \text{sign}(\mu_s + \tilde{\mu}_s) \theta(|\mu_s + \tilde{\mu}_s| - E_{0s}^-)] \text{sign}(eB_{\perp}) \right. \\ & \left. + \sum_{n=0}^{\infty} \left[\frac{(\tilde{\Delta}_s + \Delta_s) \theta(E_{ns}^+ - |\mu_s - \tilde{\mu}_s|)}{E_{ns}^+} - \frac{(\tilde{\Delta}_s - \Delta_s) \theta(E_{ns}^- - |\mu_s + \tilde{\mu}_s|)}{E_{ns}^-} \right] [1 + \theta(n-1)] \right\}, \quad (20) \end{aligned}$$

$$\begin{aligned} \tilde{\mu}_s = \frac{A}{2} & \left\{ \left[\frac{(\tilde{\Delta}_s + \Delta_s) \theta(E_{0s}^+ - |\mu_s - \tilde{\mu}_s|)}{E_{0s}^+} + \frac{(\tilde{\Delta}_s - \Delta_s) \theta(E_{0s}^- - |\mu_s + \tilde{\mu}_s|)}{E_{0s}^-} \right] \text{sign}(eB_{\perp}) \right. \\ & \left. + \sum_{n=0}^{\infty} [-\text{sign}(\mu_s - \tilde{\mu}_s) \theta(|\mu_s - \tilde{\mu}_s| - E_{ns}^+) + \text{sign}(\mu_s + \tilde{\mu}_s) \theta(|\mu_s + \tilde{\mu}_s| - E_{ns}^-)] [1 + \theta(n-1)] \right\}, \quad (21) \end{aligned}$$

$$\begin{aligned} \mu_s = \bar{\mu}_s + X + \frac{A}{2} \left\{ - \left[\frac{(\tilde{\Delta}_s + \Delta_s)\theta(E_{0s}^+ - |\mu_s - \tilde{\mu}_s|)}{E_{0s}^+} - \frac{(\tilde{\Delta}_s - \Delta_s)\theta(E_{0s}^- - |\mu_s + \tilde{\mu}_s|)}{E_{0s}^-} \right] \text{sign}(eB_\perp) \right. \\ \left. + \sum_{n=0}^{\infty} [\text{sign}(\mu_s - \tilde{\mu}_s)\theta(|\mu_s - \tilde{\mu}_s| - E_{ns}^+) + \text{sign}(\mu_s + \tilde{\mu}_s)\theta(|\mu_s + \tilde{\mu}_s| - E_{ns}^-)] [1 + \theta(n-1)] \right\}, \end{aligned} \quad (22)$$

where the step function is defined by $\theta(x) = 1$ for $x \geq 0$ and $\theta(x) = 0$ for $x < 0$. Regarding the other notation, $\bar{\mu}_\pm \equiv \mu_0 \mp Z$ is the bare electron chemical potential which includes the Zeeman energy $Z = \mu_B B$, and $E_{ns}^\pm = \sqrt{n\epsilon_B^2 + (\tilde{\Delta}_s \pm \Delta_s)^2}$ are quasiparticle energies. In these equations, we introduced a new energy scale, A , that plays an important role throughout the analysis. It is determined by the value of the magnetic field and the coupling constant strength,

$$A \equiv \frac{G_{\text{int}}|eB_\perp|}{8\pi\hbar c} = \frac{\sqrt{\pi}\lambda\epsilon_B^2}{4\Lambda}. \quad (23)$$

The second term on the right hand side in Eq. (22) is defined as follows:

$$X = \sum_{s=\pm} X_s, \quad (24)$$

where

$$\begin{aligned} X_s = -2A \left\{ - \left[\frac{(\tilde{\Delta}_s + \Delta_s)\theta(E_{0s}^+ - |\mu_s - \tilde{\mu}_s|)}{E_{0s}^+} - \frac{(\tilde{\Delta}_s - \Delta_s)\theta(E_{0s}^- - |\mu_s + \tilde{\mu}_s|)}{E_{0s}^-} \right] \text{sign}(eB_\perp) \right. \\ \left. + \sum_{n=0}^{\infty} [\text{sign}(\mu_s - \tilde{\mu}_s)\theta(|\mu_s - \tilde{\mu}_s| - E_{ns}^+) + \text{sign}(\mu_s + \tilde{\mu}_s)\theta(|\mu_s + \tilde{\mu}_s| - E_{ns}^-)] [1 + \theta(n-1)] \right\}. \end{aligned} \quad (25)$$

The following comment is in order here. Because of the Hartree term in the gap equation (5), the equations for the spin up and spin down parameters do not decouple: they are mixed via the X term in Eq. (22). Fortunately, it is the only place affected by the Hartree term. As shown in Appendix B, this fact strongly simplifies the analysis of the system of equations (19)–(22). This point also clearly reflects the essential difference between the roles played by the exchange and Hartree interactions in the quasiparticle dynamics of graphene. While the former dominates in producing the QHF and MC order parameters, the latter participates only in the renormalization of the electron chemical potential, which is relevant for the filling of LLs.

Since the step functions in the above set of equations depend on $\mu_s \pm \tilde{\mu}_s$ and $\tilde{\Delta}_s \pm \Delta_s$, it is more convenient to rewrite the gap equations for the following set of parameters

$$\Delta_s^{(\pm)} = \Delta_s \pm \tilde{\Delta}_s, \quad \mu_s^{(\pm)} = \mu_s \pm \tilde{\mu}_s. \quad (26)$$

In the numerical analysis, we always consider a nonzero temperature. This is implemented by utilizing the Matsubara formalism. Using the identities

$$T \sum_{n=-\infty}^{\infty} \frac{1}{[(2n+1)\pi T + i\mu]^2 + E^2} = \frac{1}{2E} \frac{\sinh(E/T)}{\cosh(E/T) + \cosh(\mu/T)}, \quad (27)$$

$$T \sum_{n=-\infty}^{\infty} \frac{-i(2n+1)\pi T + \mu}{[(2n+1)\pi T + i\mu]^2 + E^2} = -\frac{1}{2} \frac{\sinh(\mu/T)}{\cosh(E/T) + \cosh(\mu/T)}, \quad (28)$$

it is straightforward to write the equations at nonzero temperature. One can check that the prescription for modifying Eqs. (19)–(22) at $T \neq 0$ is to replace

$$\text{sign}(\mu_s^{(\pm)})\theta(|\mu_s^{(\pm)}| - E_{ns}^\mp) \rightarrow \frac{\sinh \frac{\mu_s^{(\pm)}}{T}}{\cosh \frac{E_{ns}^\mp}{T} + \cosh \frac{\mu_s^{(\pm)}}{T}}, \quad (29)$$

$$\theta(E_{ns}^\pm - |\mu_s^{(\mp)}|) \rightarrow \frac{\sinh \frac{E_{ns}^\pm}{T}}{\cosh \frac{E_{ns}^\pm}{T} + \cosh \frac{\mu_s^{(\mp)}}{T}}. \quad (30)$$

This leads to the following set of equations:

$$\Delta_s^{(\pm)} = Af_1\left(\Delta_s^{(\pm)}, \mu_s^{(\mp)}\right), \quad (31)$$

$$\mu_s^{(\pm)} = \tilde{\mu}_s + Af_2\left(\Delta_s^{(\mp)}, \mu_s^{(\pm)}\right) + 2Af_2\left(\Delta_s^{(\pm)}, \mu_s^{(\mp)}\right) + 2Af_2\left(\Delta_{-s}^{(\pm)}, \mu_{-s}^{(\mp)}\right) + 2Af_2\left(\Delta_{-s}^{(\mp)}, \mu_{-s}^{(\pm)}\right), \quad (32)$$

where $\Delta_s^{(\pm)}$ and $\mu_s^{(\pm)}$ are given in Eq. (26), and

$$f_1\left(\Delta_s^{(\pm)}, \mu_s^{(\mp)}\right) = \frac{\sinh\left(\frac{\Delta_s^{(\pm)}}{T}\right) - s_\perp \sinh\left(\frac{\mu_s^{(\mp)}}{T}\right)}{\cosh\left(\frac{\Delta_s^{(\pm)}}{T}\right) + \cosh\left(\frac{\mu_s^{(\mp)}}{T}\right)} + \sum_{n=1}^{\infty} \frac{2\Delta_s^{(\pm)} \sinh\left(\frac{E_{ns}^\pm}{T}\right)}{E_{ns}^\pm \left[\cosh\left(\frac{E_{ns}^\pm}{T}\right) + \cosh\left(\frac{\mu_s^{(\mp)}}{T}\right)\right]}, \quad (33)$$

$$f_2\left(\Delta_s^{(\pm)}, \mu_s^{(\mp)}\right) = \frac{s_\perp \sinh\left(\frac{\Delta_s^{(\pm)}}{T}\right) - \sinh\left(\frac{\mu_s^{(\mp)}}{T}\right)}{\cosh\left(\frac{\Delta_s^{(\pm)}}{T}\right) + \cosh\left(\frac{\mu_s^{(\mp)}}{T}\right)} - \sum_{n=1}^{\infty} \frac{2 \sinh\left(\frac{\mu_s^{(\mp)}}{T}\right)}{\cosh\left(\frac{E_{ns}^\pm}{T}\right) + \cosh\left(\frac{\mu_s^{(\mp)}}{T}\right)}, \quad (34)$$

with $s_\perp \equiv \text{sign}(eB_\perp)$ and $E_{ns}^\pm = \sqrt{n\epsilon_B^2 + \left(\Delta_s^{(\pm)}\right)^2}$.

Let us now show that the QHF and MC order parameters should always coexist in this dynamics. Suppose that Eqs. (31) and (32) have a solution with some of the chemical potentials μ_s^\mp being nonzero but the Dirac masses being zero, $\Delta_s^{(\pm)} = 0$. Then, the left hand side of Eq. (31) is equal to zero. On the other hand, taking into account expression (33) for the function f_1 , we find that for $\Delta_s^{(\pm)} = 0$ the right hand side of this equation takes the form

$$f_1\left(0, \mu_s^{(\mp)}\right) = \frac{-s_\perp \sinh\left(\frac{\mu_s^{(\mp)}}{T}\right)}{1 + \cosh\left(\frac{\mu_s^{(\mp)}}{T}\right)} = -s_\perp \tanh\left(\frac{\mu_s^{(\mp)}}{2T}\right), \quad (35)$$

and it could be zero only if *all* chemical potentials $\mu_s^{(\mp)}$ disappear, in contradiction with our assumption. Therefore we conclude that the QHF and MC order parameters in this dynamics necessarily coexist indeed. This is perhaps one of the central observations in this study.

Which factors underlie this feature of the graphene dynamics in a magnetic field? It is the relativistic nature of the free Hamiltonian H_0 in Eq. (1) and the special features of the LLs associated with it. To see this, note that while the triplet Dirac mass $\tilde{\Delta}_s$ multiplies the unit Dirac matrix I_4 , the triplet chemical potential $\tilde{\mu}_s$ comes with the matrix $\gamma^3\gamma^5\gamma^0$ in the inverse propagator G_s^{-1} in Eq. (13). Let us trace how these two structures are connected with each other. The point is that there are terms with $i\gamma^1\gamma^2\text{sign}(eB_\perp)$ matrix in the expansion of the propagator G_s over LLs [see Eq. (A21) in Appendix A]. Taking into account the definition $\gamma^5 = i\gamma^0\gamma^1\gamma^2\gamma^3$, we have $i\gamma^1\gamma^2 = \gamma^3\gamma^5\gamma^0$. Then, through the exchange term $\sim \gamma^0 G_s \gamma^0$ in gap equation (5), the $\tilde{\Delta}_s$ term in the inverse propagator G_s^{-1} necessarily induces the term with the chemical potential $\tilde{\mu}_s$. In the same way, the singlet Dirac mass Δ_s in G_s^{-1} is connected with the singlet chemical potential μ_s .

These arguments are based on the kinematic structure of gap equation (5), which is the same as that for equation (3) with the Coulomb interaction. Taking into account the universality of the MC phenomenon, we conclude that the coexistence of the QHF and MC order parameters is a robust feature of the QH dynamics in graphene.

The necessity of the coexistence of the QHF and MC order parameters can be clearly seen in the case of the dynamics on the LLL. As follows from Eq. (A27) in Appendix A, the LLL propagator contains only the combinations $-\mu_s + \Delta_s\text{sign}(eB_\perp)$ and $\tilde{\mu}_s\text{sign}(eB_\perp) + \tilde{\Delta}_s$. Therefore, in this case, the QHF and MC parameters not only coexist but they are not independent, which in turn reflects the fact that the sublattice and valley degrees of freedom are not independent on the LLL. In particular, by using Eqs. (11), (12), (15), and (16), one can easily check that, because of the projector $\mathcal{P}_- = [1 - i\gamma^1\gamma^2\text{sign}(eB_\perp)]/2$ in the LLL propagator [see Eqs. (A21) and (A22)], the operators $\Psi^\dagger P_s \Psi$ and $\bar{\Psi}\gamma^3\gamma^5 P_s \Psi$ ($\Psi^\dagger\gamma^3\gamma^5 P_s \Psi$ and $\bar{\Psi}P_s \Psi$), determining the order parameters related to μ_s and Δ_s ($\tilde{\mu}_s$ and $\tilde{\Delta}_s$), coincide up to a sign factor $\text{sign}(eB_\perp)$.⁴⁸ This fact in particular implies that in order to determine all the order parameters, it is necessary to analyze the gap equation beyond the LLL approximation.

The important point, however, is that this special feature of the LLL takes place only on an infinite plane. In real graphene samples with boundaries the situation is different: the QHF and MC parameters on the LLL become independent.^{49,50} As is discussed in Sec. VI, this leads to important consequences for the dynamics of edge states on the LLL.

IV. DYNAMICS ON LLL: $\nu = 0$, $\nu = \pm 1$, AND $\nu = \pm 2$ PLATEAUS

As was already discussed in Introduction, at magnetic fields $B \lesssim 10$ T, the plateaus with the filling factors $\nu = \pm 4(n + 1/2)$ are observed in the QH effect in graphene.^{2,3} At stronger magnetic fields, new plateaus, with $\nu = 0$ and $\nu = \pm 1$ occur: while the former arises at $B \gtrsim 10$ T, the latter appear at $B \gtrsim 20$ T.^{13,14} In this section, we will describe the dynamics underlying these new plateaus, and the plateaus $\nu = \pm 2$ corresponding to the gap between the LLL and the $n = 1$ LL, by using the solutions of the gap equation presented in the next subsection. We will consider positive ν and μ_0 (the dynamics with negative ν and μ_0 is related by electron-hole symmetry and will not be discussed separately). As will be shown below, there is a large number of the solutions corresponding to the same μ_0 . In order to find the most stable of them, we compare the free energy density Ω for the solutions. The derivation of the expression for Ω is presented in Appendix C.

A. Overview of analytic solutions at LLL

The $\nu = 0$, $\nu = \pm 1$ and $\nu = \pm 2$ plateaus are connected with a process of doping of the LLL, which is described by varying the electron chemical potential μ_0 . Therefore we start our analysis by reviewing the solutions to the gap equations in the case when μ_0 is much less than the Landau energy scale, i.e., $\mu_0 \ll \epsilon_B$. At zero temperature the corresponding gap equations are analyzed analytically in Appendix B. It is concluded there that only the following three stable solutions are realized:

- (i) The solution with *singlet* Dirac masses for both spin up and spin down quasiparticles,

$$\begin{aligned} \tilde{\Delta}_+ = \tilde{\mu}_+ = 0, & \quad \mu_+ = \bar{\mu}_+ - A, & \quad \Delta_+ = s_\perp M, \\ \tilde{\Delta}_- = \tilde{\mu}_- = 0, & \quad \mu_- = \bar{\mu}_- + A, & \quad \Delta_- = -s_\perp M. \end{aligned} \quad (36)$$

[By definition $M \equiv A/(1 - \lambda)$ and $\lambda \equiv 4A\Lambda/(\sqrt{\pi}\epsilon_B^2)$, see Eq. (B9) and its derivation in Appendix B.] This solution is energetically most favorable for $0 \leq \mu_0 < 2A + Z$.⁵¹ It is one of several solutions with nonvanishing singlet Dirac masses and we call it the *S1* solution (here *S* stands for *singlet*). Because of the opposite signs of both the masses Δ_+ and Δ_- and the chemical potentials μ_+ and μ_- , the explicit breakdown of the $U(4)$ symmetry down to $U(2)_+ \times U(2)_-$ by the Zeeman term is strongly enhanced by the dynamics. Since all triplet order parameters vanish, the flavor $U(2)_+ \times U(2)_-$ symmetry is intact in the state described by this solution. As discussed in Subsec. IV C below, the *S1* solution corresponds to the $\nu = 0$ plateau.

- (ii) The *hybrid* solution with a *triplet* Dirac mass for spin up and a *singlet* Dirac mass for spin down quasiparticles,

$$\begin{aligned} \tilde{\Delta}_+ = M, & \quad \tilde{\mu}_+ = As_\perp, & \quad \mu_+ = \bar{\mu}_+ - 4A, & \quad \Delta_+ = 0, \\ \tilde{\Delta}_- = 0, & \quad \tilde{\mu}_- = 0, & \quad \mu_- = \bar{\mu}_- - 3A, & \quad \Delta_- = -s_\perp M. \end{aligned} \quad (37)$$

It is most favorable for $2A + Z \leq \mu_0 < 6A + Z$. We call it the *H1* solution (here *H* stands for *hybrid*, meaning that the solution is a mixture of the singlet and triplet parameters). In this case, while the $SU(2)_+ \subset U(2)_+$ symmetry connected with spin up is spontaneously broken down to $U(1)_+$ (whose generator is $\gamma^3\gamma^5 \otimes P_+$), the $SU(2)_- \subset U(2)_-$ symmetry connected with spin down remains intact. As will be shown in Subsec. IV D, the *H1* solution corresponds to the $\nu = 1$ plateau.

- (iii) The solution with equal *singlet* Dirac masses for both spin up and spin down quasiparticles

$$\begin{aligned} \tilde{\Delta}_+ = \tilde{\mu}_+ = 0, & \quad \mu_+ = \bar{\mu}_+ - 7A, & \quad \Delta_+ = -s_\perp M, \\ \tilde{\Delta}_- = \tilde{\mu}_- = 0, & \quad \mu_- = \bar{\mu}_- - 7A, & \quad \Delta_- = -s_\perp M. \end{aligned} \quad (38)$$

It is most favorable for $\mu_0 > 6A + Z$. We call it the *S2* solution. (Note that the dynamics in the $n = 1$ LL will set an upper limit for the range where the *S2* solution is the ground state, see Sec V below.) In the state given by the *S2* solution, the $U(4)$ symmetry is broken down to $U(2)_+ \times U(2)_-$ only by the Zeeman term. Indeed, the singlet masses and the dynamical contributions to the chemical potentials are of the same sign for both spin orientations and thus have no effect on breaking any symmetry. As will be shown in Subsec. IV E, the *S2* solution corresponds to the $\nu = 2$ plateau connected with the gap between the filled LLL and the empty $n = 1$ LL.

The free energy densities for the above three solutions are given by the following expressions (see Subsec. B 6 in

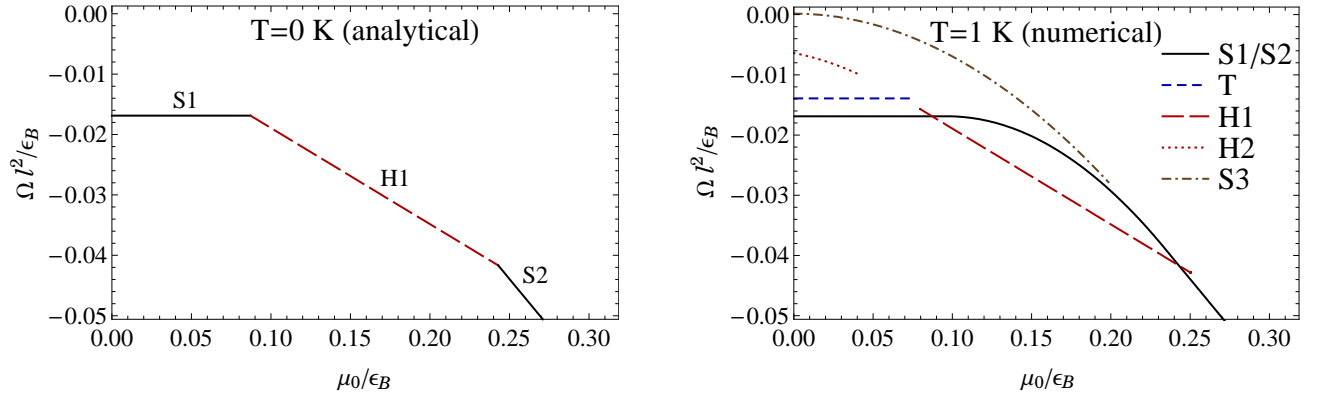


FIG. 2: Free energy density versus the electron chemical potential μ_0 for several different solutions, found analytically (left panel) and numerically (right panel) in a range of μ_0 relevant to the dynamics in the lowest Landau level. The numerical results are shown for a nonzero but small temperature, $T = 1$ K. The values of the electron chemical potential are given in units of the Landau energy scale ϵ_B , and the free energy densities are given in units of ϵ_B/l^2 , where $l = \sqrt{\hbar c/|eB_\perp|}$ is the magnetic length.

Appendix B):

$$\Omega = -\frac{|eB_\perp|}{2\pi\hbar c} (M + A + 2Z + h), \quad \text{for } 0 < \mu_0 < 2A + Z, \quad (39)$$

$$\Omega = -\frac{|eB_\perp|}{2\pi\hbar c} (M - A + Z + h + \mu_0), \quad \text{for } 2A + Z < \mu_0 < 6A + Z, \quad (40)$$

$$\Omega = -\frac{|eB_\perp|}{2\pi\hbar c} (M - 7A + h + 2\mu_0), \quad \text{for } 6A + Z < \mu_0, \quad (41)$$

where the parameter h is defined in Eq. (B56). We note that although the parameters of the solutions jump abruptly at the transition points, $\mu_0 = 2A + Z$ and $\mu_0 = 6A + Z$, their free energy densities match exactly. We conclude, therefore, that first order phase transitions take place at these values of the electron chemical potential μ_0 .

The free energy densities in Eqs. (39)-(41) are shown as functions of the chemical potential μ_0 in the left panel in Fig. 2. In order to plot the results, we took $M = 4.84 \times 10^{-2}\epsilon_B$ and $A = 3.90 \times 10^{-2}\epsilon_B$ which coincide with the values of the corresponding dynamical parameters in the numerical analysis. For comparison, the numerical results at nonzero but sufficiently small temperature are shown in the right panel of Fig. 2. As we see, the agreement is very good. It is interesting to note that the singlet-type numerical solution, given by the solid line, spans both the $S1$ and $S2$ solutions, as well as the intermediate (metastable) branch connecting them. In addition to the $S1$, $H1$, and $S2$ solutions, numerical results for several other (metastable) solutions are shown. The metastable solutions are discussed in Subsec. IV F below.

B. Numerical analysis at LLL

In this subsection, we give the key details regarding our numerical analysis.

Throughout this paper the default choice of the magnetic field in the numerical calculations is $B = 35$ T. The corresponding Landau energy scale is $\epsilon_B|_{B=35 \text{ T}} \approx 2510$ K. In order to do the numerical calculations in the model at hand, we use a simple regularization method that renders the formally defined divergent sum in Eq. (33) finite. In particular, we redefine the corresponding function as follows:

$$f_1(\Delta_s^{(\pm)}, \mu_s^{(\mp)}) = \frac{\sinh\left(\frac{\Delta_s^{(\pm)}}{T}\right) - s_\perp \sinh\left(\frac{\mu_s^{(\mp)}}{T}\right)}{\cosh\left(\frac{\Delta_s^{(\pm)}}{T}\right) + \cosh\left(\frac{\mu_s^{(\mp)}}{T}\right)} + \sum_{n=1}^{\infty} \frac{2\Delta_s^{(\pm)} \sinh\left(\frac{E_{ns}^\pm}{T}\right) \kappa(\sqrt{n}\epsilon_B, \Lambda)}{E_{ns}^\pm \left[\cosh\left(\frac{E_{ns}^\pm}{T}\right) + \cosh\left(\frac{\mu_s^{(\mp)}}{T}\right) \right]}, \quad (42)$$

where $\kappa(x, \Lambda)$ is a smooth cutoff function defined by

$$\kappa(x, \Lambda) = \frac{\sinh(\Lambda/\delta\Lambda)}{\cosh(x/\delta\Lambda) + \cosh(\Lambda/\delta\Lambda)} \quad (43)$$

with $\Lambda = 5000$ K and $\delta\Lambda = \Lambda/20 = 250$ K. The value of Λ corresponds to an approximate point of the high-energy cut-off, and the value of $\delta\Lambda$ gives the extent of the smearing region in either direction from Λ . (Note that the energy scale Λ is about the same as the energy of the $n = 4$ Landau level at $B = 35$ T.)

One should emphasize that the specific choice of the cutoff energy scale Λ has little effect on the qualitative as well as quantitative results of our analysis, provided the dynamical energy scales A and $M = A/(1 - \lambda)$ are kept fixed (see the discussion in the end of this subsection). Here we assume that the value of the cutoff is sufficiently large to avoid the reduction of the phase space relevant for the quasiparticle dynamics at the $n = 0$ and $n = 1$ LLs.

Because of the cutoff function $\kappa(x, \Lambda)$ the sum over n on the right hand side of Eq. (42) is rapidly convergent. In the numerical calculations, therefore, a sufficiently good accuracy may be achieved by keeping a finite number of terms in the sum. The optimum choice for the maximum value of index n is $n_{\max} = [14\Lambda^2/\epsilon_B^2]$, where the square brackets mean the integer number nearest to the result in the brackets. This choice is large enough to insure a high precision and, at the same time, it is small enough to make the calculation fast.

While the f_2 -function in Eq. (34) is finite, for consistency we redefine it in the same way as function f_1 by smoothly cutting off the contributions of large- n LLs,

$$f_2\left(\Delta_s^{(\pm)}, \mu_s^{(\mp)}\right) = \frac{s_{\perp} \sinh\left(\frac{\Delta_s^{(\pm)}}{T}\right) - \sinh\left(\frac{\mu_s^{(\mp)}}{T}\right)}{\cosh\left(\frac{\Delta_s^{(\pm)}}{T}\right) + \cosh\left(\frac{\mu_s^{(\mp)}}{T}\right)} - \sum_{n=1}^{\infty} \frac{2 \sinh\left(\frac{\mu_s^{(\mp)}}{T}\right) \kappa(\sqrt{n} \epsilon_B, \Lambda)}{\cosh\left(\frac{E_{ns}^{\pm}}{T}\right) + \cosh\left(\frac{\mu_s^{(\mp)}}{T}\right)}, \quad (44)$$

where $\kappa(x, \Lambda)$ is defined in Eq. (43). The numerical result for the sum in f_2 is also approximated by dropping the terms with $n > n_{\max}$ where n_{\max} is given above.

By analyzing the solutions to Eqs. (31) and (32) at very low temperatures, we reproduce all the analytic solutions derived in Appendix B. For the choice of the magnetic field $B = 35$ T the values of the two dynamical energy parameters A and M are given by

$$A \approx 98 \text{ K}, \quad M \approx 122 \text{ K}. \quad (45)$$

As is easy to check, these correspond to the dimensionless coupling $\lambda \approx 0.196$. Here one should keep in mind that the smooth-cutoff regularization used in our numerical calculations is not the same as in the analytical calculations [see, for example, Eq. (B6) in Appendix B.] Despite this difference, all analytical results agree very well even quantitatively with the corresponding numerical ones when expressed in terms of A and M parameters.

C. Plateau $\nu = 0$

The plateau $\nu = 0$ is connected with a range of electron chemical potentials in the vicinity of the Dirac neutral point with $\mu_0 = 0$. In this case the $S1$ solution with singlet Dirac masses of opposite sign for spin up and spin down quasiparticles, see Eq. (36), is most favorable energetically and therefore is the ground state solution, provided $\mu_0 < 2A + Z$ (other solutions related to the Dirac neutral point are discussed in Subsec. IV F below).

From dispersion relation (18), we find that while $\omega_+ = -\mu_0 + Z + M + A$ is positive for spin up states, $\omega_- = -\mu_0 - Z - M - A$ is negative for spin down states, i.e., the LLL is half filled (the energy spectrum in this solution is σ independent). Therefore there is a nonzero spin gap $\Delta E_0 = \omega_+ - \omega_-$ associated with the $\nu = 0$ plateau. The value of this gap is $\Delta E_0 = 2(Z + A) + 2M$.

While no exact symmetry is broken in the state described by the $S1$ solution, the explicit spin symmetry breaking by the Zeeman term Z is strongly enhanced by the dynamical contribution $M + A$. In this case, it is appropriate to talk about the dynamical symmetry breaking of the approximate spin symmetry. This is also evident from studying the temperature dependence of the MC and QHF order parameters in Fig. 3. In the two panels, we compare the results in the models with the exact (left panel) and approximate (right panel) spin symmetry. In the first case we take $Z = 0$ and see that the spontaneous spin-symmetry breaking occurs at low temperatures. The symmetry is restored at about $T \approx 0.9M$ in a typical second order phase transition (recall that we work in the mean-field approximation). In the second case, a nonzero Zeeman energy term ($Z \approx 23.51$ K at $B = 35$ T) breaks the spin symmetry explicitly and its restoration is impossible even at very high temperatures. However, even in this latter case, there is a well pronounced crossover (around $T \approx 0.9M$) between the regimes of low and high temperatures, which can be quantified by the relative strength of the bare Zeeman and dynamical contributions.

The order parameters for the solution $S1$ versus the electron chemical potential μ_0 are shown in Fig. 4 for several different values of the temperature. At $T = 0$ this solution is the ground state for $\mu_0 \lesssim 0.09\epsilon_B$. At sufficiently low temperature, the main qualitative feature of this solution is that the singlet Dirac masses for spin-up and spin-down quasiparticles have opposite signs, $\Delta_+ = -\Delta_-$. This defines the configuration of the MC order parameters that is formally invariant under the time reversal symmetry. (Of course, the time reversal symmetry is still explicitly broken

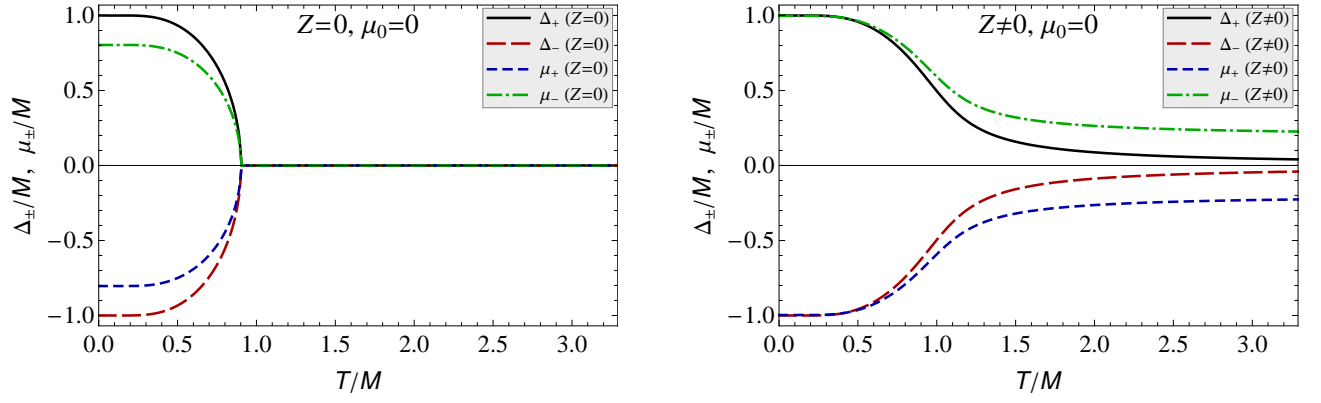


FIG. 3: Temperature dependence of the nontrivial order parameters in the $\nu = 0$ QH state, described by the $S1$ solution. The results in a model with a vanishing Zeeman energy ($Z = 0$) are shown in the left panel, and the results in a realistic model with a nonzero Zeeman energy ($Z \neq 0$) are shown in the right panel. Note that $\tilde{\mu}_{\pm} = \tilde{\Delta}_{\pm} = 0$ in both cases. The values of the temperature and the order parameters are given in units of the dynamical scale M .

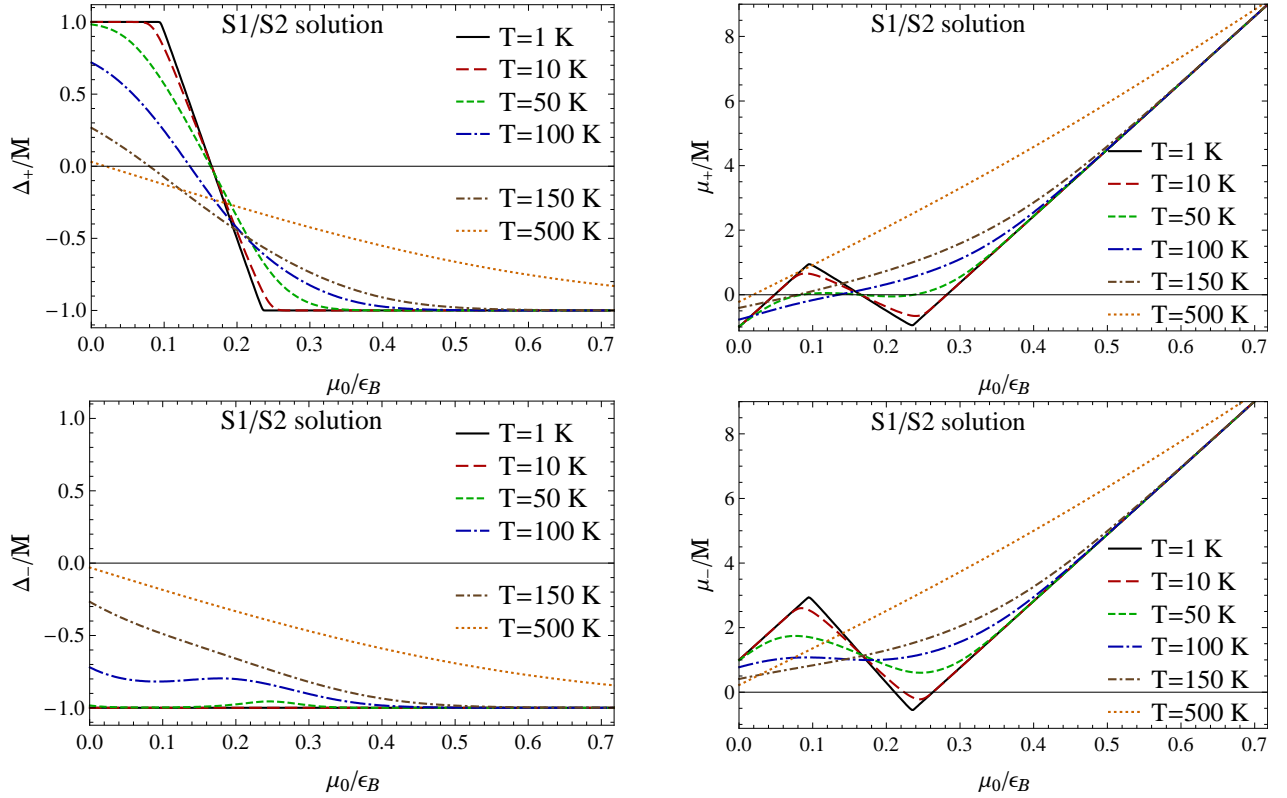


FIG. 4: Order parameters for the singlet solution $S1/S2$ as functions of the electron chemical potential μ_0 for several different values of temperature.

by the external magnetic field.) As the temperature increases, the approximate relation $\Delta_+ \approx -\Delta_-$ may hold at $\mu_0 \approx 0$, but deviations from such a relation grow with increasing μ_0 .

It should be emphasized that the solution $S1$ is continuously connected with the solution $S2$ responsible for the $\nu = 2$ QH plateau, see Subsec. IVE below. At low temperatures, the intermediate branch between the $S1$ and $S2$ solutions is metastable. At high temperatures, however, it becomes stable and the qualitative difference between the two solutions disappears.

The conclusion that the $\nu = 0$ state is related to the spin gap agrees with the scenario in Ref. 20 and the experiments

reported in Refs. 14,36. The fact established in the present paper that both μ_3 and the singlet Dirac mass Δ_3 contribute to the gap ΔE_0 is noticeable. As was already pointed out in Sec. III, unlike the case of an infinite plane, in graphene samples with boundaries, the parameters μ_3 and Δ_3 are independent on the LLL. As will be discussed in Sec. VI, this fact could have important consequences for the dynamics of edge states.

In conclusion, the following comment is in order. As one can see in the right panel in Fig.2, besides the $S1$ solution, there is another, triplet (T), solution around the Dirac neutral point. In the T solution, given in Eq.(B33) in Appendix B, both spin up and spin down quasiparticle states have a triplet Dirac mass. Calculating the difference of the free energy densities for these two solutions, one finds that $\delta\Omega = \Omega_{S1} - \Omega_T = -Z|eB|/\pi\hbar c$. Therefore, it is the Zeeman term which makes the $S1$ solution more favorable: without it, the $S1$ and T solutions would correspond to two degenerate ground states. It would be interesting to figure out the role of the small on-site repulsion interaction terms^{17,19,22,46} mentioned in Subsec. IIB in choosing the genuine ground state in the present dynamics.

D. Plateau $\nu = 1$

As was pointed out in Subsec. IVA, for larger μ_0 the hybrid $H1$ solution (37), with a triplet Dirac mass for spin up quasiparticles and a singlet Dirac mass for spin down quasiparticles, is most favorable. It is the ground state for $2A + Z < \mu_0 < 6A + Z$. As one can easily check by using Eq. (18), while now $\omega_+^{(+)} > 0$, the energies $\omega_+^{(-)}$ and $\omega_-^{(+)} = \omega_-^{(-)}$ are negative. Consequently, the LLL is now three-quarter filled and, therefore, the gap $\Delta E_1 = \omega_+^{(+)} - \omega_+^{(-)} = 2(M + A)$ corresponds to the $\nu = 1$ plateau. Notably, the Zeeman term does not enter the value of the gap. Unlike the $\nu = 0$ state, therefore, the gap in the $\nu = 1$ state is directly related to the spontaneous breakdown of the flavor symmetry $SU(2)_+$.

The last point regarding the nature of the ground state described by the $H1$ solution has important consequences for the physical properties of the $\nu = 1$ QH state. Since the coupling constant G_{int} in the present model is proportional to $1/\epsilon_B$ (see Subsec. IIA), Eq. (23) implies that the dynamical parameters A and M , and therefore the gap ΔE_1 , scale with the magnetic field as $\sqrt{|eB_\perp|}$. This fact agrees with the dependence of the activation energy in the $\nu = 1$ state observed in Ref. 14.

The critical temperature at which the $SU(2)_+$ symmetry is restored, i.e., when the triplet parameters $\tilde{\mu}_+$ and $\tilde{\Delta}_+$ vanish, is $T_c \simeq 0.9M \simeq 110K$. The restoration is described by a conventional second order phase transition.

The temperature dependence of the hybrid $H1$ solution is rather interesting too. This is summarized in Fig. 5 where the nontrivial order parameters and chemical potentials are shown for several values of the temperature in the range from 1 K to 100 K. One of the most spectacular features of this dependence is a revival of the singlet mass Δ_+ at finite temperature shown in Fig. 5 (recall that it vanishes at zero temperature). This phenomenon is intimately connected with the general conclusion in Sec. III that at a *fixed* value of spin s and *any* value of temperature, there are no nontrivial solutions of the gap equation with the both masses Δ_s and $\tilde{\Delta}_s$ being zero. Indeed, at $T > T_c$, when the triplet mass $\tilde{\Delta}_+$ vanishes, the absence of the Δ_+ would contradict this conclusion (note that as Fig. 5 shows, the revival of this mass occurs even at subcritical T). Note also that in the case of spin down quasiparticles, the triplet parameters $\tilde{\mu}_-$ and $\tilde{\Delta}_-$ are identically zero but the singlet mass Δ_- remains nonzero at all temperatures.

These results are obtained in the mean field approximation and for the Hamiltonian H_{tot} (10), which is symmetric under the $U(2)_+ \times U(2)_-$. However, as was already pointed out in Sec. IIB above, this symmetry is not exact for the Hamiltonian on the graphene lattice. In that case, it is replaced by $U(1)_+ \times Z_{2+} \times U(1)_- \times Z_{2-}$, where the elements of the discrete group $Z_{2\pm}$ are $\gamma^5 \otimes P_\pm + I_4 \otimes P_\mp$ and the unit matrix. It is important that unlike a spontaneous breakdown of continuous symmetries, a spontaneous breakdown of the discrete symmetry $Z_{2\pm}$, with the order parameters $\langle \tilde{\Psi} P_\pm \Psi \rangle$ and $\langle \Psi^\dagger \gamma^3 \gamma^5 P_\pm \Psi \rangle$, is not forbidden by the Mermin-Wagner theorem at finite temperatures in a planar system.⁴⁷ This point strongly suggests that there exists a genuine phase transition in temperature related to the $\nu = 1$ state in graphene.

E. Plateau $\nu = 2$

At zero temperature, the $S2$ solution (38) with equal singlet Dirac masses for spin up and spin down states is most favorable for $\mu_0 > 6A + Z$. It is easy to check from Eq. (18) that both ω_+ and ω_- are negative in this case, i.e., the LLL is completely filled. This solution corresponds to the $\nu = 2$ plateau when the value of the electron chemical potential is in the gap between the LLL and the $n = 1$ LL.

The nonzero temperature results for the order parameters of the solution $S2$ versus the electron chemical potential μ_0 are shown in Fig. 4. At $T = 0$ this solution is the ground state for $\mu_0 \gtrsim 0.24\epsilon_B$. As we see, even at high

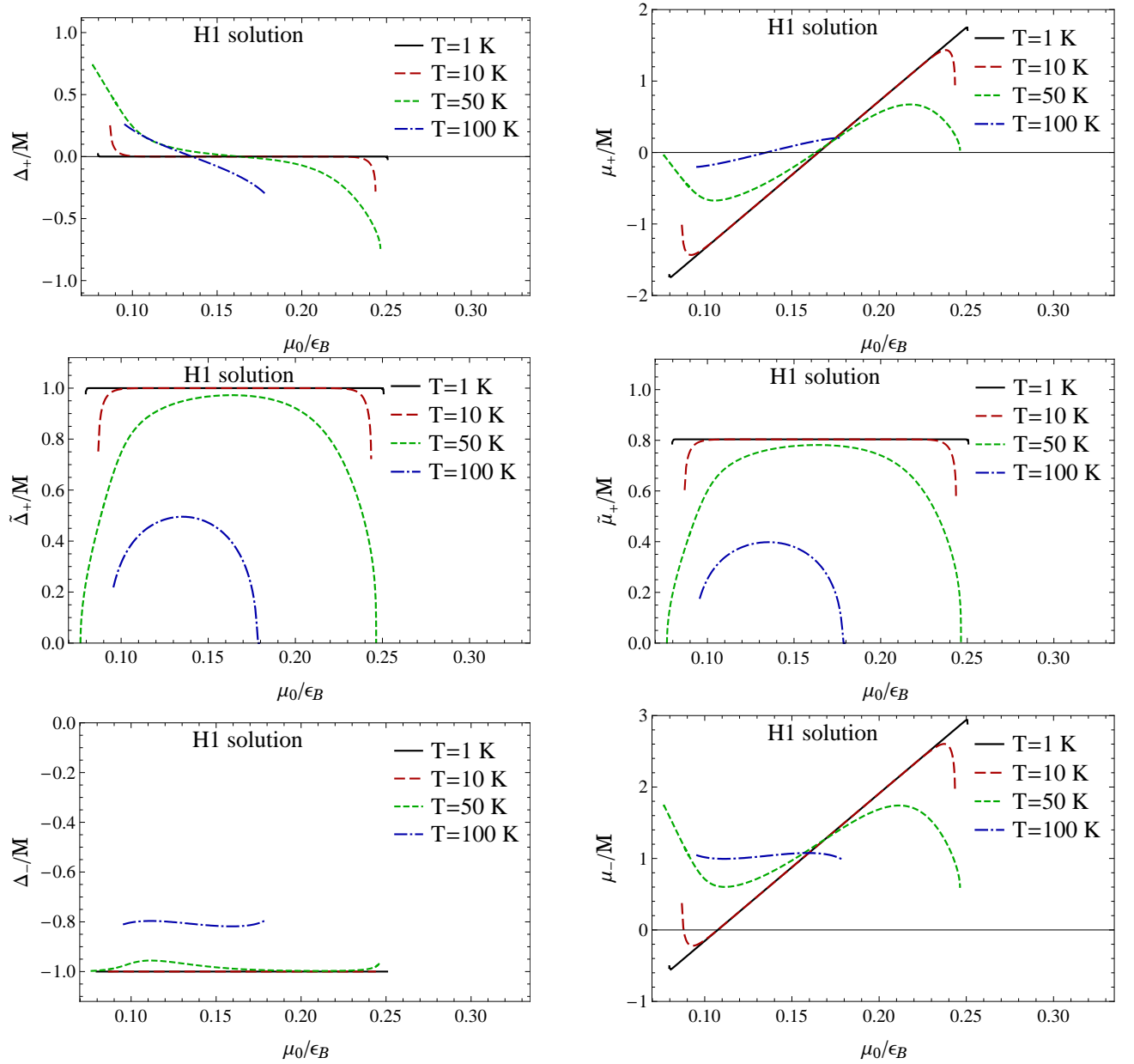


FIG. 5: Order parameters for the solution $H1$ as functions of the electron chemical potential μ_0 for several different values of temperature.

temperatures, the MC order parameters satisfy the same approximate relation, $\Delta_+ \approx \Delta_-$. Such a configuration breaks neither spin nor sublattice-valley symmetry of graphene.

F. Metastable solutions on LLL

As was already pointed out above, in addition to the three stable solutions $S1$, $H1$, and $S2$, describing the $\nu = 0$, $\nu = \pm 1$, and $\nu = \pm 2$ QH plateaus, the numerical analysis of the gap equations reveals other, metastable, solutions.

One of such solutions is the T solution with nonzero *triplet* Dirac masses for both spin up and spin down quasiparticles. In the model of graphene used in this paper, the explicit analytical form of this solution is given in Eq. (B33) in Appendix B. Note that because there is a contribution of the bare Zeeman term $Z \propto eB$ in the gap ΔE_1 for this solution, the corresponding activation energy in the $\nu = 1$ state scales with eB differently from the $\sqrt{|eB|}$ law in the

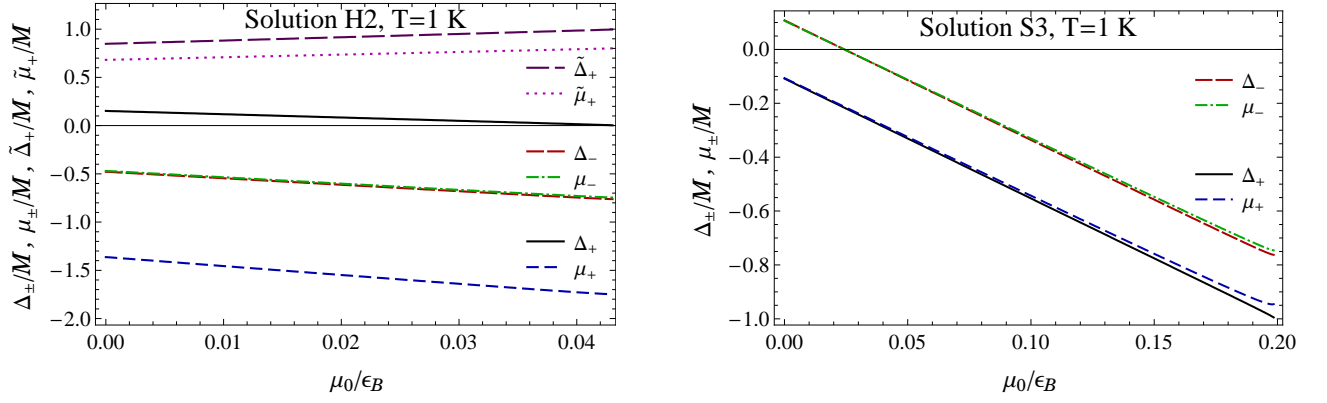


FIG. 6: Nontrivial order parameters of metastable solutions *H2* (left panel) and *S3* (right panel) as functions of the electron chemical potential μ_0 . In calculation, the temperature is taken nonzero but small, $T = 1$ K. The values of the electron chemical potential are given in units of the Landau energy scale ϵ_B , while the order parameters are given in units of the dynamical scale M .

hybrid *H1* solution.

In addition to the triplet solution, there exist also metastable hybrid (*H2*) and singlet (*S3*) solutions. Their free energy densities are shown in Fig. 2 together with the energy densities of the other solutions. As seen, neither the *H2* solution nor the *S3* one can have sufficiently low free energy density to become the genuine ground state.

The following remark is in order. Unlike all the other solutions, the solutions *H2* and *S3* cannot be found analytically at $T = 0$, see Appendix B. By making use of the numerical analysis, we find that these two extra solutions are such that $\mu_s^{(\pm)} \approx \pm E_{0s}^\mp$. At exactly zero temperature, it is problematic to get such solutions analytically because Eqs. (19)–(22) contain undetermined values of the step functions, e.g., $\theta(|\mu_s^{(\pm)}| - E_{0s}^\mp)$. In contrast, at a nonzero temperature, the step functions are replaced by smooth expressions, see Eqs. (29) and (30), and numerical solutions with $\mu_s^{(\pm)} \approx \pm E_{0s}^\mp$ are easily found. The order parameters for the solutions *H2* and *S3* are shown in Fig. 6.

V. DYNAMICS ON $n = 1$ LL

In the previous section, we analyzed solutions of the gap equations under the condition that only states on the LLL can be filled, $|\mu_s \pm \tilde{\mu}_s| \ll \epsilon_B = \sqrt{2\hbar} |eB_\perp| v_F^2 / c$. Since all the dynamically generated parameters are much less than ϵ_B , this condition implies that the bare chemical potential μ_0 also has to satisfy a similar inequality, $\mu_0 \ll \epsilon_B$. In this section, we extend the analysis by considering the dynamics with μ_0 being of the order of the Landau scale ϵ_B , i.e., we study the regime when quasiparticle states on the first Landau level, $n = 1$ LL, can be filled.

A. Analytic solutions at $T = 0$

We will start from the gap equations at zero temperature, which are given in Eqs. (19)–(22) in Sec. III. In order to get their solutions for $\mu_0 \sim \epsilon_B$, we will follow the same steps of the analysis as in Appendix B for the LLL. The corresponding analysis for the $n = 1$ LL, including the calculation of the free energy density for the solutions, is done in Appendix D. It is shown there that the following five stable solutions are realized (see the end of Subsec. D3):

- (f-i) The singlet type solution (f-I–f-I) (here *f* stands for *first*; the nomenclature used for the $n = 1$ LL solutions is defined in Appendix D):

$$\begin{aligned} \tilde{\Delta}_+ = \tilde{\mu}_+ = 0, & \quad \mu_+ = \bar{\mu}_+ - 7A, & \quad \Delta_+ = -s_\perp M, \\ \tilde{\Delta}_- = \tilde{\mu}_- = 0, & \quad \mu_- = \bar{\mu}_- - 7A, & \quad \Delta_- = -s_\perp M \end{aligned} \quad (46)$$

coincides with the solution S2 given by Eq. (38) in the analysis of the LLL. It takes place for $6A + Z < \mu_0 <$

$7A + \sqrt{\epsilon_B^2 + M^2} - Z$, and its free energy density is

$$\Omega = -\frac{|eB_\perp|}{2\pi\hbar c} (M + 2\mu_0 - 7A + h), \quad (47)$$

where h is given in Eq. (B56). According to Subsec. IV E, this solution corresponds to the regime with the filled LLL and the empty $n = 1$ LL and is connected with the $\nu = 2$ plateau.

(f-ii) The hybrid type solution (f-I-f-II)

$$\begin{aligned} \tilde{\Delta}_+ &= \tilde{\mu}_+ = 0, & \mu_+ &= \bar{\mu}_+ - 11A, & \Delta_+ &= -s_\perp M, \\ \tilde{\Delta}_- &= \frac{M - M_1}{2}, & \tilde{\mu}_- &= -As_\perp, & \mu_- &= \bar{\mu}_- - 10A, & \Delta_- &= -s_\perp \frac{M + M_1}{2}, \end{aligned} \quad (48)$$

with M_1 given in Eq. (D5) in Appendix D, takes place for $9A + \sqrt{\epsilon_B^2 + M_1^2} - Z < \mu_0 < 11A + \sqrt{\epsilon_B^2 + M^2} - Z$, and its free energy density is

$$\Omega = -\frac{|eB_\perp|}{2\pi\hbar c} \left(\frac{3M + M_1}{4} + 3\mu_0 - 15A - \epsilon_B + Z + \frac{3h + h_1}{4} \right), \quad (49)$$

where h_1 is given in Eq. (D22). As is shown in Subsec. V B below, this solution corresponds to the $\nu = 3$ plateau.

(f-iii) The singlet type solution (f-I-f-III)

$$\begin{aligned} \tilde{\Delta}_+ &= \tilde{\mu}_+ = 0, & \mu_+ &= \bar{\mu}_+ - 15A, & \Delta_+ &= -s_\perp M, \\ \tilde{\Delta}_- &= \tilde{\mu}_- = 0, & \mu_- &= \bar{\mu}_- - 13A, & \Delta_- &= -s_\perp M_1 \end{aligned} \quad (50)$$

is realized for $13A + \sqrt{\epsilon_B^2 + M_1^2} - Z < \mu_0 < 15A + \sqrt{\epsilon_B^2 + M^2} + Z$, and its free energy density is

$$\Omega = -\frac{|eB_\perp|}{2\pi\hbar c} \left(\frac{M + M_1}{2} + 4\mu_0 - 27A - 2\epsilon_B + 2Z + \frac{h + h_1}{2} \right). \quad (51)$$

As is discussed in Subsec. V B, this solution corresponds to the $\nu = 4$ plateau.

(f-iv) The hybrid type solution (f-II-f-III)

$$\begin{aligned} \tilde{\Delta}_+ &= \frac{M - M_1}{2}, & \tilde{\mu}_+ &= -As_\perp, & \mu_+ &= \bar{\mu}_+ - 18A, & \Delta_+ &= -s_\perp \frac{M + M_1}{2}, \\ \tilde{\Delta}_- &= \tilde{\mu}_- = 0, & \mu_- &= \bar{\mu}_- - 17A, & \Delta_- &= -s_\perp M_1 \end{aligned} \quad (52)$$

takes place for $17A + \sqrt{\epsilon_B^2 + M_1^2} + Z < \mu_0 < 19A + \sqrt{\epsilon_B^2 + M^2} + Z$, and its free energy density is

$$\Omega = -\frac{|eB_\perp|}{2\pi\hbar c} \left(\frac{3M_1 + M}{4} + 5\mu_0 - 43A - 3\epsilon_B + Z + \frac{3h_1 + h}{4} \right). \quad (53)$$

This solution corresponds to the $\nu = 5$ plateau (see Subsec. V B).

(f-v) The singlet type solution (f-III-f-III)

$$\begin{aligned} \tilde{\Delta}_+ &= \tilde{\mu}_+ = 0, & \mu_+ &= \bar{\mu}_+ - 21A, & \Delta_+ &= -s_\perp M_1, \\ \tilde{\Delta}_- &= \tilde{\mu}_- = 0, & \mu_- &= \bar{\mu}_- - 21A, & \Delta_- &= -s_\perp M_1 \end{aligned} \quad (54)$$

is realized for $\mu_0 > 21A + \sqrt{\epsilon_B^2 + M_1^2} + Z$, and its free energy density is

$$\Omega = -\frac{|eB_\perp|}{2\pi\hbar c} (M_1 + 6\mu_0 - 63A - 4\epsilon_B + h_1). \quad (55)$$

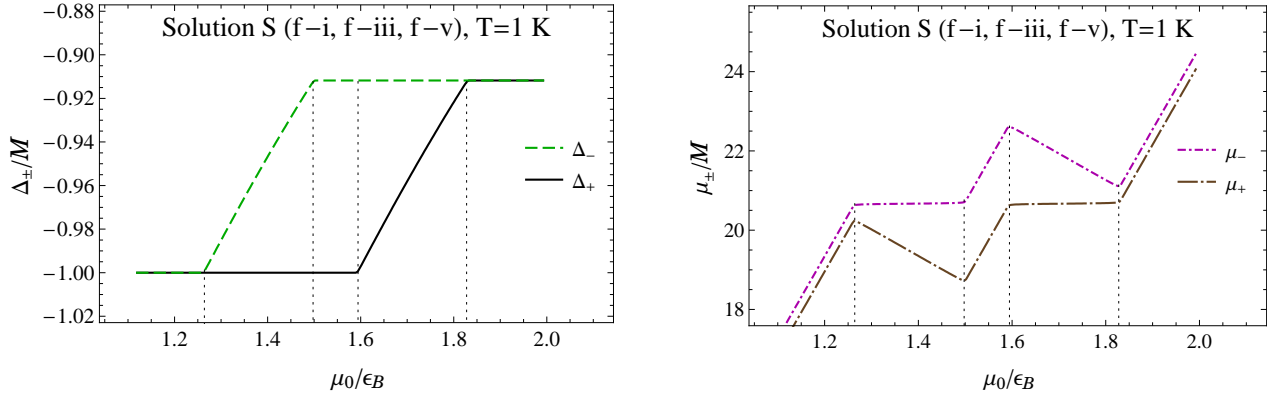


FIG. 7: Nontrivial order parameters of the S -type numerical solution that contains the analytical solutions (f-i), (f-iii) and (f-v) as parts, connected by two intermediate solutions.

This solution corresponds to the $\nu = 6$ plateau connected with the gap between the filled $n = 1$ LL and the empty $n = 2$ LL.

It should be emphasized that the above analytical solutions do not cover the whole range of the values of the electron chemical potential around the $n = 1$ LL. In particular, there are no analytical solutions found in the following four intervals:

$$7A + \sqrt{\epsilon_B^2 + M^2} - Z < \mu_0 < 9A + \sqrt{\epsilon_B^2 + M_1^2} - Z, \quad (56)$$

$$11A + \sqrt{\epsilon_B^2 + M^2} - Z < \mu_0 < 13A + \sqrt{\epsilon_B^2 + M_1^2} - Z, \quad (57)$$

$$15A + \sqrt{\epsilon_B^2 + M^2} + Z < \mu_0 < 17A + \sqrt{\epsilon_B^2 + M_1^2} + Z, \quad (58)$$

$$19A + \sqrt{\epsilon_B^2 + M^2} + Z < \mu_0 < 21A + \sqrt{\epsilon_B^2 + M_1^2} + Z. \quad (59)$$

The difficulty in finding analytical solutions at $T = 0$ on these intervals is related to the ambiguities in the definition of some step functions in gap equations (19)–(22). The same problem, albeit in a weaker form, was also encountered in the analysis of dynamics at the LLL (see Subsec. IV F). As in that case, we remove the ambiguities by considering a nonzero temperature case. The results at $T = 0$ can then be obtained by taking the limit $T \rightarrow 0$. The details of our numerical analysis are given in the next subsection.

B. Numerical analysis, $n = 1$ LL

By performing a nonzero temperature analysis numerically, we find that the solutions (f-i), (f-iii), and (f-v), found analytically, are in fact continuously connected. They are parts of a more general solution S (here S stands for *singlet*) that exists at all values of μ_0 . At small and intermediate values of μ_0 , this solution includes solutions $S1$ and $S2$, see Fig. 4. At larger values of μ_0 , relevant for the dynamics of $n = 1$ LL, the solution S is shown in Fig. 7.

As seen in Fig. 7, the solution S consists of five pieces defined on five adjacent intervals of μ_0 . Three of them are the analytical solutions (f-i), (f-iii), and (f-v), as defined in the previous subsection. Their intervals of existence are $\mu_0/\epsilon_B \lesssim 1.27$, $1.5 \lesssim \mu_0/\epsilon_B \lesssim 1.6$ and $\mu_0/\epsilon_B \gtrsim 1.83$, respectively. These intervals are in agreement with the analytical results if one takes $M_1 \approx 111$ K, or in terms of the Landau energy scale, $M_1 = 4.42 \times 10^{-2} \epsilon_B$. The other two pieces of the solution S extend the singlet-type analytical solution to the intermediate intervals.

At $T = 0$ the solution S describes the ground state in exactly the same regions of validity that are found analytically for solutions (f-i), (f-iii), and (f-v) in the previous subsection. This can be concluded from the energy consideration: among all numerical solutions the parts of the solution S have the lowest free energy density there. Analyzing the quasiparticle spectra by using the dispersion relation in Eq. (17), we find that the solutions (f-i), (f-iii), and (f-v) describe the $\nu = 2$, $\nu = 4$, and $\nu = 6$ QH states, respectively.

From the symmetry viewpoint, none of the three parts of the singlet solution break any exact symmetries in the model. However, the part (f-iii) of the solution, describing the $\nu = 4$ QH state, corresponds to a quasi-spontaneous breakdown of the $U(4)$ symmetry down to the $U(2)_+ \times U(2)_-$. Indeed, by using Eq. (17), one can check that the

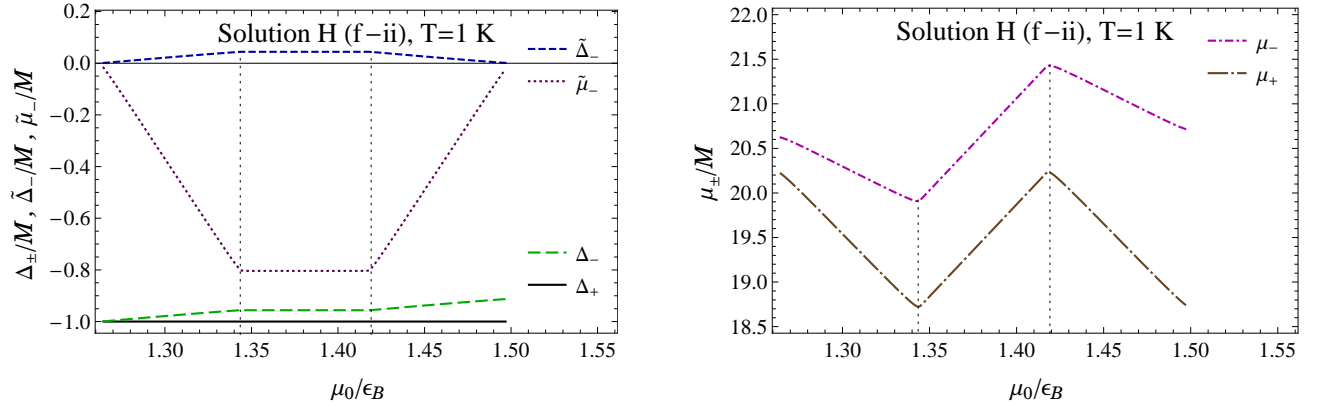


FIG. 8: Nontrivial order parameters of the extended hybrid solution (f-ii) which determines the ground state for the $\nu = 3$ QH plateau in graphene.

LLL is half filled and the energy gap between the pairs of the pseudospin degenerate spin-up and spin-down states of the $n = 1$ LL is given by $\Delta E_4 \simeq 2(Z + A) + (M^2 - M_1^2)/2\epsilon_B$. As we see, the spin splitting by the Zeeman term $2Z$ is strongly enhanced by the dynamical contribution $2A$.

This is somewhat similar to the enhancement of the spin splitting in the $\nu = 0$ QH state, discussed in Subsec. IV C. However, there is an important qualitative difference between the cases of the LLL and the $n = 1$ LL: It is only the dynamical contribution to the chemical potentials (but not the Dirac masses) that substantially affects the splitting in the $\nu = 4$ QH state. Indeed, the dynamical contribution due to the Dirac masses in the gap ΔE_4 , i.e., $(M^2 - M_1^2)/2\epsilon_B$, is very small because $M \simeq M_1 \ll \epsilon_B$.) As a result, the gap ΔE_4 is substantially smaller than the LLL spin gap ΔE_0 ($\Delta E_4 \lesssim \Delta E_0/2$).

Because of having nonvanishing triplet order parameters in the extended hybrid solutions (f-ii) and (f-iv), the flavor $U(2)_+ \times U(2)_-$ symmetry of graphene is partially broken in the corresponding ground states. By using dispersion relation (17) in the analysis of the quasiparticle spectra, we find that these solutions describe the $\nu = 3$ and $\nu = 5$ plateaus corresponding to the quarter and three-quarter filled $n = 1$ LL, respectively. In the case of the extended solution (f-ii), the spin-down flavor subgroup $SU(2)_- \subset U(2)_-$ is broken down to $U(1)_-$, while the spin-up flavor subgroup $U(2)_+$ is intact. Similarly, in the case of the extended solution (f-iv), the spin-up flavor subgroup $SU(2)_+ \subset U(2)_+$ is broken down to $U(1)_+$, while the spin-down flavor subgroup $U(2)_-$ is intact. Up to small corrections due nonzero Dirac masses, the energy gaps ΔE_3 and ΔE_5 associated with the (f-ii) and (f-iv) solutions are equal to $2A$. Note that these gaps are substantially smaller than the LLL gap ΔE_1 ($\Delta E_3, \Delta E_5 \lesssim \Delta E_1/2$).

The analytical hybrid solutions (f-ii) and (f-iv) get continuous extensions to the left and to the right from their regions of validity found analytically in the previous subsection. In fact, they extend all the way to cover the neighboring “forbidden” regions defined in Eqs. (56)–(59). The first two “forbidden” interval are covered by the extension of the solution (f-ii) to the interval $7A + \sqrt{\epsilon_B^2 + M^2} - Z < \mu_0 < 13A + \sqrt{\epsilon_B^2 + M_1^2} - Z$. The non-trivial Dirac masses and chemical potentials for this numerical solution are shown in Fig. 8. The last two “forbidden” intervals, see Eqs. (58) and (59), are covered by the extension of the solution (f-iv) to the interval $15A + \sqrt{\epsilon_B^2 + M^2} + Z < \mu_0 < 21A + \sqrt{\epsilon_B^2 + M_1^2} + Z$. The non-trivial parameters for this solution are shown in Fig. 9.

In fact, the extended solutions (f-ii) and (f-iv) are the ground states in their whole regions of existence. This is seen in Fig. 10, where we plot the difference between the free energy density of the hybrid type solutions and the singlet one. The results for the extended hybrid solutions (f-ii) and (f-iv) are shown by the solid line and the long-dashed line, respectively.

In Fig. 10 we also show the results for another hybrid solution that was found numerically. It exists in the interval of μ_0 that could potentially be relevant for the $\nu = 4$ QH state. However, its free energy density is higher than that for the solution S , and therefore it is unstable.

With increasing the temperature, we find that the extended hybrid solutions (f-ii) and (f-iv) responsible for the $\nu = 3$ and $\nu = 5$ QH states gradually vanish. Their regions of existence shrink and their free energy densities approach the free energy density of the singlet solution S . At temperatures above $T_{\text{cr}}^{(\nu=3)} \simeq T_{\text{cr}}^{(\nu=5)} \simeq 0.4M \simeq T_{\text{cr}}^{(\nu=1)}/2$, they cease to exist altogether, and the ground state is described by the singlet solution which does not break any exact symmetries of the model.

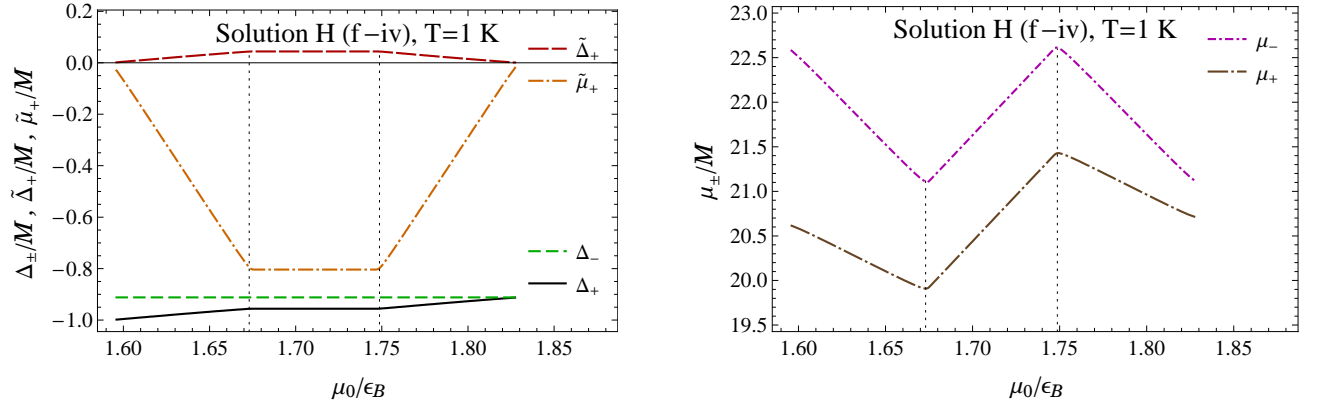


FIG. 9: Nontrivial order parameters of the extended hybrid solution (f-iv) which determines the ground state for the $\nu = 5$ QH plateau in graphene.

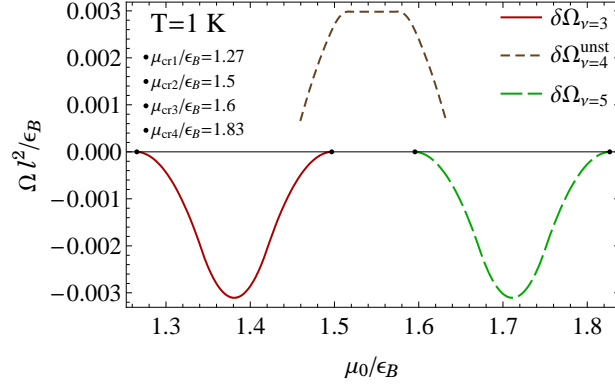


FIG. 10: The difference between the free energy density of three hybrid type solutions and the free energy density of the S -type solution in the range of μ_0 , associated with the dynamics of the $n = 1$ LL. In calculations, the temperature is taken nonzero but small, $T = 1$ K. The values of the free energy density and the electron chemical potential are given in the same units as in Fig 2.

VI. DISCUSSION: PHASE DIAGRAM, EXPERIMENT, DISORDER, AND EDGE STATES

By summarizing the numerical results for the ground states at different temperatures, we obtain the phase diagram of graphene in the plane of temperature T and electron chemical potential μ_0 shown in Fig. 11. The areas highlighted in green correspond to hybrid solutions with a lowered symmetry in the ground state. These regions are separated from the rest of the diagram by phase transitions. At the boundary of the $\nu = 1$ region, the transition is of first order at low temperatures and of second order at higher temperatures. The transitions to/from the QH $\nu = 3$ and $\nu = 5$ states are of second order. It should be kept in mind, however, that here the analysis is done in the mean-field approximation and in a model with a simplified contact interaction. Therefore, the predicted types of the phase transitions may not be reliable. In particular, the contributions of collective excitations, which are beyond the mean-field approximation, may change the transitions to first order type. Also, the types of the transitions may be affected by the inclusion of disorder and a more realistic long-range Coulomb interaction. Despite the model limitations, we still expect that Fig. 11 correctly represents the key qualitative features of the phase diagram of graphene at least in the case of the highest quality samples.

In Fig. 11 the regions highlighted in blue correspond to the ground states with a quasi-spontaneous breakdown of the spin symmetry. In the case of the LLL and the $n = 1$ LL, such are the $\nu = 0$ and $\nu = 4$ QH states, in which the quasi-spontaneous breakdown of the approximate $U(4)$ symmetry down to $U(2)_+ \times U(2)_-$ is enhanced by dynamical contributions. Because of the explicit breakdown by the Zeeman term, there is no well-defined order parameter associated with this symmetry breakdown. Also, there is no well-defined boundary of the corresponding regions in the diagram. In the plot, this feature is represented by the fading shades of blue at the approximate boundaries of

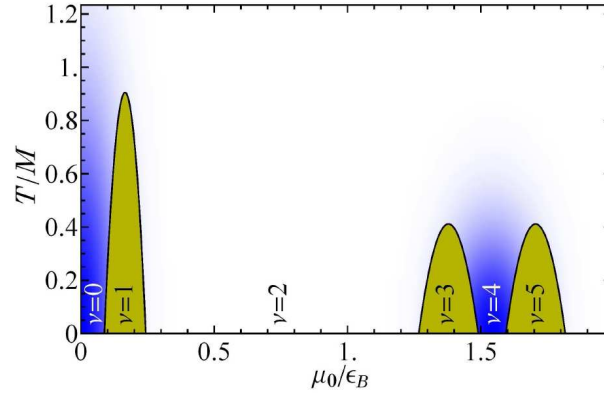


FIG. 11: Schematic phase diagram of graphene in the plane of temperature and electron chemical potential. The values of chemical potential are given in units of the Landau energy scale ϵ_B , and the values of temperature are given in units of the dynamical scale M .

the $\nu = 0$ and $\nu = 4$ regions.

As considered in detail in Sec. IV, the physical properties of the $\nu = 0$ and $\nu = 1$ QH states are determined by the dynamics of the LLL. The corresponding values of the gaps, $\Delta E_0 = 2(Z + A + M)$ and $\Delta E_1 = 2(A + M)$, are largely determined by the dynamical contributions A and M of about equal magnitude. These two contributions are associated with the QHF and MC order parameters, respectively.

The results of this study for the LLL at least qualitatively agree with the experimental data.^{13,14} By taking the dimensionless coupling $\lambda = 4A\Lambda/(\sqrt{\pi}\epsilon_B^2)$ to be a free parameter and utilizing the cutoff Λ to be of the order of the Landau scale ϵ_B , we arrive at the following scaling relations: $A \sim \lambda\sqrt{|eB_\perp|}$ and $M \sim \lambda\sqrt{|eB_\perp|}$. This implies the same type of scaling for the gap, $\Delta E_1 = 2(A + M) \sim \lambda\sqrt{|eB_\perp|}$, associated with the $\nu = \pm 1$ plateaus. [Recently, the square root scaling of the activation energy in the $\nu = 1$ QH state was also obtained in the large- N approximation in Ref. 52.] By making use of our results, we find that the experimental value $\Delta E_1 \sim 100$ K for $B_\perp = 30$ T from Ref. 14 corresponds to $\lambda \sim 0.02$. This estimate, however, should be taken with great caution: Because interactions with impurities are ignored and no disorder of any type is accounted for in the present model, it may not be unreasonable to assume that actual values of λ are up to an order of magnitude larger.

As to the $n = 1$ LL, we found that there are the gaps $\Delta E_3 = \Delta E_5 \simeq 2A$ and $\Delta E_4 \simeq 2(Z + A)$ corresponding to the plateaus $\nu = 3, 5$ and $\nu = 4$, respectively [the contributions of Dirac masses are suppressed by a factor of order $(M/\epsilon_B)^2$ there]. Therefore the gaps $\Delta E_3 = \Delta E_5$ and ΔE_4 are mostly due to the QHF type order parameters and are about a factor of two smaller than the LLL gaps ΔE_1 and ΔE_0 , respectively. On the other hand, the experimental data yield $\Delta E_4 \simeq 2Z$, and no gaps ΔE_3 , ΔE_5 have been observed.^{13,14} We believe that a probable explanation of this discrepancy is that, unlike Z , the value of the *dynamically* generated parameter A corresponding to the $|n| \geq 1$ LLs will be strongly reduced if a considerable broadening of higher LLs in a magnetic field is taken into account.²¹ If so, the gap ΔE_4 will be reduced to $2Z$, while the gaps ΔE_3 and ΔE_5 will become unobservable.

In order to estimate the value of a magnetic field at which the plateaus $\nu = 3$ and 5 could become observable, one can use the following arguments. Recently, in Ref. 33, a large width Γ_1 of 400 K was determined for the $n = 1$ LL. On the other hand, the plateaus $\nu = 3, 5$ could become observable if the gaps $\Delta E_3 = \Delta E_5 \simeq 2A$ calculated in the clean limit are at least of order Γ_1 or larger.²¹ The LLL gap $\Delta E_1 \simeq 100$ K at $|B_\perp| = 30$ T corresponds to $\Delta E_{3,5} \lesssim 50$ K. Then, taking a conservative estimate $\Gamma_1 = 100$ K and using $A \sim \sqrt{|eB_\perp|}$, we conclude that to observe the $\nu = 3, 5$ plateaus, the magnetic fields should be at least as large as $B \sim 100$ T.

Here it is also appropriate to mention the dynamics of gapless edge states, whose importance for the physics of the $\nu = 0$ plateau has been recently discussed in Refs. 20,36,37. Generalizing the analysis in Ref. 36, it has been recently found^{49,50} that for the $S1$ solution (36) with the zigzag boundary conditions, such states exist only when the full Zeeman energy $(\mu_+ - \mu_-)/2 = Z + A$ is larger than the Dirac mass $\Delta_\pm = M$ (at an armchair edge, gapless edge states exist for any value of a singlet Dirac mass). Because of that, for λ smaller than 1, we find from the constraint $Z > \lambda A/(1 - \lambda)$ in the solution (i) and Eq. (23) with $\Lambda \sim \epsilon_B$ that the gapless edge states exist when $|B_\perp| > B_\perp^{(\text{cr})} \sim 8 \times 10^4 \lambda^4 / (1 - \lambda)^2$ T. Then, for the values of the dimensionless coupling λ in the range $0.02 \lesssim \lambda \lesssim 0.2$, we find that 0.01 T $\lesssim B_\perp^{(\text{cr})} \lesssim 200$ T. As we see, $B_\perp^{(\text{cr})}$ is very sensitive to the choice of λ . Therefore, in order to fix the critical value $B_\perp^{(\text{cr})}$ more accurately, one should first utilize more realistic models of graphene that incorporate

disorder among other things.^{31,32} This is a topic for future studies however.

These results are of interest in connection with the interpretation of the $\nu = 0$ Hall plateau. Indeed, the gapless edge states should play an important role in transport properties of graphene in a strong magnetic field. Their presence is expected to make graphene a so-called quantum Hall metal, while their absence should make it an insulator.^{20,36} The actual temperature dependence of the longitudinal resistivity at the $\nu = 0$ plateau in Refs. 13,36 is consistent with the metal type. This conclusion may be disputed in view of the recent data from Ref. 37 that reveal a clear plateau at $\nu = 0$, but the temperature dependence of the diagonal component of the resistivity signals a crossover to an insulating state in high fields. The latter observations do not seem to support the existence of gapless edge states.

The analysis in this paper as well as in Refs. 49,50 suggests that the conditions for the existence and absence of gapless edge states depend sensitively on the type of the boundary conditions and the values of QHF and MC order parameters that characterize the nature of the corresponding QH state. Therefore, the dynamics of the edge states is very likely to be rich and full of surprises.

In conclusion, we have shown that the QHF and MC order parameters in graphene are two sides of the same coin and they necessarily coexist. This feature could have important consequences for the QH dynamics, in particular, for edge states. The present model leads to a reasonable and consistent description of the new QH plateaus in graphene in strong magnetic fields. It would be desirable to extend the present analysis to a more realistic model setup, including the Coulomb interaction between quasiparticles, the quasiparticle width, and various types of disorder.

Acknowledgments

Useful discussions with S.G. Sharapov are acknowledged. V.A.M. is grateful to G.W. Semenoff for enjoyable discussions. The work of E.V.G and V.P.G. was supported by the SCOPES under Project No. IB 7320-110848 of the NSF-CH, by Ukrainian State Foundation for Fundamental Research under the grant No. F16-457-2007, and by the National Academy of Sciences of Ukraine under the grants No. 10/07-N and No. II-1-07. The work of V.A.M. was supported by the Natural Sciences and Engineering Research Council of Canada. He is grateful to the Aspen Center for Physics and the Institute for Nuclear Theory at the University of Washington for their hospitality and the Department of Energy for partial support during the completion of this work.

APPENDIX A: QUASIPARTICLE PROPAGATOR AND THE GAP EQUATION

1. Quasiparticle propagator: Expansion over LLs

In this Appendix, the units with $\hbar = 1$ and $c = 1$ are used.

The full propagator $G_s(u, u')$ that corresponds to the inverse propagator in Eq. (13) is given by the following expression:

$$\begin{aligned}
G_s(u, u') &= i\langle u | \left[(i\partial_t + \mu_s)\gamma^0 - v_F(\boldsymbol{\pi} \cdot \boldsymbol{\gamma}) + i\tilde{\mu}_s\gamma^1\gamma^2 + i\Delta_s\gamma^0\gamma^1\gamma^2 - \tilde{\Delta}_s \right]^{-1} | u' \rangle \\
&= i\langle u | \left[(i\partial_t + \mu_s)\gamma^0 - v_F(\boldsymbol{\pi} \cdot \boldsymbol{\gamma}) + i\tilde{\mu}_s\gamma^1\gamma^2 - i\Delta_s\gamma^0\gamma^1\gamma^2 + \tilde{\Delta}_s \right] \\
&\quad \times \left[(i\partial_t + \mu_s)\gamma^0 - v_F(\boldsymbol{\pi} \cdot \boldsymbol{\gamma}) + i\tilde{\mu}_s\gamma^1\gamma^2 + i\Delta_s\gamma^0\gamma^1\gamma^2 - \tilde{\Delta}_s \right] \\
&\quad \times \left[(i\partial_t + \mu_s)\gamma^0 - v_F(\boldsymbol{\pi} \cdot \boldsymbol{\gamma}) + i\tilde{\mu}_s\gamma^1\gamma^2 - i\Delta_s\gamma^0\gamma^1\gamma^2 + \tilde{\Delta}_s \right]^{-1} | u' \rangle \\
&= i\langle u | \left[(i\partial_t + \mu_s)\gamma^0 - v_F(\boldsymbol{\pi} \cdot \boldsymbol{\gamma}) + i\tilde{\mu}_s\gamma^1\gamma^2 - i\Delta_s\gamma^0\gamma^1\gamma^2 + \tilde{\Delta}_s \right] \\
&\quad \times \left[(i\partial_t + \mu_s)^2 - v_F^2\boldsymbol{\pi}^2 + 2i\tilde{\mu}_s(i\partial_t + \mu_s)\gamma^0\gamma^1\gamma^2 + 2i\Delta_s\tilde{\Delta}_s\gamma^0\gamma^1\gamma^2 \right. \\
&\quad \left. - ieB_\perp v_F^2\gamma^1\gamma^2 + \tilde{\mu}_s^2 - \tilde{\Delta}_s^2 - \Delta_s^2 \right]^{-1} | u' \rangle. \tag{A1}
\end{aligned}$$

where $u = (t, \mathbf{r})$ and $\mathbf{r} = (x, y)$. Our aim is to get an expression for this propagator as an expansion over LLs. For the Fourier transform in time we need to calculate

$$G_s(\omega; \mathbf{r}, \mathbf{r}') = i [W - v_F(\boldsymbol{\pi}_r \cdot \boldsymbol{\gamma})] \langle \mathbf{r} | (\mathcal{M} - v_F^2\boldsymbol{\pi}^2 - ieB_\perp v_F^2\gamma^1\gamma^2)^{-1} | \mathbf{r}' \rangle, \tag{A2}$$

where the matrices W and \mathcal{M} are

$$W = (\omega + \mu_s)\gamma^0 + i\tilde{\mu}_s\gamma^1\gamma^2 - i\Delta_s\gamma^0\gamma^1\gamma^2 + \tilde{\Delta}_s, \quad (\text{A3})$$

$$\mathcal{M} = (\omega + \mu_s + i\tilde{\mu}_s\gamma^0\gamma^1\gamma^2)^2 - (\tilde{\Delta}_s - i\Delta_s\gamma^0\gamma^1\gamma^2)^2. \quad (\text{A4})$$

The operator $\boldsymbol{\pi}^2$ has well known eigenvalues $(2n+1)|eB_\perp|$ with $n = 0, 1, 2, \dots$ and its normalized wave functions in the Landau gauge $\mathbf{A} = (0, B_\perp x)$ are

$$\psi_{np}(\mathbf{r}) = \frac{1}{\sqrt{2\pi l}} \frac{1}{\sqrt{2^n n! \sqrt{\pi}}} H_n\left(\frac{x}{l} + pl\right) e^{-\frac{1}{2l^2}(x+pl)^2} e^{ipy}, \quad (\text{A5})$$

where $H_n(x)$ are the Hermite polynomials and $l = \sqrt{\hbar c/|eB_\perp|}$ is the magnetic length. These wave functions satisfy the conditions of normalizability

$$\int d^2r \psi_{np}^*(\mathbf{r}) \psi_{n'p'}(\mathbf{r}) = \delta_{nn'} \delta(p-p'), \quad (\text{A6})$$

and completeness

$$\sum_{n=0}^{\infty} \int_{-\infty}^{\infty} dp \psi_{np}^*(\mathbf{r}) \psi_{np}(\mathbf{r}') = \delta(\mathbf{r} - \mathbf{r}'). \quad (\text{A7})$$

Using the spectral expansion of the unit operator (A7), we can write

$$\begin{aligned} \langle \mathbf{r} | (\mathcal{M} - v_F^2 \boldsymbol{\pi}^2 - ieB_\perp v_F^2 \gamma^1 \gamma^2)^{-1} | \mathbf{r}' \rangle &= \frac{1}{2\pi l^2} \exp\left(-\frac{(\mathbf{r} - \mathbf{r}')^2}{4l^2} - i\frac{(x+x')(y-y')}{2l^2}\right) \\ &\times \sum_{n=0}^{\infty} \frac{1}{\mathcal{M} - (2n+1)v_F^2|eB_\perp| - iv_F^2 eB_\perp \gamma^1 \gamma^2} L_n\left(\frac{(\mathbf{r} - \mathbf{r}')^2}{2l^2}\right), \end{aligned} \quad (\text{A8})$$

where we integrated over the quantum number p by making use of the formula 7.378 in Ref. 53,

$$\int_{-\infty}^{\infty} e^{-x^2} H_m(x+y) H_n(x+z) dx = 2^n \pi^{1/2} m! z^{n-m} L_m^{n-m}(-2yz), \quad (\text{A9})$$

assuming $m \leq n$. Here L_n^α are the generalized Laguerre polynomials, and $L_n \equiv L_n^0$. The matrix $iv_F^2 eB_\perp \gamma^1 \gamma^2$ has eigenvalues $\pm v_F^2 |eB_\perp|$, and thus one can write

$$\frac{L_n(\xi)}{\mathcal{M} - (2n+1)v_F^2|eB_\perp| - iv_F^2 eB_\perp \gamma^1 \gamma^2} = \frac{\mathcal{P}_- L_n(\xi)}{\mathcal{M} - (2n+1)v_F^2|eB_\perp| + v_F^2|eB_\perp|} + \frac{\mathcal{P}_+ L_n(\xi)}{\mathcal{M} - (2n+1)v_F^2|eB_\perp| - v_F^2|eB_\perp|}, \quad (\text{A10})$$

where the variable ξ and the projectors \mathcal{P}_\pm are

$$\xi = \frac{(\mathbf{r} - \mathbf{r}')^2}{2l^2}, \quad (\text{A11})$$

$$\mathcal{P}_\pm = \frac{1}{2} [1 \pm i\gamma^1 \gamma^2 \text{sign}(eB_\perp)]. \quad (\text{A12})$$

Now, by redefining $n \rightarrow n-1$ in the second term in Eq. (A10), equality (A8) can be rewritten as

$$\langle \mathbf{r} | [\mathcal{M} - v_F^2 \boldsymbol{\pi}^2 - ieB_\perp v_F^2 \gamma^1 \gamma^2]^{-1} | \mathbf{r}' \rangle = \frac{1}{2\pi l^2} e^{i\Phi(\mathbf{r}, \mathbf{r}')} e^{-\xi/2} \sum_{n=0}^{\infty} \frac{\mathcal{P}_- L_n(\xi) + \mathcal{P}_+ L_{n-1}(\xi)}{\mathcal{M} - 2nv_F^2|eB_\perp|}, \quad (\text{A13})$$

where $L_{-1} \equiv 0$ by definition and the phase

$$\Phi(\mathbf{r}, \mathbf{r}') = -\frac{(x+x')(y-y')}{2l^2} = -e \int_{\mathbf{r}'}^{\mathbf{r}} dz_i A_i(z) \quad (\text{A14})$$

appears because in the presence of a constant magnetic field, the commutative group of translations is replaced by the noncommutative group of magnetic translations⁵⁴ (note that the integration in Eq. (A14) is taken along the straight line). This implies that it has a universal character. By noting that

$$\pi_x e^{i\Phi} = e^{i\Phi} \left(-i\partial_x - \frac{y-y'}{2l^2} \right), \quad (\text{A15})$$

$$\pi_y e^{i\Phi} = e^{i\Phi} \left(-i\partial_y + \frac{x-x'}{2l^2} \right), \quad (\text{A16})$$

we see that propagator (A2) can be presented in the form of a product of the phase factor and a translation invariant part $\bar{G}_s(\omega; \mathbf{r} - \mathbf{r}')$,

$$G_s(\omega; \mathbf{r}, \mathbf{r}') = e^{i\Phi(\mathbf{r}, \mathbf{r}')} \bar{G}_s(\omega; \mathbf{r} - \mathbf{r}'), \quad (\text{A17})$$

where

$$\bar{G}_s(\omega; \mathbf{r} - \mathbf{r}') = i \left[W - v_F \gamma^1 \left(-i\partial_x - \frac{y-y'}{2l^2} \right) - v_F \gamma^2 \left(-i\partial_y + \frac{x-x'}{2l^2} \right) \right] \frac{e^{-\xi/2}}{2\pi l^2} \sum_{n=0}^{\infty} \frac{\mathcal{P}_- L_n(\xi) + \mathcal{P}_+ L_{n-1}(\xi)}{\mathcal{M} - 2nv_F^2 |eB_{\perp}|}. \quad (\text{A18})$$

It is important to emphasize that the phase factor does not affect the gap equation (5) because the latter contains the full propagator only at $u' = u$.

The Fourier transform of the translation invariant part of propagator (A18) can be evaluated by first performing the integration over the angle,

$$\int_0^{2\pi} d\theta e^{ikr \cos \theta} = 2\pi J_0(kr), \quad (\text{A19})$$

where $J_0(x)$ is the Bessel function, and then using the formula 7.421.1 in Ref. 53,

$$\int_0^{\infty} x e^{-\frac{1}{2}\alpha x^2} L_n \left(\frac{1}{2}\beta x^2 \right) J_0(xy) dx = \frac{(\alpha - \beta)^n}{\alpha^{n+1}} e^{-\frac{1}{2\alpha}y^2} L_n \left(\frac{\beta y^2}{2\alpha(\beta - \alpha)} \right), \quad (\text{A20})$$

valid for $y > 0$ and $\text{Re } \alpha > 0$. The result is given by

$$\bar{G}_s(\omega, \mathbf{k}) = i e^{-k^2 l^2} \sum_{n=0}^{\infty} \frac{(-1)^n D_{ns}(\omega, \mathbf{k})}{\mathcal{M} - 2nv_F^2 |eB_{\perp}|}, \quad (\text{A21})$$

with

$$D_{ns}(\omega, \mathbf{k}) = 2W [\mathcal{P}_- L_n(2k^2 l^2) - \mathcal{P}_+ L_{n-1}(2k^2 l^2)] + 4v_F (\mathbf{k} \cdot \boldsymbol{\gamma}) L_{n-1}^1(2k^2 l^2), \quad L_{-1}^{\alpha} \equiv 0, \quad (\text{A22})$$

describing the n th Landau level contribution (compare with corresponding expression for the standard Dirac propagator in Ref. 28).

2. Equations for Dirac masses and chemical potentials

In order to derive Eqs. (19)–(22) for masses and chemical potentials, we need to know the full propagator at $u' = u$, $G_s(u, u')|_{u=u'} = \bar{G}_s(u, u)$. As follows from Eq. (A18), it is

$$G_s(u, u) = \int_{-\infty}^{\infty} \frac{d\omega}{2\pi} \bar{G}_s(\omega, 0) = \frac{i}{2\pi l^2} \sum_{n=0}^{\infty} \int_{-\infty}^{\infty} \frac{d\omega}{2\pi} W \frac{\mathcal{P}_- + \mathcal{P}_+ \theta(n-1)}{\mathcal{M} - 2nv_F^2 |eB_{\perp}|}. \quad (\text{A23})$$

In what follows, it is convenient to work with eigenvectors of the matrices $\gamma^1 \gamma^2$ and γ^0 . Since $(\gamma^1 \gamma^2)^2 = -1$, the eigenvectors $|s_{12}\rangle$ of the matrix $\gamma^1 \gamma^2$ correspond to imaginary eigenvalues $is_{12} = \pm i$, i.e.,

$$\gamma^1 \gamma^2 |s_{12}\rangle = is_{12} |s_{12}\rangle. \quad (\text{A24})$$

Similarly, since $(\gamma^0)^2 = 1$, the eigenvectors $|s_0\rangle$ of the matrix γ^0 correspond to eigenvalues $s_0 = \pm 1$, i.e.,

$$\gamma^0 |s_0\rangle = s_0 |s_0\rangle. \quad (\text{A25})$$

Because γ^0 and $\gamma^1\gamma^2$ commute, we can use states $|s_{12}s_0\rangle$ which are simultaneously eigenvectors of $\gamma^1\gamma^2$ and γ^0 with eigenvalues is_{12} and s_0 , respectively. The vectors $|s_{12}s_0\rangle$ form a complete basis. Therefore, any 4×4 matrix \mathcal{O} can be represented as

$$\mathcal{O} = \sum_{s'_{12}, s'_0, s_{12}, s_0} \mathcal{O}_{s'_{12}s'_0 s_{12}s_0} |s'_{12}s'_0\rangle \langle s_{12}s_0|. \quad (\text{A26})$$

Now, taking into account that propagator (A23) contains only the unit, γ^0 , $\gamma^1\gamma^2$, and $\gamma^0\gamma^1\gamma^2$ matrices [see Eqs. (A3) and (A4)], its expansion in the form (A26) has only diagonal terms with $s'_{12} = s_{12}$ and $s'_0 = s_0$. Therefore, we can rewrite it as follows:

$$G_s(u, u) = \frac{i}{4\pi l^2} \sum_{s_{12}, s_0} \int_{-\infty}^{\infty} \frac{d\omega}{2\pi} \sum_{n=0}^{\infty} \frac{(\omega + \mu_s - \tilde{\mu}_s s_{12} s_0) s_0 + \tilde{\Delta}_s + \Delta_s s_{12} s_0}{(\omega + \mu_s - \tilde{\mu}_s s_{12} s_0)^2 - (\tilde{\Delta}_s + \Delta_s s_{12} s_0)^2 - 2v_F^2 |eB_{\perp}| n} \times \{1 + s_{12} \text{sign}(eB_{\perp}) + [1 - s_{12} \text{sign}(eB_{\perp})] \theta(n-1)\} |s_{12}s_0\rangle \langle s_{12}s_0|. \quad (\text{A27})$$

The zeros of the denominator in the integrand define the dispersion relations for the Landau levels. In the case of $n \geq 1$, they are given by

$$\omega_{ns}^{(\sigma)} = -\mu_s + \sigma \tilde{\mu}_s \pm \sqrt{2v_F^2 |eB_{\perp}| n + (\tilde{\Delta}_s + \sigma \Delta_s)^2}, \quad (\text{A28})$$

where $\sigma \equiv s_{12}s_0$ (i.e., $\sigma = \pm 1$) and the two signs in front of the square root correspond to the energy levels above and below the Dirac point. The case of the LLL is special because the numerator in the $n = 0$ term in Eq. (A27) coincides with one of the zeros in the denominator. After taking this into account, we find the following dispersion relation:

$$\omega_s^{(\sigma)} = -\mu_s + \sigma [\tilde{\mu}_s \text{sign}(eB_{\perp}) + \tilde{\Delta}_s] + \Delta_s \text{sign}(eB_{\perp}). \quad (\text{A29})$$

Note that the parameter $\sigma = \pm 1$ in Eqs. (A28) and (A29) is connected with the eigenvalues of the diagonal pseudospin matrix $\gamma_3\gamma_5$ in Eq. (9). Indeed, from the expression $\gamma^5 = i\gamma^0\gamma^1\gamma^2\gamma^3$, one gets $\gamma^3\gamma^5 = i\gamma^0\gamma^1\gamma^2$, i.e., the eigenvalues of $\gamma^3\gamma^5$ are $-s_0s_{12}$. It is now easy to check for higher LLs that $\sigma = \pm 1$ in Eq. (A28) corresponds to the eigenvalues ∓ 1 of $\gamma^3\gamma^5$. On the other hand, as follows from Eq. (A21), $s_{12} = \text{sign}(eB_{\perp})$ on the LLL, and we find that in this case $\sigma = \pm 1$ corresponds to $\text{sign}(eB_{\perp}) \times (\mp 1)$, with ∓ 1 being the eigenvalues of $\gamma^3\gamma^5$.

Integrating over ω in Eq. (A27), we obtain

$$G_s(u, u) = \frac{1}{8\pi l^2} \sum_{s_{12}, s_0} \sum_{n=0}^{\infty} \left(-s_0 \text{sign}(\mu_s - \tilde{\mu}_s s_{12} s_0) \theta(|\mu_s - \tilde{\mu}_s s_{12} s_0| - E_{ns}^{\sigma}) + \frac{(\tilde{\Delta}_s + \Delta_s s_{12} s_0) \theta(E_{ns}^{\sigma} - |\mu_s - \tilde{\mu}_s s_{12} s_0|)}{E_{ns}^{\sigma}} \right) \times \{1 + s_{12} \text{sign}(eB_{\perp}) + [1 - s_{12} \text{sign}(eB_{\perp})] \theta(n-1)\} |s_{12}s_0\rangle \langle s_{12}s_0|, \quad (\text{A30})$$

where $E_{ns}^{\sigma} = \sqrt{2v_F^2 |eB_{\perp}| n + (\tilde{\Delta}_s + \sigma \Delta_s)^2}$.

Using this expression and the inverse bare and full propagators in Eqs. (4) and (13), we arrive at the following form of gap equation (5):

$$\begin{aligned} & -\mu_s s_0 + \tilde{\mu}_s s_{12} + \Delta_s s_{12} s_0 + \tilde{\Delta}_s = -\tilde{\mu}_s s_0 + A \sum_{n=0}^{\infty} \left[1 + s_{12} \text{sign}(eB_{\perp}) + (1 - s_{12} \text{sign}(eB_{\perp})) \theta(n-1) \right] \\ & \times \left[-s_0 \text{sign}(\mu_s - \tilde{\mu}_s s_{12} s_0) \theta(|\mu_s - \tilde{\mu}_s s_{12} s_0| - E_{ns}^{\sigma}) + \frac{(\tilde{\Delta}_s + \Delta_s s_{12} s_0) \theta(E_{ns}^{\sigma} - |\mu_s - \tilde{\mu}_s s_{12} s_0|)}{E_{ns}^{\sigma}} \right] \\ & - A s_0 \sum_{n=0}^{\infty} \sum_{s'=\pm} \sum_{s'_{12}, s'_0} \left[1 + s'_{12} \text{sign}(eB_{\perp}) + (1 - s'_{12} \text{sign}(eB_{\perp})) \theta(n-1) \right] \\ & \times \left[-s'_0 \text{sign}(\mu_{s'} - \tilde{\mu}_{s'} s'_{12} s'_0) \theta(|\mu_{s'} - \tilde{\mu}_{s'} s'_{12} s'_0| - E_{ns'}^{\sigma}) + \frac{(\tilde{\Delta}_{s'} + \Delta_{s'} s'_{12} s'_0) \theta(E_{ns'}^{\sigma} - |\mu_{s'} - \tilde{\mu}_{s'} s'_{12} s'_0|)}{E_{ns'}^{\sigma}} \right], \quad (\text{A31}) \end{aligned}$$

where $A \equiv G_{\text{int}}/(8\pi l^2)$. The last term on the right-hand side of Eq. (A31) proportional to s_0 is the Hartree contribution. Finally, multiplying (A31) by 1, $s_{12}s_0$, s_{12} , and s_0 , respectively, and taking the sum over s_{12} and s_0 , we obtain Eqs. (19)–(22).

APPENDIX B: ANALYTIC SOLUTIONS OF GAP EQUATION FOR LLL AT $T = 0$

In order to solve Eqs. (19)–(21) for Δ_s , $\tilde{\Delta}_s$, $\tilde{\mu}_s$ as functions of μ_s , note that these equations contain θ -functions whose arguments suggest that the following three cases have to be considered:

1. $|\mu_s \mp \tilde{\mu}_s| < |\tilde{\Delta}_s \pm \Delta_s|$;
2. $|\mu_s - \tilde{\mu}_s| > |\tilde{\Delta}_s + \Delta_s|$, $|\mu_s + \tilde{\mu}_s| < |\tilde{\Delta}_s - \Delta_s|$ or $|\mu_s - \tilde{\mu}_s| < |\tilde{\Delta}_s + \Delta_s|$, $|\mu_s + \tilde{\mu}_s| > |\tilde{\Delta}_s - \Delta_s|$;
3. $|\mu_s \mp \tilde{\mu}_s| > |\tilde{\Delta}_s \pm \Delta_s|$.

1. The first case

For $|\mu_s \mp \tilde{\mu}_s| < |\tilde{\Delta}_s \pm \Delta_s|$, the gap equations for Dirac masses take the form

$$\tilde{\Delta}_s + \Delta_s = A \sum_{n=0}^{\infty} \frac{\tilde{\Delta}_s + \Delta_s}{E_{ns}^+} [1 + \theta(n-1)], \quad (\text{B1})$$

$$\tilde{\Delta}_s - \Delta_s = A \sum_{n=0}^{\infty} \frac{\tilde{\Delta}_s - \Delta_s}{E_{ns}^-} [1 + \theta(n-1)]. \quad (\text{B2})$$

Equations for $\tilde{\Delta}_s + \Delta_s$ and $\tilde{\Delta}_s - \Delta_s$ are equivalent and since each equation admits both positive and negative solutions with the same absolute value, we have

$$\tilde{\Delta}_s + \Delta_s = \pm(\tilde{\Delta}_s - \Delta_s). \quad (\text{B3})$$

This implies that one of the following should be true

$$(a) \quad \Delta_s = 0, \quad \text{or} \quad (b) \quad \tilde{\Delta}_s = 0. \quad (\text{B4})$$

Then, the gap equation for the nonvanishing parameter $\tilde{\Delta}_s$ (or Δ_s) takes the form

$$\tilde{\Delta}_s = A \sum_{n=0}^{\infty} \frac{\tilde{\Delta}_s}{\sqrt{n\epsilon_B^2 + \tilde{\Delta}_s^2}} [1 + \theta(n-1)]. \quad (\text{B5})$$

Let us first consider the case (a) and show that Eq. (B5) can be equivalently represented in the following integral form:

$$\tilde{\Delta}_s = \frac{A\tilde{\Delta}_s}{\sqrt{\pi}} \int_{1/\Lambda^2}^{\infty} \frac{dy}{\sqrt{y}} e^{-y\tilde{\Delta}_s^2} \coth\left(\frac{\epsilon_B^2}{2}y\right), \quad (\text{B6})$$

where Λ is a high energy cut-off up to which the low-energy effective theory is valid. After taking into account the identity $\coth(\epsilon_B^2 y/2) = 1 + 2 \sum_{n=1}^{\infty} e^{-yn\epsilon_B^2}$, we can integrate over y in Eq. (B6) by using the following table integral:

$$\int_{1/\Lambda^2}^{\infty} \frac{dy}{\sqrt{y}} e^{-y(n\epsilon_B^2 + \tilde{\Delta}_s^2)} \simeq \int_0^{\infty} \frac{dy}{\sqrt{y}} e^{-y(n\epsilon_B^2 + \tilde{\Delta}_s^2)} = \frac{\sqrt{\pi}}{\sqrt{n\epsilon_B^2 + \tilde{\Delta}_s^2}}, \quad (\text{B7})$$

where we replaced the lower limit of integration by 0 because the integral is convergent for $y \rightarrow 0$. Therefore, up to corrections suppressed by the inverse powers of cutoff Λ , Eq. (B6) is indeed equivalent to Eq. (B5). Then, by using the same approach as in the second paper in Ref. 28, we expand the result on the right hand side of Eq. (B6) in powers of $1/\Lambda$ and arrive at the following form of the gap equation:

$$\tilde{\Delta}_s = \lambda\tilde{\Delta}_s + A + \frac{2A\tilde{\Delta}_s}{\epsilon_B} \zeta\left(\frac{1}{2}, 1 + \frac{\tilde{\Delta}_s^2}{\epsilon_B^2}\right) + O\left(\lambda \frac{\tilde{\Delta}_s^2}{\Lambda^2}\right), \quad (\text{B8})$$

where $\lambda \equiv 4A\Lambda/(\sqrt{\pi}\epsilon_B^2) = G_{\text{int}}\Lambda/(4\pi^{3/2}\hbar^2v_F^2)$ is the dimensionless coupling constant and $\zeta(z, q)$ is the generalized Riemann zeta function.⁵³ By assuming that the gap $\tilde{\Delta}_s$ is much smaller than the Landau energy scale ϵ_B , we find the solution in an analytical form,

$$\tilde{\Delta}_s = M \equiv \frac{A}{1-\lambda}, \quad \tilde{\mu}_s = A s_{\perp}. \quad (\text{B9})$$

Here, in order to get the result for the chemical potential $\tilde{\mu}_s$ we used Eq. (21). It is easy to check that the gap equation also has another solution, which is obtained from Eq. (B9) by replacing $\tilde{\Delta}_s$ and $\tilde{\mu}_s$ with $-\tilde{\Delta}_s$ and $-\tilde{\mu}_s$. However, the second solution is equivalent to that in Eq. (B9): one can see this from dispersion relations (17), (18) by transforming $\sigma \rightarrow -\sigma$ there. In other words, these solutions describe two degenerate ground states connected by a $Z_{2s} [\subset SU(2)_s]$ symmetry transformation.

Turning to case (b) in Eq. (B4), we have $\tilde{\Delta}_s = 0$,

$$\Delta_s = \pm M \quad \text{and} \quad \tilde{\mu}_s = 0, \quad (\text{B10})$$

where the last relation follows from Eq. (21).

Finally, we would like to note that by analyzing the inequalities $|\mu_s \mp \tilde{\mu}_s| < |\tilde{\Delta}_s \pm \Delta_s|$, one can show that solution (B9) with a triplet Dirac mass exists for

$$|\mu_s| < M - A \quad (\text{B11})$$

and solution (B10) with a singlet Dirac mass exists for

$$|\mu_s| < M. \quad (\text{B12})$$

2. The second case

There are two possibilities $|\mu_s + \tilde{\mu}_s| < |\tilde{\Delta}_s - \Delta_s|$, $|\mu_s - \tilde{\mu}_s| > |\tilde{\Delta}_s + \Delta_s|$ or $|\mu_s - \tilde{\mu}_s| < |\tilde{\Delta}_s + \Delta_s|$, $|\mu_s + \tilde{\mu}_s| > |\tilde{\Delta}_s - \Delta_s|$. In the first case, the equations for Dirac masses take the form

$$\tilde{\Delta}_s + \Delta_s = -A s_{\perp} \text{sign}(\mu_s - \tilde{\mu}_s) + 2A \sum_{n=1}^{\infty} \frac{\tilde{\Delta}_s + \Delta_s}{E_{ns}^+}, \quad (\text{B13})$$

$$\tilde{\Delta}_s - \Delta_s = A \sum_{n=0}^{\infty} \frac{\tilde{\Delta}_s - \Delta_s}{E_{ns}^-} [1 + \theta(n-1)], \quad (\text{B14})$$

where $s_{\perp} \equiv \text{sgn}(eB_{\perp})$. While the equation for $\tilde{\Delta}_s - \Delta_s$ coincides with Eq. (B2), the equation for $\tilde{\Delta}_s + \Delta_s$ is slightly different from its counterpart in Eq. (B1). Unlike Eq. (B1), the above equation for $\tilde{\Delta}_s + \Delta_s$ does not contain the sign factor $\text{sign}(\tilde{\Delta}_s + \Delta_s)$ in the LLL contribution. The absence of such a factor in Eq. (B13) means that the sign of the LLL contribution is fixed for a given set of values of μ_s , $\tilde{\mu}_s$, and eB_{\perp} . In turn, this implies that Eq. (B13) [unlike the gap equation (B1)] has only one solution whose sign is correlated with the sign of the LLL contribution. In order to prove this, let us consider the following equation:

$$x = -A + 2A \sum_{n=1}^{\infty} \frac{x}{\sqrt{n\epsilon_B^2 + x^2}}. \quad (\text{B15})$$

By taking x negative, we see that its absolute value $|x|$ satisfies an equation that is equivalent to the equation for positive $\tilde{\Delta}_s$ that follows from Eq. (B5). Therefore, the solution for $|x|$ coincides with the positive solution for $\tilde{\Delta}_s$ in (B9). We can also show that Eq. (B15) does not have a solution for positive x by using the integral form of (B15), i.e.,

$$1 = \frac{A}{\sqrt{\pi}} \int_{1/\Lambda^2}^{\infty} \frac{dy}{\sqrt{y}} e^{-yx^2} \left[\coth\left(\frac{\epsilon_B^2}{2}y\right) - 2 \right], \quad (\text{B16})$$

where the term -2 is subtracted in order to get the negative LLL contribution as in (B15) [cf. Eq. (B6)].

In order to prove that Eq. (B16) does not have solution, we will use the fact that Eq. (B6) does not have a nontrivial solution for $B_{\perp} \rightarrow 0$ in the case when the coupling constant G_{int} is subcritical, i.e., $G_{\text{int}} < 4\pi^{3/2}v_F^2\hbar^2/\Lambda$,

or equivalently $\lambda < 1$. Note that the coupling constant should indeed be subcritical because, as we know from experiment, there is no gap generation at $B_\perp = 0$. It is not difficult to prove that the right hand side of Eq. (B16) is less than λ after taking into account that $t(\coth t - 2) < 1$ for $t > 0$. Then we conclude that Eq. (B16) does not have a solution for a subcritical coupling constant $\lambda < 1$. As for Eq. (B15), it has only one solution which, in fact, coincides with the solution for $\tilde{\Delta}_s$ in (B9) times -1 . Thus, the solutions of Eqs. (B13) and (B14) are

$$\tilde{\Delta}_s + \Delta_s = -\text{sign}(\mu_s - \tilde{\mu}_s) s_\perp M \quad (\text{B17})$$

and

$$\tilde{\Delta}_s - \Delta_s = \pm(\tilde{\Delta}_s + \Delta_s). \quad (\text{B18})$$

From the fact that the solutions for $\tilde{\Delta}_s + \Delta_s$ and $\tilde{\Delta}_s - \Delta_s$ have the same absolute value, we conclude that either $\tilde{\Delta}_s \neq 0, \Delta_s = 0$ or vice versa $\Delta_s \neq 0, \tilde{\Delta}_s = 0$ depending on the sign in Eq. (B18). If Eq. (B16) had solution, there would exist solutions with both nonzero $\tilde{\Delta}_s$ and Δ_s .

Further, solution of Eq. (21) for $\tilde{\mu}_s$ in the case under consideration takes the form

$$\tilde{\mu}_s = \frac{A}{2} [-\text{sign}(\mu_s - \tilde{\mu}_s) + \text{sign}(\tilde{\Delta}_s - \Delta_s) s_\perp]. \quad (\text{B19})$$

Using (B17), it is easy to check that for the plus sign in (B18) (when $\tilde{\Delta}_s \neq 0$ and $\Delta_s = 0$) $\tilde{\mu}_s = A \text{sign}(\tilde{\Delta}_s) s_\perp$ and for the sign minus in (B18) (when $\tilde{\Delta}_s = 0$ and $\Delta_s \neq 0$) $\tilde{\mu}_s = 0$. In the latter case, the assumed inequalities $|\mu_s + \tilde{\mu}_s| < |\tilde{\Delta}_s - \Delta_s|$ and $|\mu_s - \tilde{\mu}_s| > |\tilde{\Delta}_s + \Delta_s|$ cannot be satisfied, therefore, only solution with triplet Dirac mass $\tilde{\Delta}_s$ is realized

$$\tilde{\Delta}_s = -s_\perp \text{sign}(\mu_s - \tilde{\mu}_s) M, \quad \Delta_s = 0, \quad \tilde{\mu}_s = A \text{sign}(\tilde{\Delta}_s) s_\perp. \quad (\text{B20})$$

In the other case $|\mu_s + \tilde{\mu}_s| > |\tilde{\Delta}_s - \Delta_s|$ and $|\mu_s - \tilde{\mu}_s| < |\tilde{\Delta}_s + \Delta_s|$, we find the following solution:

$$\tilde{\Delta}_s = s_\perp \text{sign}(\mu_s + \tilde{\mu}_s) M, \quad \Delta_s = 0, \quad \tilde{\mu}_s = A \text{sign}(\tilde{\Delta}_s) s_\perp. \quad (\text{B21})$$

One can show that it is possible to join solutions (B20) and (B21) into one solution with triplet Dirac mass

$$\tilde{\Delta}_s = M, \quad \tilde{\mu}_s = A s_\perp, \quad \Delta_s = 0, \quad (\text{B22})$$

which exists for

$$M - A < |\mu_s| < M + A. \quad (\text{B23})$$

In fact, like in the previous subsection, there is another solution, with $\tilde{\Delta}_s, \tilde{\mu}_s$ replaced by $-\tilde{\Delta}_s, -\tilde{\mu}_s$. However, such a solution is equivalent to solution (B22) by a $SU(2)_s$ (or Z_{2s}) symmetry transformation.

3. The third case

For $|\mu_s \pm \tilde{\mu}_s| > |\tilde{\Delta}_s \mp \Delta_s|$, the equations for Dirac masses take the form

$$\tilde{\Delta}_s + \Delta_s = -A \text{sign}(\mu_s - \tilde{\mu}_s) s_\perp + 2A \sum_{n=1}^{\infty} \frac{\tilde{\Delta}_s + \Delta_s}{E_{ns}^+}, \quad (\text{B24})$$

$$\tilde{\Delta}_s - \Delta_s = A \text{sign}(\mu_s + \tilde{\mu}_s) s_\perp + 2A \sum_{n=1}^{\infty} \frac{\tilde{\Delta}_s - \Delta_s}{E_{ns}^-}. \quad (\text{B25})$$

Solutions of Eqs. (B24) and (B25) are

$$\tilde{\Delta}_s + \Delta_s = -s_\perp \text{sign}(\mu_s - \tilde{\mu}_s) M, \quad (\text{B26})$$

$$\tilde{\Delta}_s - \Delta_s = s_\perp \text{sign}(\mu_s + \tilde{\mu}_s) M. \quad (\text{B27})$$

Using these solutions and taking into account the inequalities $|\mu_s \pm \tilde{\mu}_s| > |\tilde{\Delta}_s \mp \Delta_s|$, one can check that Eq. (21) has only the trivial solution. Then it follows from Eqs. (B26) and (B27) that

$$\Delta_s = -s_\perp \text{sign}(\mu_s) M, \quad \tilde{\Delta}_s = \tilde{\mu}_s = 0. \quad (\text{B28})$$

Taking into account the assumed inequalities $|\mu_s \pm \tilde{\mu}_s| > |\tilde{\Delta}_s \mp \Delta_s|$, we find that this solution with singlet Dirac mass exists for

$$|\mu_s| > M. \quad (\text{B29})$$

4. Final solutions for Δ_s , $\tilde{\Delta}_s$, and $\tilde{\mu}_s$ as functions of μ_s

Using the results derived above and calculating the quantity X_s in Eq. (25) (which is needed for solving the equation for μ_s), we obtain the following three distinct solutions.

- Solution I (triplet Dirac mass). By joining the two solutions of the same type in Eqs. (B9) and (B22), considered in Subsecs. B 1 and B 2, respectively, we arrive at the following solution:

$$\tilde{\Delta}_s = M, \quad \tilde{\mu}_s = A s_\perp, \quad \Delta_s = 0, \quad X_s = 0 \quad (\text{B30})$$

which exists over the combined range of validity $|\mu_s| < M + A$. Let us mention that there is also another solution, in which $\tilde{\Delta}_s$ and $\tilde{\mu}_s$ are replaced by $-\tilde{\Delta}_s$ and $-\tilde{\mu}_s$, respectively. However, this second solution is equivalent to that in Eq. (B30): one can see this from dispersion relations (17), (18) by transforming $\sigma \rightarrow -\sigma$ there. In other words, the two solutions are related to two degenerate ground states connected by a $SU(2)_s$ (or Z_{2s}) flavor transformation.

- Solution II (singlet Dirac mass). This is one of the two solutions in Eq. (B10) from Subsec. B 1 that corresponds to a particular choice of the sign for the singlet Dirac mass,

$$\Delta_s = s_\perp \text{sign}(\mu_s) M, \quad \tilde{\Delta}_s = \tilde{\mu}_s = 0, \quad X_s = 4A \text{sign}(\mu_s). \quad (\text{B31})$$

It exists for $|\mu_s| < M$.

- Solution III (singlet Dirac mass). This combines the remaining solution in Eq. (B10) from Subsec. B 1 with solution (B28) in Subsec. B 3 to give

$$\Delta_s = -s_\perp \text{sign}(\mu_s) M, \quad \tilde{\Delta}_s = \tilde{\mu}_s = 0, \quad X_s = -4A \text{sign}(\mu_s). \quad (\text{B32})$$

This solution exists for *all* values of μ_s .

A noticeable point is that unlike the case with a triplet Dirac mass, the solutions II and III, with a different sign for a singlet Dirac mass, are different. This in particular can be seen from dispersion relation (18). This feature is directly connected with the fact that while the triplet mass is even under time reversal \mathcal{T} , the singlet mass is \mathcal{T} -odd. The latter is in turn connected with the fact that $\Delta \propto s_\perp = \text{sign}(B_\perp)$ (recall that a magnetic field is also \mathcal{T} -odd).

Let us also emphasize that the expressions for Dirac masses in solutions I, II, and III are valid only for $\lambda < 1$: in the supercritical regime, with $\lambda > 1$, a Dirac mass $\tilde{\Delta}$ is generated even with no magnetic field.²⁸ Experiments clearly show that the subcritical regime, with $\lambda < 1$, takes place in graphene.^{2,3} As argued in Sec. IV in the main text, realistic values for λ in this model are $\lambda \lesssim 0.2$.

5. Including both spin up and spin down states

In the previous subsection, the solutions for masses and chemical potentials were found for a fixed spin, treating the electron chemical potential μ_s as a free parameter. Here we will describe full solutions, including both spin up and spin down states. For this purpose, we need to solve Eq. (22) for the chemical potentials μ_\pm . Since the X term in that equation contains both spin up and spin down contributions, the equations for μ_+ and μ_- are now coupled and have to be solved together. As a result, the full chemical potentials μ_\pm will be expressed through the bare electron chemical potentials $\bar{\mu}_\pm = \mu_0 \mp Z$.

At a fixed spin, there are 3 different types of solutions for masses and $\tilde{\mu}_s$ described in Subsec. B 4. Since we can choose any of them for each spin, there are nine possible types and, therefore, nine systems of coupled equations for μ_+ and μ_- . Fortunately, noting that the solutions for the types II-I, III-I, and III-II can be obtained from those for I-II, I-III, and II-III by interchanging the spin subscripts $+$ and $-$ in the latter, this number can be reduced to six coupled systems. We will analyze them below case by case.

It will be convenient to separate these systems of equations into 3 groups. The first group includes one system, I-I. This is the simplest case with triplet masses $\tilde{\Delta}_\pm$ for both spins, when the Hartree diagram does not contribute in the equations for μ_\pm . The second group consists of hybrid systems I-II and I-III, where while fields with spin up have a triplet mass $\tilde{\Delta}_+$, the fields with spin down have a singlet mass Δ_- . The third group, II-II, II-III, and III-III, consists of solutions with singlet masses Δ_\pm only.

In the analysis, it will be assumed that the Zeeman energy $Z < A$. As argued in Sec. IV, this assumption is valid for magnetic fields $|B_\perp| \lesssim 45T$ used in experiments.^{13,14}

- *The first group: Triplet Dirac masses*

- I-I. In this simplest case, using Eq. (B30), we immediately find from Eq. (22) that $\mu_{\pm} = \bar{\mu}_{\pm}$ and the solution is:

$$\begin{aligned}\tilde{\Delta}_+ &= M, & \tilde{\mu}_+ &= A s_{\perp}, & \mu_+ &= \bar{\mu}_+, & \Delta_+ &= 0, \\ \tilde{\Delta}_- &= M, & \tilde{\mu}_- &= A s_{\perp}, & \mu_- &= \bar{\mu}_-, & \Delta_- &= 0.\end{aligned}\tag{B33}$$

It exists for

$$|\bar{\mu}_+| < A + M, \quad |\bar{\mu}_-| < A + M.\tag{B34}$$

The physical meaning of these constraints is clear: they imply that the LLL is neither completely filled nor empty.

- *The second group: Hybrid solutions*

- I-II. By using Eqs. (B30) and (B31), we analyze the system of two equations (22) for μ_+ and μ_- and find that the solution

$$\begin{aligned}\tilde{\Delta}_+ &= M, & \tilde{\mu}_+ &= A s_{\perp}, & \mu_+ &= \bar{\mu}_+ - 4A \text{sign}(\bar{\mu}_+), & \Delta_+ &= 0, \\ \tilde{\Delta}_- &= \tilde{\mu}_- = 0, & \mu_- &= \bar{\mu}_- - 3A \text{sign}(\bar{\mu}_-), & \Delta_- &= -s_{\perp} \text{sign}(\bar{\mu}_-) M\end{aligned}\tag{B35}$$

exists for

$$3A - M < |\bar{\mu}_+| < 5A + M, \quad 3A - M < |\bar{\mu}_-| < 3A, \quad \text{sign}(\bar{\mu}_+) \text{sign}(\bar{\mu}_-) > 0.\tag{B36}$$

- I-III. In this case, using Eqs. (22), (B30), and (B32), we find the solution

$$\begin{aligned}\tilde{\Delta}_+ &= M, & \tilde{\mu}_+ &= A s_{\perp}, & \mu_+ &= \bar{\mu}_+ - 4A \text{sign}(\bar{\mu}_+), & \Delta_+ &= 0, \\ \tilde{\Delta}_- &= \tilde{\mu}_- = 0, & \mu_- &= \bar{\mu}_- - 3A \text{sign}(\bar{\mu}_-), & \Delta_- &= -s_{\perp} \text{sign}(\bar{\mu}_-) M,\end{aligned}\tag{B37}$$

which exists for

$$3A - M < |\bar{\mu}_+| < 5A + M, \quad |\bar{\mu}_-| > 3A, \quad \text{sign}(\bar{\mu}_+) \text{sign}(\bar{\mu}_-) > 0.\tag{B38}$$

- *The third group: Singlet Dirac masses*

- II-II. Using Eq. (B31) and analyzing equations (22) for μ_+ and μ_- , we find the solution

$$\begin{aligned}\tilde{\Delta}_+ &= \tilde{\mu}_+ = 0, & \mu_+ &= \bar{\mu}_+ - 7A \text{sign}(\bar{\mu}_+), & \Delta_+ &= -s_{\perp} \text{sign}(\bar{\mu}_+) M, \\ \tilde{\Delta}_- &= \tilde{\mu}_- = 0, & \mu_- &= \bar{\mu}_- - 7A \text{sign}(\bar{\mu}_-), & \Delta_- &= -s_{\perp} \text{sign}(\bar{\mu}_-) M,\end{aligned}\tag{B39}$$

which exists for

$$7A - M < |\bar{\mu}_+| < 7A, \quad 7A - M < |\bar{\mu}_-| < 7A, \quad \text{sign}(\bar{\mu}_+) \text{sign}(\bar{\mu}_-) > 0.\tag{B40}$$

[Formally, there is also another solution,

$$\begin{aligned}\tilde{\Delta}_+ &= \tilde{\mu}_+ = 0, & \mu_+ &= \bar{\mu}_+ - A \text{sign}(\bar{\mu}_+), & \Delta_+ &= s_{\perp} \text{sign}(\bar{\mu}_+) M, \\ \tilde{\Delta}_- &= \tilde{\mu}_- = 0, & \mu_- &= \bar{\mu}_- - A \text{sign}(\bar{\mu}_-), & \Delta_- &= s_{\perp} \text{sign}(\bar{\mu}_-) M,\end{aligned}\tag{B41}$$

which exists for

$$A < |\bar{\mu}_+| < A + M, \quad A < |\bar{\mu}_-| < A + M, \quad \text{sign}(\bar{\mu}_+) \text{sign}(\bar{\mu}_-) < 0.\tag{B42}$$

However, because of the latter inequalities, it is easy to check that this solution does not satisfy the condition $Z < A$ and therefore is not realized for magnetic fields $|B_{\perp}| \lesssim 45T$.]

◦ II-III. As in the previous case, there are two solutions. The first solution, II-III-1,

$$\begin{aligned}\tilde{\Delta}_+ = \tilde{\mu}_+ = 0, & \quad \mu_+ = \bar{\mu}_+ - A \operatorname{sign}(\bar{\mu}_+), & \quad \Delta_+ = s_\perp \operatorname{sign}(\bar{\mu}_+) M, \\ \tilde{\Delta}_- = \tilde{\mu}_- = 0, & \quad \mu_- = \bar{\mu}_- + A \operatorname{sign}(\bar{\mu}_+), & \quad \Delta_- = -s_\perp \operatorname{sign}(\bar{\mu}_+) M\end{aligned}\tag{B43}$$

exists for

$$A < |\bar{\mu}_+| < A + M, \quad \bar{\mu}_- \operatorname{sign}(\bar{\mu}_+) > -A.\tag{B44}$$

The second solution, II-III-2,

$$\begin{aligned}\tilde{\Delta}_+ = \tilde{\mu}_+ = 0, & \quad \mu_+ = \bar{\mu}_+ - 7A \operatorname{sign}(\bar{\mu}_+), & \quad \Delta_+ = -s_\perp \operatorname{sign}(\bar{\mu}_+) M, \\ \tilde{\Delta}_- = \tilde{\mu}_- = 0, & \quad \mu_- = \bar{\mu}_- - 7A \operatorname{sign}(\bar{\mu}_-), & \quad \Delta_- = -s_\perp \operatorname{sign}(\bar{\mu}_-) M\end{aligned}\tag{B45}$$

exists for

$$7A - M < |\bar{\mu}_+| < 7A, \quad \bar{\mu}_- \operatorname{sign}(\bar{\mu}_+) > 7A.\tag{B46}$$

◦ III-III. There are three solutions in this case. The first solution, III-III-1,

$$\begin{aligned}\tilde{\Delta}_+ = \tilde{\mu}_+ = 0, & \quad \mu_+ = \bar{\mu}_+ - 7A \operatorname{sign}(\bar{\mu}_+), & \quad \Delta_+ = -s_\perp \operatorname{sign}(\bar{\mu}_+) M, \\ \tilde{\Delta}_- = \tilde{\mu}_- = 0, & \quad \mu_- = \bar{\mu}_- - 7A \operatorname{sign}(\bar{\mu}_-), & \quad \Delta_- = -s_\perp \operatorname{sign}(\bar{\mu}_-) M\end{aligned}\tag{B47}$$

exists for

$$|\bar{\mu}_+| > 7A, \quad |\bar{\mu}_-| > 7A, \quad \operatorname{sign}(\bar{\mu}_+) \operatorname{sign}(\bar{\mu}_-) > 0.\tag{B48}$$

The second solution, III-III-2, is

$$\begin{aligned}\tilde{\Delta}_+ = \tilde{\mu}_+ = 0, & \quad \mu_+ = \bar{\mu}_+ + A, & \quad \Delta_+ = -s_\perp M, \\ \tilde{\Delta}_- = \tilde{\mu}_- = 0, & \quad \mu_- = \bar{\mu}_- - A, & \quad \Delta_- = s_\perp M.\end{aligned}\tag{B49}$$

It is realized for

$$\bar{\mu}_+ > -A, \quad \bar{\mu}_- < A.\tag{B50}$$

The third solution, III-III-3,

$$\begin{aligned}\tilde{\Delta}_+ = \tilde{\mu}_+ = 0, & \quad \mu_+ = \bar{\mu}_+ - A, & \quad \Delta_+ = s_\perp M, \\ \tilde{\Delta}_- = \tilde{\mu}_- = 0, & \quad \mu_- = \bar{\mu}_- + A, & \quad \Delta_- = -s_\perp M\end{aligned}\tag{B51}$$

takes place for

$$\bar{\mu}_+ < A, \quad \bar{\mu}_- > -A,\tag{B52}$$

i.e., in fact, it is obtained from the second solution by interchanging spin subscripts + and -.

6. Dependence of solutions on electron chemical potential μ_0 and free energy density of their ground states

The process of filling LLs is described by varying the electron chemical potential μ_0 . Therefore, it will be convenient to express the intervals of the existence of the solutions found in the previous subsection in terms of μ_0 . Henceforth we will consider $\mu_0 \geq 0$. (Dynamics with negative μ_0 is related by electron-hole symmetry and will not be discussed separately.)

Some intermediate results of the analysis in this subsection will depend on whether the inequality $M > 2Z$ or $M < 2Z$ is satisfied. We will consider both these cases and indicate explicitly which inequality is satisfied for a particular solution. If nothing will be said, this means that the corresponding results are valid in both cases. Fortunately, the final results do not depend on whether $M > 2Z$ or $M < 2Z$.

TABLE I: Intervals of the existence of solutions, relevant for the dynamics in the LLL at $T = 0$.

	$M > 2Z$	$M < 2Z$
I-I	$0 \leq \mu_0 < M + A - Z$	$0 \leq \mu_0 < M + A - Z$
I-II	$M + A + Z < \mu_0 < 3A - Z$	no solution
II-I	$3A - M + Z < \mu_0 < 3A + Z$	$3A - M + Z < \mu_0 < 3A + Z$
I-III	$3A - Z < \mu_0 < 5A + M + Z$	$3A - M + Z < \mu_0 < 5A + M + Z$
III-I	$3A + Z < \mu_0 < 5A + M - Z$	$3A + Z < \mu_0 < 5A + M - Z$
II-II	$7A - M + Z < \mu_0 < 7A - Z$	no solution
II-III-1	$A + Z < \mu_0 < M + A + Z$	$A + Z < \mu_0 < M + A + Z$
II-III-2	$7A - Z < \mu_0 < 7A + Z$	$7A - M + Z < \mu_0 < 7A + Z$
III-II-1	$A - Z < \mu_0 < M + A - Z$	$A - Z < \mu_0 < M + A - Z$
III-II-2	no solution	no solution
III-III-1	$7A + Z < \mu_0$	$7A + Z < \mu_0$
III-III-2	$0 < \mu_0 < A - Z$	$0 < \mu_0 < A - Z$
III-III-3	$0 < \mu_0 < A + Z$	$0 < \mu_0 < A + Z$

TABLE II: The list of solutions that coexist in a set of non-overlapping intervals of μ_0 , relevant for the dynamics in the LLL at $T = 0$. The solutions with the lowest free energy density are marked by stars.

#	Interval	$M > 2Z$	$M < 2Z$
1	$0 \leq \mu_0 < A - Z$	I-I, III-III-2, III-III-3*	I-I, III-III-2, III-III-3*
2	$A - Z < \mu_0 < A + Z$	I-I, III-II, III-III-3*	I-I, III-II, III-III-3*
3	$A + Z < \mu_0 < M + A - Z$	I-I, III-II, II-III-1*	I-I, III-II, II-III-1*
4	$M + A - Z < \mu_0 < 3A - M + Z$	II-III-1*	II-III-1*
5	$3A - M + Z < \mu_0 < 2A + Z$	I-II, II-I, II-III-1*	I-III, II-I, II-III-1*
6	$2A + Z < \mu_0 < M + A + Z$	I-II*, II-I, II-III-1	I-III*, II-I, II-III-1
7	$M + A + Z < \mu_0 < 3A - Z$	I-II*, II-I	I-III*, II-I
8	$3A - Z < \mu_0 < 3A + Z$	I-III*, II-I	I-III*, II-I
9	$3A + Z < \mu_0 < 5A + M - Z$	I-III*, III-I	I-III*, III-I
10	$5A + M - Z < \mu_0 < 7A - M + Z$	I-III*	I-III*
11	$7A - M + Z < \mu_0 < 6A + Z$	I-III*, II-II	I-III*, II-III-2
12	$6A + Z < \mu_0 < 5A + M + Z$	I-III, II-II*	I-III, II-III-2*
13	$5A + M + Z < \mu_0 < 7A - Z$	II-II*	II-III-2*
14	$7A - Z < \mu_0 < 7A + Z$	II-III-2*	II-III-2*
15	$7A + Z < \mu_0$	III-III-1*	III-III-1*

Taking into account that $\bar{\mu}_{\pm} = \mu_0 \mp Z$, we find the intervals of existence for solutions. These are given in Table I. Using this information, we see that some solutions may coexist. The list of coexisting solutions for a set of non-overlapping intervals of μ_0 is summarized in Table II. [We assume that $Z > M - A \equiv A\lambda/(1 - \lambda)$ which is likely to be satisfied because, as will be shown in Sec. IV, realistic values for λ in this model are relatively small, $\lambda \lesssim 0.2$.]

Thus, there are several coexistent solutions on different intervals of μ_0 . In order to find the most stable solution among them, we have to calculate the free energy density Ω of the ground states corresponding to these solutions. To facilitate this, we first calculate the free energy densities of the fixed spin solutions I, II and III considered in

Subsec. B 4 by using expression (C19) for Ω derived in Appendix C. The results are

$$\text{solution I:} \quad \Omega_{\text{I}} = -\frac{|eB_{\perp}|}{4\pi\hbar c} [M + A + h], \quad (\text{B53})$$

$$\text{solution II:} \quad \Omega_{\text{II}} = -\frac{|eB_{\perp}|}{4\pi\hbar c} [M - (\mu + \bar{\mu})\text{sign}(\mu) + h], \quad (\text{B54})$$

$$\text{solution III:} \quad \Omega_{\text{III}} = -\frac{|eB_{\perp}|}{4\pi\hbar c} [M + (\mu + \bar{\mu})\text{sign}(\mu) + h], \quad (\text{B55})$$

where h is the higher LLs contribution, defined by

$$h \equiv \sum_{n=1}^{\infty} \frac{2M^4}{\sqrt{n\epsilon_B^2 + M^2} \left(\sqrt{n\epsilon_B^2 + M^2} + \sqrt{n}\epsilon_B \right)^2} \simeq \frac{M^4}{2\epsilon_B^3} \left[\zeta\left(\frac{3}{2}\right) - \zeta\left(\frac{5}{2}\right) \frac{M^2}{\epsilon_B^2} + O\left(\frac{M^4}{\epsilon_B^4}\right) \right], \quad (\text{B56})$$

where $\zeta(x)$ is the Riemann zeta function. On the right hand side we used the expansion in powers of $(M/\epsilon_B)^2$. When keeping only the first two terms in the expansion, we find that the result deviates by less than 1% from the exact one for $M \lesssim 0.4\epsilon_B$. Note that the above contribution from higher LLs is the same for all solutions. Therefore, it is only the LLL contribution that is relevant for choosing the lowest free energy density.

It is not difficult now to calculate the free energy densities for all the solutions. In Table II, the solutions that have the lowest values of Ω and thus correspond to the ground states in the given intervals of μ_0 are marked by stars. As for the explicit expression for the energy density in the ground state, it reads

$$\Omega = -\frac{|eB_{\perp}|}{2\pi\hbar c} [M + A + 2Z + h], \quad \text{for } 0 < \mu_0 < 2A + Z, \quad (\text{B57})$$

$$\Omega = -\frac{|eB_{\perp}|}{2\pi\hbar c} [M - A + Z + h + \mu_0], \quad \text{for } 2A + Z < \mu_0 < 6A + Z, \quad (\text{B58})$$

$$\Omega = -\frac{|eB_{\perp}|}{2\pi\hbar c} [M - 7A + h + 2\mu_0], \quad \text{for } 6A + Z < \mu_0, \quad (\text{B59})$$

Using now the explicit form of the solutions obtained in Subsec. B 5, we can significantly reduce the number of the cases. As result, we conclude that only the following three solutions are realized:

- (i) The solution with singlet Dirac masses for both spin up and spin down:

$$\begin{aligned} \tilde{\Delta}_+ = \tilde{\mu}_+ = 0, & \quad \mu_+ = \bar{\mu}_+ - A, & \quad \Delta_+ = s_{\perp}M, \\ \tilde{\Delta}_- = \tilde{\mu}_- = 0, & \quad \mu_- = \bar{\mu}_- + A, & \quad \Delta_- = -s_{\perp}M. \end{aligned} \quad (\text{B60})$$

It is the most favorable for $0 \leq \mu_0 < 2A + Z$.⁵¹ We will call it the *S1* solution, which is one of several solutions with nonvanishing *singlet* Dirac masses.

- (ii) The hybrid solution with a triplet Dirac mass for spin up and a singlet mass for spin down:

$$\begin{aligned} \tilde{\Delta}_+ = M, & \quad \tilde{\mu}_+ = As_{\perp}, & \quad \mu_+ = \bar{\mu}_+ - 4A, & \quad \Delta_+ = 0, \\ \tilde{\Delta}_- = \tilde{\mu}_- = 0, & \quad \mu_- = \bar{\mu}_- - 3A, & \quad \Delta_- = -s_{\perp}M. \end{aligned} \quad (\text{B61})$$

It is the most favorable for $2A + Z \leq \mu_0 < 6A + Z$. We will call it the *H1* solution.

- (iii) The solution with equal singlet masses for both spin up and spin down:

$$\begin{aligned} \tilde{\Delta}_+ = \tilde{\mu}_+ = 0, & \quad \mu_+ = \bar{\mu}_+ - 7A, & \quad \Delta_+ = -s_{\perp}M, \\ \tilde{\Delta}_- = \tilde{\mu}_- = 0, & \quad \mu_- = \bar{\mu}_- - 7A, & \quad \Delta_- = -s_{\perp}M. \end{aligned} \quad (\text{B62})$$

It is the most favorable for $\mu_0 > 6A + Z$. We will call it the *S2* solution.

APPENDIX C: FREE ENERGY DENSITY

In this Appendix, the units with $\hbar = 1$ and $c = 1$ are used.

In order to calculate a free energy density Ω , it is convenient to use the Baym-Kadanoff formalism (the effective action formalism for composite operators) developed in Ref. 55 (see in particular the last paper there). In the mean field approximation that we use, the corresponding effective action Γ has the following form:

$$\Gamma(G) = -i \text{Tr} [\text{Ln}G^{-1} + S^{-1}G - 1] + \frac{G_{int}}{2} \int d^3x \left\{ \text{tr} [\gamma^0 G(x, x) \gamma^0 G(x, x)] - (\text{tr} [\gamma^0 G(x, x)])^2 \right\}, \quad (\text{C1})$$

where the trace, the logarithm, and the product $S^{-1}G$ are taken in the functional sense, and $G = \text{diag}(G_+, G_-)$. The free energy density Ω is expressed through Γ as $\Omega = -\Gamma/TV$, where TV is a space-time volume. The stationarity condition $\delta\Gamma(G)/\delta G = 0$ leads to the gap equation (5). On its solutions we have

$$\Gamma = -i \text{Tr} \left[\text{Ln}G^{-1} + \frac{1}{2} (S^{-1}G - 1) \right]. \quad (\text{C2})$$

Henceforth we will use the symmetric gauge with $\mathbf{A}(\mathbf{r}) = (-B_\perp y/2, B_\perp x/2)$. Then, as was shown in Appendix A, the Green's function $G_s(u, u')$, with $u = (t, \mathbf{r})$, has the form:

$$G_s(u, u') = e^{i\Phi(u, u')} \bar{G}_s(u - u'), \quad (\text{C3})$$

where $\Phi(u, u') = -e\mathbf{r} \cdot \mathbf{A}(\mathbf{r}')$ is the Schwinger phase in the symmetric gauge.

Because of the translation invariance in time, we have

$$G_s(u, u') = \int_{-\infty}^{\infty} \frac{d\omega}{2\pi} e^{-i\omega(t-t')} G_s(\omega; \mathbf{r}, \mathbf{r}'). \quad (\text{C4})$$

Then the effective action Γ can be rewritten as

$$\Gamma = -iT \int_{-\infty}^{\infty} \frac{d\omega}{2\pi} \text{Tr} \left[\ln G^{-1}(\omega) + \frac{1}{2} (S^{-1}(\omega)G(\omega) - 1) \right], \quad (\text{C5})$$

where

$$G_s^{-1}(\omega; \mathbf{r}, \mathbf{r}') = -i \left[(\omega + \mu_s) \gamma^0 - v_F (\boldsymbol{\pi} \cdot \boldsymbol{\gamma}) + i\tilde{\mu}_s \gamma^1 \gamma^2 + i\Delta_s \gamma^0 \gamma^1 \gamma^2 - \tilde{\Delta}_s \right] \delta(\mathbf{r} - \mathbf{r}'), \quad (\text{C6})$$

$$S_s^{-1}(\omega; \mathbf{r}, \mathbf{r}') = -i \left[(\omega + \bar{\mu}_s) \gamma^0 - v_F (\boldsymbol{\pi} \cdot \boldsymbol{\gamma}) \right] \delta(\mathbf{r} - \mathbf{r}'). \quad (\text{C7})$$

In Eq. (C5) the functional operation Tr includes now the integration over the space coordinates only and the trace over matrix indices.

Integrating by parts the logarithm term in Eq. (C5) and omitting the irrelevant surface term (independent of the physical parameters), we arrive at the expression

$$\Gamma = -iT \int_{-\infty}^{\infty} \frac{d\omega}{2\pi} \text{Tr} \left[-\omega \frac{\partial G^{-1}(\omega)}{\partial \omega} G(\omega) + \frac{1}{2} (S^{-1}(\omega)G(\omega) - 1) \right] \quad (\text{C8})$$

with

$$\frac{\partial G^{-1}(\omega)}{\partial \omega} = -i\gamma^0 \delta(\mathbf{r} - \mathbf{r}'). \quad (\text{C9})$$

Substituting now expression (C3) for the Green's function in Γ , one can see that the Schwinger phase goes away and we get

$$\Gamma = -iTV \int_{-\infty}^{\infty} \frac{d\omega}{2\pi} \text{tr} \left[i\gamma^0 \omega \bar{G}(\omega; 0) + \frac{1}{2} \left(-i \left[(\omega + \bar{\mu}) \gamma^0 - v_F (\boldsymbol{\pi} \cdot \boldsymbol{\gamma}) \right] \bar{G}(\omega; \mathbf{r})|_{r=0} - \delta(0) \right) \right]. \quad (\text{C10})$$

Dividing Γ by the space-time volume TV , we find the free energy density:

$$\begin{aligned}\Omega &= i \int_{-\infty}^{\infty} \frac{d\omega}{2\pi} \int \frac{d^2k}{(2\pi)^2} \text{tr} \left\{ i\omega\gamma^0 \bar{G}(\omega, \mathbf{k}) + \frac{1}{2} (-i [(\omega + \bar{\mu})\gamma^0 - v_F(\mathbf{k} \cdot \boldsymbol{\gamma})] \bar{G}(\omega, \mathbf{k}) - 1) \right\} \\ &= - \int_{-\infty}^{\infty} \frac{d\omega}{4\pi} \int \frac{d^2k}{(2\pi)^2} \text{tr} \left\{ [(\omega - \bar{\mu})\gamma^0 + v_F(\mathbf{k} \cdot \boldsymbol{\gamma})] \bar{G}(\omega, \mathbf{k}) + i \right\},\end{aligned}\quad (\text{C11})$$

where the propagator $\bar{G}_s(\omega, \mathbf{k})$ is given in Eq. (A21) in Appendix A. By making use of its explicit form, we can calculate the following two integrals that contribute to the free energy density,

$$\int \frac{d^2k}{(2\pi)^2} \gamma^0 \bar{G}_s(\omega, \mathbf{k}) = \frac{i}{4\pi l^2} \sum_{n=0}^{\infty} \frac{(\omega + \mu_s + i\tilde{\mu}_s\gamma^0\gamma^1\gamma^2 - i\Delta_s\gamma^1\gamma^2 + \tilde{\Delta}_s\gamma^0) P_n}{(\omega + \mu_s + i\tilde{\mu}_s\gamma^0\gamma^1\gamma^2)^2 - (\tilde{\Delta}_s - i\Delta_s\gamma^0\gamma^1\gamma^2)^2 - 2v_F^2|eB_{\perp}|n}, \quad (\text{C12})$$

$$\int \frac{d^2k}{(2\pi)^2} v_F(\mathbf{k} \cdot \boldsymbol{\gamma}) \bar{G}_s(\omega, \mathbf{k}) = \frac{i}{\pi l^2} \sum_{n=0}^{\infty} \frac{v_F^2|eB_{\perp}|n\theta(n-1)}{(\omega + \mu_s + i\tilde{\mu}_s\gamma^0\gamma^1\gamma^2)^2 - (\tilde{\Delta}_s - i\Delta_s\gamma^0\gamma^1\gamma^2)^2 - 2v_F^2|eB_{\perp}|n}, \quad (\text{C13})$$

where

$$P_n = 1 - i\gamma^1\gamma^2\text{sign}(eB_{\perp}) + [1 + i\gamma^1\gamma^2\text{sign}(eB_{\perp})]\theta(n-1). \quad (\text{C14})$$

In the calculation, we used formula 7.414.7 from Ref. 53, i.e.,

$$\int_0^{\infty} e^{-at} t^{\alpha} L_n^{\alpha}(t) dt = \frac{\Gamma(\alpha + n + 1)(a-1)^n}{n! a^{\alpha+n+1}}, \quad \text{Re } \alpha > -1, \text{ Re } a > 0. \quad (\text{C15})$$

By dropping an infinite divergent term which is independent of the physical parameters, from Eq. (C11) we derive the following expression for the free energy density:

$$\Omega = -\frac{i}{(4\pi l)^2} \sum_{s=\pm} \int_{-\infty}^{\infty} d\omega \text{tr}_D \sum_{n=0}^{\infty} \frac{(\omega - \bar{\mu}_s) [\omega + \mu_s + i\tilde{\mu}_s\gamma^0\gamma^1\gamma^2 - i\Delta_s\gamma^1\gamma^2 + \tilde{\Delta}_s\gamma^0] P_n + 4v_F^2|eB_{\perp}|n\theta(n-1)}{(\omega + \mu_s + i\tilde{\mu}_s\gamma^0\gamma^1\gamma^2)^2 - (\tilde{\Delta}_s - i\Delta_s\gamma^0\gamma^1\gamma^2)^2 - 2v_F^2|eB_{\perp}|n}. \quad (\text{C16})$$

Here the trace tr_D is taken over the Dirac indices.

The free energy density Ω is a function of $\tilde{\Delta}_s$, $\tilde{\mu}_s$, μ_s , Δ_s , $\bar{\mu}_s$, and B_{\perp} . Normalizing Ω by subtracting its value at $\tilde{\Delta}_s = \tilde{\mu}_s = \mu_s = \Delta_s = \bar{\mu}_s = 0$, we obtain:

$$\begin{aligned}\Omega &= -\frac{i}{(4\pi l)^2} \sum_{s=\pm} \sum_{n=0}^{\infty} \int_{-\infty}^{\infty} d\omega \text{tr}_D \left[\frac{(\omega - \bar{\mu}_s) [\omega + \mu_s + i\tilde{\mu}_s\gamma^0\gamma^1\gamma^2 - i\Delta_s\gamma^1\gamma^2 + \tilde{\Delta}_s\gamma^0] P_n + 4v_F^2|eB_{\perp}|n\theta(n-1)}{(\omega + i\epsilon\text{sign}(\omega) + \mu_s + i\tilde{\mu}_s\gamma^0\gamma^1\gamma^2)^2 - (\tilde{\Delta}_s - i\Delta_s\gamma^0\gamma^1\gamma^2)^2 - 2v_F^2|eB_{\perp}|n} \right. \\ &\quad \left. - \frac{\omega^2 P_n + 4v_F^2|eB_{\perp}|n\theta(n-1)}{(\omega + i\epsilon\text{sign}(\omega))^2 - 2v_F^2|eB_{\perp}|n} \right].\end{aligned}\quad (\text{C17})$$

One can check that for $\tilde{\mu}_s = \Delta_s = \mu_s = \bar{\mu}_s = B_{\perp} = 0$ and $\tilde{\Delta}_+ = \tilde{\Delta}_- = \tilde{\Delta}$ this expression reduces to

$$\Omega(\tilde{\Delta}, 0, 0, 0, 0, 0) = -\frac{\tilde{\Delta}^4}{4\pi} \int_0^{\infty} \frac{dx}{\sqrt{\tilde{\Delta}^2 + x} (\sqrt{\tilde{\Delta}^2 + x} + \sqrt{x})^2} = -\frac{\tilde{\Delta}^3}{6\pi}, \quad (\text{C18})$$

which coincides with the known expression for the vacuum energy density in 2 + 1 dimension.⁵⁶

Finally, integrating over ω and taking trace, we find the following expression for the free energy density:

$$\begin{aligned} \Omega = & -\frac{1}{8\pi l^2} \sum_{s=\pm} \left\{ \left[\mu_s + \bar{\mu}_s - \tilde{\mu}_s - (\tilde{\Delta}_s + \Delta_s) \text{sign}(eB_\perp) \right] \text{sign}(\mu_s - \tilde{\mu}_s) \theta(|\mu_s - \tilde{\mu}_s| - |\tilde{\Delta}_s + \Delta_s|) \right. \\ & + \left[\tilde{\Delta}_s + \Delta_s - (\mu_s + \bar{\mu}_s - \tilde{\mu}_s) \text{sign}(eB_\perp) \right] \text{sign}(\tilde{\Delta}_s + \Delta_s) \theta(|\tilde{\Delta}_s + \Delta_s| - |\mu_s - \tilde{\mu}_s|) \\ & + 2 \sum_{n=1}^{\infty} \left[[(\mu_s + \bar{\mu}_s - \tilde{\mu}_s) \text{sign}(\mu_s - \tilde{\mu}_s) - 2\epsilon_B \sqrt{n}] \theta(|\mu_s - \tilde{\mu}_s| - E_{ns}^+) + \frac{(\tilde{\Delta}_s + \Delta_s)^4 \theta(E_{ns}^+ - |\mu_s - \tilde{\mu}_s|)}{E_{ns}^+ (E_{ns}^+ + \epsilon_B \sqrt{n})^2} \right] \\ & \left. + [\tilde{\mu}_s \rightarrow -\tilde{\mu}_s, \Delta_s \rightarrow -\Delta_s, \text{sign}(eB_\perp) \rightarrow -\text{sign}(eB_\perp)] \right\}, \end{aligned} \quad (\text{C19})$$

where $E_{ns}^\pm = \sqrt{n\epsilon_B^2 + (\tilde{\Delta}_s \pm \Delta_s)^2}$ and $\epsilon_B = \sqrt{2v_F^2 |eB_\perp|}$.

APPENDIX D: ANALYTIC SOLUTIONS OF GAP EQUATION FOR $n = 1$ LL AT $T = 0$

1. Fixed spin

In Appendix B, we analyzed solutions of the gap equations under the condition that only states on the LLL can be filled, $|\mu_s \pm \tilde{\mu}_s| \ll \epsilon_B = \sqrt{2\hbar|eB_\perp|v_F^2/c}$. Since all the dynamically generated parameters are much less than ϵ_B , this condition implies that the bare chemical potential μ_0 also has to satisfy $\mu_0 \ll \epsilon_B$ in that case.

In this section, we will consider the case when μ_0 is of the order of the Landau scale ϵ_B , i.e., we will study the dynamics when states on the first Landau level, $n = 1$ LL, can be filled. The gap equations are given in Eqs. (19)–(22) in Sec. III. In order to get their solutions for $\mu_0 \sim \epsilon_B$, we will follow the steps in the analysis in Appendix B. The equations for the dynamical parameters $\tilde{\Delta}_s$, Δ_s , and $\tilde{\mu}_s$ form independent systems of equations for each spin. From these systems, we can find their solutions as functions of μ_s . We obtain the following three solutions.

- Solution f-I. This solution corresponds to the case with $|\mu_s - \tilde{\mu}_s| < \sqrt{\epsilon_B^2 + (\tilde{\Delta}_s + \Delta_s)^2}$ and $|\mu_s + \tilde{\mu}_s| < \sqrt{\epsilon_B^2 + (\tilde{\Delta}_s - \Delta_s)^2}$. It is

$$\Delta_s = -s_\perp \text{sign}(\mu_s) M, \quad \tilde{\Delta}_s = \tilde{\mu}_s = 0. \quad (\text{D1})$$

This solution exists for $M < |\mu_s| < \sqrt{\epsilon_B^2 + M^2}$. Actually, it is exactly the same as solution (B28) considered in Subsec. 3 of Appendix B. For positive μ_s , this solution corresponds to a state with the completely filled LLL and the empty $n = 1$ LL. With increasing μ_s , this solution exists up to the point where the first LL starts to fill, which is defined by the upper limit of the above inequality for μ_s . Recall that $X_s = -4A \text{sign}(\mu_s)$ for such a solution.

- Solution f-II. This solution is realized when the inequalities $|\mu_s - \tilde{\mu}_s| < \sqrt{\epsilon_B^2 + (\tilde{\Delta}_s + \Delta_s)^2}$ and $|\mu_s + \tilde{\mu}_s| > \sqrt{\epsilon_B^2 + (\tilde{\Delta}_s - \Delta_s)^2}$ are satisfied. In this solution, all three dynamical parameters Δ_s , $\tilde{\Delta}_s$, and $\tilde{\mu}_s$ are nonzero:

$$\tilde{\Delta}_s = -s_\perp \text{sign}(\mu_s) \frac{M - M_1}{2}, \quad \Delta_s = -s_\perp \text{sign}(\mu_s) \frac{M_1 + M}{2}, \quad \tilde{\mu}_s = \text{sign}(\mu_s) A. \quad (\text{D2})$$

Here M_1 satisfies the following equation:

$$1 = \frac{A}{\sqrt{\pi}} \int_{1/\Lambda^2}^{\infty} \frac{dy}{\sqrt{y}} e^{-yM_1^2} \left[\coth\left(\frac{\epsilon_B^2}{2} y\right) - 2 \exp(-y\epsilon_B^2) \right]. \quad (\text{D3})$$

Note that the last term in the square brackets of the integrand appears because the $n = 1$ LL contribution is absent in the equation for $\tilde{\Delta} - \Delta$ [cf. Eq. (B6) where all LLs are included].

Utilizing the analysis in the second paper in Ref. 28, we arrive at the following gap equation for M_1 :

$$1 = \lambda + \frac{A}{M_1} + \frac{2A}{\epsilon_B} \zeta\left(\frac{1}{2}, 1 + \frac{M_1^2}{\epsilon_B^2}\right) - \frac{2A}{\sqrt{\epsilon_B^2 + M_1^2}} + O\left(\lambda \frac{M_1^2}{\Lambda^2}\right), \quad (\text{D4})$$

where $\zeta(z, q)$ is the generalized Riemann zeta function.⁵³ In the subcritical regime ($\lambda < 1$) its solution is given by

$$M_1 \simeq \frac{A}{1 - \lambda + 2[1 - \zeta(1/2)] A/\epsilon_B}. \quad (\text{D5})$$

Since the last term in the denominator is positive, we have $M_1 < M$ that is consistent with the fact that the equation for $\tilde{\Delta} - \Delta$ misses the contribution of the $n = 1$ LL.

This solution exists for $\sqrt{\epsilon_B^2 + M_1^2} - A < |\mu_s| < \sqrt{\epsilon_B^2 + M^2} + A$. One can check that the corresponding parameter X_s is $X_s = -8A \text{sign}(\mu_s)$. As in the case of the LLL (see Subsec. B 4), there is another solution with $\tilde{\Delta}_s, \tilde{\mu}_s$ replaced by $-\tilde{\Delta}_s, -\tilde{\mu}_s$, which takes place for $|\mu_s - \tilde{\mu}_s| > \sqrt{\epsilon_B^2 + (\tilde{\Delta}_s + \Delta_s)^2}$ and $|\mu_s + \tilde{\mu}_s| < \sqrt{\epsilon_B^2 + (\tilde{\Delta}_s - \Delta_s)^2}$. These two solutions are equivalent: one can see this from dispersion relations (17), (18) by transforming $\sigma \rightarrow -\sigma$ there, i.e., as in the case of the LLL solution I (B30), these solutions are related to two degenerate ground states connected by a $SU(2)_s$ (or Z_{2s}) flavor transformation.

- Solution f-III. This solution corresponds to the case with $|\mu_s - \tilde{\mu}_s| > \sqrt{\epsilon_B^2 + (\tilde{\Delta}_s + \Delta_s)^2}$ and $|\mu_s + \tilde{\mu}_s| > \sqrt{\epsilon_B^2 + (\tilde{\Delta}_s - \Delta_s)^2}$. Its explicit form reads

$$\tilde{\Delta}_s = \tilde{\mu}_s = 0, \quad \Delta_s = -s_\perp \text{sign}(\mu_s) M_1. \quad (\text{D6})$$

This solution takes place for $|\mu_s| > \sqrt{\epsilon_B^2 + M_1^2}$ and the corresponding X_s is $X_s = -12A \text{sign}(\mu_s)$.

2. Including both spin up and spin down

In Subsec. D 1, the solutions for the dynamical parameters $\Delta_s, \tilde{\Delta}_s$, and $\tilde{\mu}_s$ at fixed spin were described. Since X contains contribution of fields of both spins, the equations for chemical potentials μ_+ and μ_- for fields of different spin are coupled and have to be solved together. Since we can choose any of the found three solutions for masses at a fixed spin, we should solve 9 systems of coupled equations for μ_+ and μ_- . Like in the case of the LLL, it is enough to consider only 6 systems. The simplest case is the solution f-I–f-I because it corresponds to the case of completely filled LLL, which was already considered in Subsec. B 5. We have

- f-I–f-I solution is given by

$$\begin{aligned} \tilde{\Delta}_+ &= \tilde{\mu}_+ = 0, & \mu_+ &= \bar{\mu}_+ - 7A \text{sign}(\bar{\mu}_+), & \Delta_+ &= -s_\perp \text{sign}(\bar{\mu}_+) M, \\ \tilde{\Delta}_- &= \tilde{\mu}_- = 0, & \mu_- &= \bar{\mu}_- - 7A \text{sign}(\bar{\mu}_-), & \Delta_- &= -s_\perp \text{sign}(\bar{\mu}_-) M. \end{aligned} \quad (\text{D7})$$

It exists when $\text{sign}(\bar{\mu}_+) \text{sign}(\bar{\mu}_-) > 0$ and

$$7A + M < |\bar{\mu}_+| < 7A + \sqrt{\epsilon_B^2 + M^2}, \quad 7A + M < |\bar{\mu}_-| < 7A + \sqrt{\epsilon_B^2 + M^2}. \quad (\text{D8})$$

It coincides with the solution III-III-1 in Eq. (B47) in Subsec. B 5, except for having a different lower limit for $|\bar{\mu}_\pm|$. The latter is connected with the point that while the solution III in Eq. (B32) exists for all values of μ_s , the solution f-I in Eq. (D1) exists only for $|\mu_s| > M$. This is because, according to the analysis in Subsec. B 4, the solution III is a combination of two solutions: the solution (B28), which is equivalent to the solution f-I, and one of the two solutions in Eq. (B10).

- f-I–f-II solution is given by

$$\begin{aligned} \tilde{\Delta}_+ &= \tilde{\mu}_+ = 0, & \mu_+ &= \bar{\mu}_+ - 11A \text{sign}(\bar{\mu}_+), & \Delta_+ &= -s_\perp \text{sign}(\bar{\mu}_+) M, \\ \tilde{\Delta}_- &= \frac{M - M_1}{2}, & \tilde{\mu}_- &= -As_\perp, & \mu_- &= \bar{\mu}_- - 10A \text{sign}(\bar{\mu}_-), & \Delta_- &= -s_\perp \text{sign}(\bar{\mu}_-) \frac{M + M_1}{2}. \end{aligned} \quad (\text{D9})$$

It exists when $\text{sign}(\bar{\mu}_+) \text{sign}(\bar{\mu}_-) > 0$ and

$$11A + M < |\bar{\mu}_+| < 11A + \sqrt{\epsilon_B^2 + M^2}, \quad 9A + \sqrt{\epsilon_B^2 + M_1^2} < |\bar{\mu}_-| < 11A + \sqrt{\epsilon_B^2 + M^2}. \quad (\text{D10})$$

- f-I–f-III solution reads

$$\begin{aligned}\tilde{\Delta}_+ &= \tilde{\mu}_+ = 0, & \mu_+ &= \bar{\mu}_+ - 15A \operatorname{sign}(\bar{\mu}_+), & \Delta_+ &= -s_\perp \operatorname{sign}(\bar{\mu}_+)M, \\ \tilde{\Delta}_- &= \tilde{\mu}_- = 0, & \mu_- &= \bar{\mu}_- - 13A \operatorname{sign}(\bar{\mu}_-), & \Delta_- &= -s_\perp \operatorname{sign}(\bar{\mu}_-)M_1,\end{aligned}\quad (\text{D11})$$

and takes place when $\operatorname{sign}(\bar{\mu}_+) \operatorname{sign}(\bar{\mu}_-) > 0$ and

$$15A + M < |\bar{\mu}_+| < 15A + \sqrt{\epsilon_B^2 + M^2}, \quad 13A + \sqrt{\epsilon_B^2 + M_1^2} < |\bar{\mu}_-|. \quad (\text{D12})$$

- f-II–f-II solution is given by

$$\begin{aligned}\tilde{\Delta}_+ &= \frac{M - M_1}{2}, & \tilde{\mu}_+ &= -As_\perp, & \mu_+ &= \bar{\mu}_+ - 14A \operatorname{sign}(\bar{\mu}_+), & \Delta_+ &= -s_\perp \operatorname{sign}(\bar{\mu}_+) \frac{M + M_1}{2}, \\ \tilde{\Delta}_- &= \frac{M - M_1}{2}, & \tilde{\mu}_- &= -As_\perp, & \mu_- &= \bar{\mu}_- - 14A \operatorname{sign}(\bar{\mu}_-), & \Delta_- &= -s_\perp \operatorname{sign}(\bar{\mu}_-) \frac{M + M_1}{2},\end{aligned}\quad (\text{D13})$$

and exists when $\operatorname{sign}(\bar{\mu}_+) \operatorname{sign}(\bar{\mu}_-) > 0$ and

$$13A + \sqrt{\epsilon_B^2 + M_1^2} < |\bar{\mu}_\pm| < 15A + \sqrt{\epsilon_B^2 + M^2}. \quad (\text{D14})$$

- f-II–f-III solution is given by

$$\begin{aligned}\tilde{\Delta}_+ &= \frac{M - M_1}{2}, & \tilde{\mu}_+ &= -As_\perp, & \mu_+ &= \bar{\mu}_+ - 18A \operatorname{sign}(\bar{\mu}_+), & \Delta_+ &= -s_\perp \operatorname{sign}(\bar{\mu}_+) \frac{M + M_1}{2}, \\ \tilde{\Delta}_- &= \tilde{\mu}_- = 0, & \mu_- &= \bar{\mu}_- - 17A \operatorname{sign}(\bar{\mu}_-), & \Delta_- &= -s_\perp \operatorname{sign}(\bar{\mu}_-)M_1,\end{aligned}\quad (\text{D15})$$

and takes place when $\operatorname{sign}(\bar{\mu}_+) \operatorname{sign}(\bar{\mu}_-) > 0$ and

$$17A + \sqrt{\epsilon_B^2 + M_1^2} < |\bar{\mu}_+| < 19A + \sqrt{\epsilon_B^2 + M^2}, \quad |\bar{\mu}_-| > 17A + \sqrt{\epsilon_B^2 + M_1^2}. \quad (\text{D16})$$

- f-III–f-III solution is given by

$$\begin{aligned}\tilde{\Delta}_+ &= \tilde{\mu}_+ = 0, & \mu_+ &= \bar{\mu}_+ - 21A \operatorname{sign}(\bar{\mu}_+), & \Delta_+ &= -s_\perp \operatorname{sign}(\bar{\mu}_+)M_1, \\ \tilde{\Delta}_- &= \tilde{\mu}_- = 0, & \mu_- &= \bar{\mu}_- - 21A \operatorname{sign}(\bar{\mu}_-), & \Delta_- &= -s_\perp \operatorname{sign}(\bar{\mu}_-)M_1,\end{aligned}\quad (\text{D17})$$

and exists when $\operatorname{sign}(\bar{\mu}_+) \operatorname{sign}(\bar{\mu}_-) > 0$ and

$$|\bar{\mu}_+| > 21A + \sqrt{\epsilon_B^2 + M_1^2}, \quad |\bar{\mu}_-| > 21A + \sqrt{\epsilon_B^2 + M_1^2}. \quad (\text{D18})$$

3. Dependence of solutions on μ_0 and their free energy density energy

Using the solutions found in the previous subsection, we find that the intervals of their existence in terms of μ_0 for $\mu_0 \geq 0$ (dynamics with negative μ_0 is related by the electron-hole symmetry and will not be discussed separately). These are given in Table III. By making use of this information, we can also determine the complete set of non-overlapping intervals of μ_0 and the solutions that (co-)exist on such intervals. This is summarized in Table IV.

Thus, there are several coexistent solutions on certain intervals of μ_0 . In order to define which solutions are realized, we have to calculate their free energy densities. To facilitate this calculation, first we will calculate free energy densities of solutions f-I, f-II, and f-III. Using the effective potential given by Eq. (C19), we have

$$\text{solution f-I:} \quad \Omega_{\text{f-I}} = -\frac{|eB_\perp|}{4\pi\hbar c} [M + (\mu + \bar{\mu}) \operatorname{sign}(\mu) + h], \quad (\text{D19})$$

$$\text{solution f-II:} \quad \Omega_{\text{f-II}} = -\frac{|eB_\perp|}{4\pi\hbar c} \left(\frac{M + M_1}{2} + A + 2(\mu + \bar{\mu}) \operatorname{sign}(\mu) - 2\epsilon_B + \frac{h + h_1}{2} \right), \quad (\text{D20})$$

$$\text{solution f-III:} \quad \Omega_{\text{f-III}} = -\frac{|eB_\perp|}{4\pi\hbar c} (M_1 + 3(\mu + \bar{\mu}) \operatorname{sign}(\mu) - 4\epsilon_B + h_1), \quad (\text{D21})$$

TABLE III: Intervals of the existence of solutions, relevant for the dynamics in the $n = 1$ LL at $T = 0$.

f-I-f-I	$7A + M + Z < \mu_0 < 7A + \sqrt{\epsilon_B^2 + M^2} - Z$
f-I-f-II	$9A + \sqrt{\epsilon_B^2 + M_1^2} - Z < \mu_0 < 11A + \sqrt{\epsilon_B^2 + M^2} - Z$
f-II-f-I	$9A + \sqrt{\epsilon_B^2 + M_1^2} + Z < \mu_0 < 11A + \sqrt{\epsilon_B^2 + M^2} - Z$
f-I-f-III	$13A + \sqrt{\epsilon_B^2 + M_1^2} - Z < \mu_0 < 15A + \sqrt{\epsilon_B^2 + M^2} + Z$
f-III-f-I	$13A + \sqrt{\epsilon_B^2 + M_1^2} + Z < \mu_0 < 15A + \sqrt{\epsilon_B^2 + M^2} - Z$
f-II-f-II	$13A + \sqrt{\epsilon_B^2 + M_1^2} + Z < \mu_0 < 15A + \sqrt{\epsilon_B^2 + M^2} - Z$
f-II-f-III	$17A + \sqrt{\epsilon_B^2 + M_1^2} + Z < \mu_0 < 19A + \sqrt{\epsilon_B^2 + M^2} + Z$
f-III-f-II	$17A + \sqrt{\epsilon_B^2 + M_1^2} + Z < \mu_0 < 19A + \sqrt{\epsilon_B^2 + M^2} - Z$
f-III-f-III	$\mu_0 > 21A + \sqrt{\epsilon_B^2 + M_1^2} + Z$

TABLE IV: The list of solutions that coexist in a set of non-overlapping intervals of μ_0 , relevant for the dynamics in the $n = 1$ LL at $T = 0$. The solutions with the lowest free energy density are marked by stars.

#	Interval	Solution(s)
1	$7A + M + Z < \mu_0 < 7A + \sqrt{\epsilon_B^2 + M^2} - Z$	f-I-f-I*
2	$9A + \sqrt{\epsilon_B^2 + M_1^2} - Z < \mu_0 < 9A + \sqrt{\epsilon_B^2 + M_1^2} + Z$	f-I-f-II*
3	$9A + \sqrt{\epsilon_B^2 + M_1^2} + Z < \mu_0 < 11A + \sqrt{\epsilon_B^2 + M^2} - Z$	f-I-f-II*, f-II-f-I
4	$13A + \sqrt{\epsilon_B^2 + M_1^2} - Z < \mu_0 < 13A + \sqrt{\epsilon_B^2 + M_1^2} + Z$	f-I-f-III*
5	$13A + \sqrt{\epsilon_B^2 + M_1^2} + Z < \mu_0 < 15A + \sqrt{\epsilon_B^2 + M^2} - Z$	f-I-f-III*, f-III-f-I, f-II-f-II
6	$15A + \sqrt{\epsilon_B^2 + M^2} - Z < \mu_0 < 15A + \sqrt{\epsilon_B^2 + M^2} + Z$	f-I-f-III*
7	$17A + \sqrt{\epsilon_B^2 + M_1^2} + Z < \mu_0 < 19A + \sqrt{\epsilon_B^2 + M^2} - Z$	f-II-f-III*, f-III-f-II
8	$19A + \sqrt{\epsilon_B^2 + M^2} - Z < \mu_0 < 19A + \sqrt{\epsilon_B^2 + M^2} + Z$	f-II-f-III*
9	$\mu_0 > 21A + \sqrt{\epsilon_B^2 + M_1^2} + Z$	f-III-f-III*

where h is given in Eq. (B56) and

$$h_1 \equiv \sum_{n=2}^{\infty} \frac{2M_1^4}{\sqrt{n\epsilon_B^2 + M_1^2} \left(\sqrt{n\epsilon_B^2 + M_1^2} + \sqrt{n\epsilon_B} \right)^2} \simeq \frac{M_1^4}{2\epsilon_B^3} \left[\zeta(3/2) - 1 - [\zeta(5/2) - 1] \frac{M_1^2}{\epsilon_B^2} + O\left(\frac{M_1^4}{\epsilon_B^4}\right) \right]. \quad (\text{D22})$$

Now it is not difficult to calculate free energy densities for all solutions and determine the ground state on each interval. The solutions with the lowest free energy density are marked by stars in Table IV. The explicit form of the corresponding energy densities are

$$\text{f-I-f-I:} \quad \Omega = -\frac{|eB_{\perp}|}{2\pi\hbar c} (M + 2\mu_0 - 7A + h), \quad (\text{D23})$$

$$\text{f-I-f-II:} \quad \Omega = -\frac{|eB_{\perp}|}{2\pi\hbar c} \left(\frac{3M + M_1}{4} + 3\mu_0 - 15A - \epsilon_B + Z + \frac{3h + h_1}{4} \right), \quad (\text{D24})$$

$$\text{f-I-f-III:} \quad \Omega = -\frac{|eB_{\perp}|}{2\pi\hbar c} \left(\frac{M + M_1}{2} + 4\mu_0 - 27A - 2\epsilon_B + 2Z + \frac{h + h_1}{2} \right), \quad (\text{D25})$$

$$\text{f-II-f-III:} \quad \Omega = -\frac{|eB_{\perp}|}{2\pi\hbar c} \left(\frac{3M_1 + M}{4} + 5\mu_0 - 43A - 3\epsilon_B + Z + \frac{3h_1 + h}{4} \right), \quad (\text{D26})$$

$$\text{f-III-f-III:} \quad \Omega = -\frac{|eB_{\perp}|}{2\pi\hbar c} (M_1 + 6\mu_0 - 63A - 4\epsilon_B + h_1). \quad (\text{D27})$$

Therefore, the number of different solutions is reduced down to following five.

(f-i) The solution f-I-f-I

$$\begin{aligned}\tilde{\Delta}_+ &= \tilde{\mu}_+ = 0, & \mu_+ &= \bar{\mu}_+ - 7A, & \Delta_+ &= -s_\perp M, \\ \tilde{\Delta}_- &= \tilde{\mu}_- = 0, & \mu_- &= \bar{\mu}_- - 7A, & \Delta_- &= -s_\perp M\end{aligned}\quad (\text{D28})$$

is realized for $7A + M + Z < \mu_0 < 7A + \sqrt{\epsilon_B^2 + M^2} - Z$ and has free energy density in Eq. (D23). This result means that the solution S2 given by Eq. (B62) in Subsec. B 6 takes place for $\mu_0 < 7A + \sqrt{\epsilon_B^2 + M^2} - Z$.

(f-ii) The solution f-I-f-II

$$\begin{aligned}\tilde{\Delta}_+ &= \tilde{\mu}_+ = 0, & \mu_+ &= \bar{\mu}_+ - 11A, & \Delta_+ &= -s_\perp M, \\ \tilde{\Delta}_- &= \frac{M - M_1}{2}, & \tilde{\mu}_- &= -As_\perp, & \mu_- &= \bar{\mu}_- - 10A, & \Delta_- &= -s_\perp \frac{M + M_1}{2}\end{aligned}\quad (\text{D29})$$

takes place for $9A + \sqrt{\epsilon_B^2 + M_1^2} - Z < \mu_0 < 11A + \sqrt{\epsilon_B^2 + M^2} - Z$ and has free energy density in Eq. (D24).

(f-iii) The solution f-I-f-III

$$\begin{aligned}\tilde{\Delta}_+ &= \tilde{\mu}_+ = 0, & \mu_+ &= \bar{\mu}_+ - 15A, & \Delta_+ &= -s_\perp M, \\ \tilde{\Delta}_- &= \tilde{\mu}_- = 0, & \mu_- &= \bar{\mu}_- - 13A, & \Delta_- &= -s_\perp M_1\end{aligned}\quad (\text{D30})$$

is realized for $13A + \sqrt{\epsilon_B^2 + M_1^2} - Z < \mu_0 < 15A + \sqrt{\epsilon_B^2 + M^2} + Z$ and has free energy density in Eq. (D25).

(f-iv) The solution f-II-f-III

$$\begin{aligned}\tilde{\Delta}_+ &= \frac{M - M_1}{2}, & \tilde{\mu}_+ &= -As_\perp, & \mu_+ &= \bar{\mu}_+ - 18A, & \Delta_+ &= -s_\perp \frac{M + M_1}{2}, \\ \tilde{\Delta}_- &= \tilde{\mu}_- = 0, & \mu_- &= \bar{\mu}_- - 17A, & \Delta_- &= -s_\perp M_1\end{aligned}\quad (\text{D31})$$

takes place for $17A + \sqrt{\epsilon_B^2 + M_1^2} + Z < \mu_0 < 19A + \sqrt{\epsilon_B^2 + M^2} + Z$ and has free energy density in Eq. (D26).

(f-v) The solution f-III-f-III

$$\begin{aligned}\tilde{\Delta}_+ &= \tilde{\mu}_+ = 0, & \mu_+ &= \bar{\mu}_+ - 21A, & \Delta_+ &= -s_\perp M_1, \\ \tilde{\Delta}_- &= \tilde{\mu}_- = 0, & \mu_- &= \bar{\mu}_- - 21A, & \Delta_- &= -s_\perp M_1\end{aligned}\quad (\text{D32})$$

is realized for $\mu_0 > 21A + \sqrt{\epsilon_B^2 + M_1^2} + Z$ and has free energy density in Eq. (D27).

* Electronic address: gorbar@bitp.kiev.ua

† Electronic address: vgosynin@bitp.kiev.ua

‡ Electronic address: vmiransk@uwo.ca; On leave from Bogolyubov Institute for Theoretical Physics, 03680, Kiev, Ukraine

§ Electronic address: i-shovkovy@wiu.edu; On leave from Bogolyubov Institute for Theoretical Physics, 03680, Kiev, Ukraine

¹ K.S. Novoselov, A.K. Geim, S.V. Morozov, D. Jaing, Y. Zhang, S.V. Dubonos, I.V. Grigorieva, and A.A. Firsov, *Science* **306**, 666 (2004).

² K.S. Novoselov, A.K. Geim, S.V. Morozov, D. Jaing, M.I. Katsnelson, I.V. Grigorieva, S.V. Dubonos, and A.A. Firsov, *Nature* **438**, 197 (2005).

³ Y. Zhang, Y.-W. Tan, H.L. Störmer, and P. Kim, *Nature* **438**, 201 (2005).

⁴ Y. Zheng and T. Ando, *Phys. Rev. B* **65**, 245420 (2002).

⁵ V.P. Gusynin and S.G. Sharapov, *Phys. Rev. Lett.* **95**, 146801 (2005); *Phys. Rev. B* **73**, 245411 (2006).

⁶ N.M.R. Peres, F. Guinea, and A.H. Castro Neto, *Phys. Rev. B* **73**, 125411 (2006).

⁷ G.W. Semenoff, *Phys. Rev. Lett.* **53**, 2449 (1984).

⁸ F.D.M. Haldane, *Phys. Rev. Lett.* **61**, 2015 (1988).

⁹ D.V. Khveshchenko, *Phys. Rev. Lett.* **87**, 206401 (2001); *ibid.* **87**, 246802 (2001).

- ¹⁰ E.V. Gorbar, V.P. Gusynin, V.A. Miransky, and I.A. Shovkovy, Phys. Rev. B **66**, 045108 (2002).
- ¹¹ S.G. Sharapov, V.P. Gusynin, and H. Beck, Phys. Rev. B **69**, 075104 (2004).
- ¹² I.A. Luk'yanchuk and Y. Kopelevich, Phys. Rev. Lett. **93**, 166402 (2004).
- ¹³ Y. Zhang, Z. Jiang, J. P. Small, M. S. Purewal, Y.-W. Tan, M. Fazlollahi, J.D. Chudow, J.A. Jaszczak, H.L. Störmer, and P. Kim, Phys. Rev. Lett. **96**, 136806 (2006).
- ¹⁴ Z. Jiang, Y. Zhang, H.L. Störmer, and P. Kim, Phys. Rev. Lett. **99**, 106802 (2007).
- ¹⁵ K. Nomura and A.H. MacDonald, Phys. Rev. Lett. **96**, 256602 (2006); K. Yang, S. Das Sarma, and A.H. MacDonald, Phys. Rev. B **74**, 075423 (2006).
- ¹⁶ M.O. Goerbig, R. Moessner, and B. Douçot, Phys. Rev. B **74**, 161407(R) (2006).
- ¹⁷ J. Alicea and M.P.A. Fisher, Phys. Rev. B **74**, 075422 (2006).
- ¹⁸ L. Sheng, D.N. Sheng, F.D.M. Haldane, and L. Balents, Phys. Rev. Lett. **99**, 196802 (2007).
- ¹⁹ V. Lukose and R. Shankar, arXiv:0706.4280 [cond-mat.mes-hall].
- ²⁰ D.A. Abanin, P.A. Lee, and L.S. Levitov, Phys. Rev. Lett. **96**, 176803 (2006); Solid State Comm. **143**, 77 (2007).
- ²¹ V.P. Gusynin, V.A. Miransky, S.G. Sharapov, and I.A. Shovkovy, Phys. Rev. B **74**, 195429 (2006); arXiv:cond-mat/0612488.
- ²² I.F. Herbut, Phys. Rev. Lett. **97**, 146401 (2006); Phys. Rev. B **75**, 165411 (2007); *ibid*, **76**, 085432 (2007).
- ²³ J.-N. Fuchs and P. Lederer, Phys. Rev. Lett. **98**, 016803 (2007).
- ²⁴ M. Ezawa, J. Phys. Soc. Jpn. **76** (2007) 094701; Physica E **40**, 269 (2007).
- ²⁵ K. Yang, Solid State Comm. **143**, 27 (2007).
- ²⁶ M.M. Fogler and B.I. Shklovskii, Phys. Rev. B **52**, 17366 (1995).
- ²⁷ D.P. Arovas, A. Karlhelde, and D. Lilliehook, Phys. Rev. B **59**, 13147 (1999); Z.F. Ezawa and K. Hasebe, Phys. Rev. B **65**, 075311 (2002).
- ²⁸ V.P. Gusynin, V.A. Miransky, and I.A. Shovkovy, Phys. Rev. Lett. **73**, 3499 (1994); Phys. Rev. D **52**, 4718 (1995); Nucl. Phys. B **462**, 249 (1996).
- ²⁹ E.V. Gorbar, V.P. Gusynin, and V.A. Miransky, arXiv:0710.3527 [cond-mat.mes-hall].
- ³⁰ M. Koshino and T. Ando, Phys. Rev. B **75**, 033412 (2007).
- ³¹ P. Goswami, X. Jia, and S. Chakravarty, Phys. Rev. B **76**, 205408 (2007); X. Jia, P. Goswami, and S. Chakravarty, Phys. Rev. Lett. **101**, 036805 (2008).
- ³² K. Nomura, S. Ryu, M. Koshino, C. Mudry, and A. Furusaki, arXiv:0801.3121 [cond-mat.mes-hall].
- ³³ A.J.M. Giesbers, U. Zeitler, M.I. Katsnelson, L.A. Ponomarenko, T.M.G. Mohiuddin, and J.C. Maan, Phys. Rev. Lett. **99**, 206803 (2007).
- ³⁴ K.I. Bolotin, K.J. Sikes, Z. Jiang, G. Fudenberg, J. Hone, P. Kim, and H. L. Störmer, Solid State Comm. **146** (2008) 351.
- ³⁵ G. Li, A. Luican, and E.Y. Andrei, arXiv:0803.4016 [cond-mat.mes-hall].
- ³⁶ D.A. Abanin, K.S. Novoselov, U. Zeitler, P.A. Lee, A.K. Geim, and L.S. Levitov, Phys. Rev. Lett. **98**, 196806 (2007).
- ³⁷ J.G. Checkelsky, L. Li, and N.P. Ong, Phys. Rev. Lett. **100**, 206801 (2008).
- ³⁸ For Dirac matrices γ^0 and $\vec{\gamma}$, we use the same representation as in Ref. 21.
- ³⁹ The Zeeman coupling $\mu_B \vec{B} \vec{\sigma}$ can be always diagonalized in the spin space as $\mu_B B \sigma^3$.
- ⁴⁰ V.A. Miransky, *Dynamical Symmetry Breaking in Quantum Field Theories* (World Scientific, Singapore, 1993).
- ⁴¹ By definition, the values of the subcritical coupling constant are those at which no dynamical gaps are generated without a magnetic field.
- ⁴² M.I. Katsnelson, Phys. Rev. B **74**, 201401(R) (2006); B. Wunsch, T. Stauber, F. Sols, and F. Guinea, New J. Phys. **8**, 318 (2006).
- ⁴³ A.V. Shytov, M.I. Katsnelson, and L.S. Levitov, Phys. Rev. Lett. **99**, 236801 (2007).
- ⁴⁴ The energy gap $\tilde{\Delta}_{\pm}$ is expressed through the corresponding Dirac mass \tilde{m}_{\pm} as $\tilde{\Delta}_{\pm} = \tilde{m}_{\pm} v_F^2$. In what follows, we will ignore this difference between them and use the term “Dirac mass”.
- ⁴⁵ V.P. Gusynin, S.G. Sharapov, and J.P. Carbotte, Int. J. Mod. Phys. B **21**, 4611 (2007).
- ⁴⁶ I.L. Aleiner, D.E. Kharzeev, and A.M. Tsvelik, Phys. Rev. B **76**, 195415 (2007).
- ⁴⁷ N.D. Mermin and H. Wagner, Phys. Rev. Lett. **17**, 1133 (1966).
- ⁴⁸ For $\text{sign}(eB_{\perp}) > 0$, one has $\Psi^{\dagger} P_s \Psi = \bar{\Psi} \gamma^3 \gamma^5 P_s \Psi = \psi_{K'As}^{\dagger} \psi_{KAs} + \psi_{K'Bs}^{\dagger} \psi_{K'Bs}$ and $\Psi^{\dagger} \gamma^3 \gamma^5 P_s \Psi = \bar{\Psi} P_s \Psi = \psi_{KAs}^{\dagger} \psi_{KAs} - \psi_{K'Bs}^{\dagger} \psi_{K'Bs}$. For $\text{sign}(eB_{\perp}) < 0$, the relations are $\Psi^{\dagger} P_s \Psi = -\bar{\Psi} \gamma^3 \gamma^5 P_s \Psi = \psi_{K'As}^{\dagger} \psi_{K'As} + \psi_{KBs}^{\dagger} \psi_{KBs}$ and $\Psi^{\dagger} \gamma^3 \gamma^5 P_s \Psi = -\bar{\Psi} P_s \Psi = -\psi_{K'As}^{\dagger} \psi_{K'As} + \psi_{KBs}^{\dagger} \psi_{KBs}$.
- ⁴⁹ V.P. Gusynin, V.A. Miransky, S.G. Sharapov, and I.A. Shovkovy, arXiv:0801.0708 [cond-mat.mes-hall].
- ⁵⁰ V.P. Gusynin, V.A. Miransky, S.G. Sharapov, and I.A. Shovkovy, Phys. Rev. B **77**, 205409 (2008).
- ⁵¹ In dynamics in a magnetic field at zero temperature, there is no one-to-one correspondence between electron density and chemical potential. As a result, different values of the latter may correspond to the same physics, as it takes place for this solution.
- ⁵² I.F. Herbut and B. Roy, Phys. Rev. B **77**, 245438 (2008).
- ⁵³ I.S. Gradshteyn, I.M. Ryzhik, *Tables of Integrals, Series, and Products* (Academic Press, Orlando, 1980).
- ⁵⁴ J. Zak, Phys. Rev. **134**, A1602 (1964).
- ⁵⁵ J.M. Luttinger and J.D. Ward, Phys. Rev. **118**, 1417 (1960); L.P. Kadanoff and G. Baym, *ibid* **124**, 287 (1961); G. Baym, *ibid* **127**, 1391 (1962); J.M. Cornwall, R. Jackiw, and E. Tomboulis, Phys. Rev. D **10**, 2428 (1974).
- ⁵⁶ E.V. Gorbar, V.P. Gusynin, V.A. Miransky, and I.A. Shovkovy, Phys. Lett. A **313**, 472 (2003).